Low Power Thermal Reactor for Deep Space Probes

by

Matt L. Orians

**A dissertation submitted in partial fulfillment
of the requirements for the degree of
Doctor of Philosophy
(Nuclear Engineering and Radiological Sciences)
in the University of Michigan
2013**

Doctoral Committee:

Associate Professor John E. Foster, Chair
Professor Alec D. Gallimore
Michael R. Hartman, Puget Sound Naval Shipyard
Emeritus Professor Terry Kammash
Professor William R. Martin

Preface

My research started with an interest in small low power reactors. I started using MCNP to try to design as small of a critical reactor as possible. To simplify the design and improve reliability, the designs eliminated cooling pumps and other moving components. It soon became apparent that the only practical use for my reactor would be as a small space reactor.

I then started a detailed study of space energy and propulsion. From this it became apparent that Nuclear Thermal propulsion would be limited to an $I_{SP} \approx 10^3$ seconds based on fuel temperatures [2,000-3,500˚K]. While this is better than liquid hydrogen and oxygen combustion [I_{SP}=455 seconds], the high engine mass and low thrust to weight ratio makes nuclear thermal rockets ineffective for Earth liftoff and lunar missions. Additionally nuclear thermal propulsion would need a larger volume of propellant which increases the size and cost [liquid hydrogen is 6x less dense than the combined density of liquid hydrogen and oxygen fuel] and as a result will be only a slight improvement even at mars distance. It was clear that the next step further in space propulsion would be electric propulsion and that the role of nuclear power in space would be to provide electricity. This resulted in Chapter 1 of this work which develops the region of feasibility for nuclear power in space.

This region of feasibility was limited to deep space [away from solar power, ≥10 Au] and overlapped with Radioisotope Thermoelectric Generators [RTG]. I then set about analyzing the current and proposed RTG technology and deep space probes. This resulted in Chapter 2 which is the design specifications that my reactor would need to meet.

I then returned to the design of the small reactors and using computational tools, refining my earlier designs for use in deep space. This quickly created tradeoffs between opposing design goals, for example minimizing the reactor mass is desired but requires highly enriched fuel which is worse from a proliferation standpoint. Finally, there turned out to be not one unique design that was better than the rest but a variety of designs with similar characteristics. This formed the basis for Chapter 3 which is the neutronic design of the reactor.

With the generic reactor designs my attention turned to maximizing power and lifetime. The heat transfer through the core was modeled to maximize the thermal power and outlet temperature and then the issue of the best heat engine for the size and temperature of the reactor was researched-this formed the basis of Chapter 4. Without moving control rods the lifetime of the reactor would rely on burnable poisons so models of core burn-up were created to examine the maximum lifetime that the reactor could achieve [Chapter 5]. To examine the reactor in further detail a single design was chosen to be refined.

At my thesis prospectus I presented my designs to date and planned future work [improved thermal model which completed Chapter 4, Characterizing the shielding which is Chapter 6 and transient analysis which became Chapters 8]. Out of this meeting additional content was added which included an improved burn-up model and safety considerations which are presented in Chapter 7.

The design of the reactor has been refined considerably and reached a point where additional modeling is no longer useful. Further work would customize the reactor based on the actual construction [for example: machine tolerances and impurities in the materials] and specifics of the space mission [duration, instruments and power demand]. This is however cannot be completed computationally and would require facilities [and resources] not present at the University of Michigan.

At the conclusion of this semester I will be working at Hill Air Force Base on nuclear hardness for the next three years, due to the terms of my fellowship. There are parallel lines of research on space nuclear power such as the Demonstration Using Flattop Fissions [DUFF] reactor at Los Alamos/NASA-Glenn [started summer 2012] which may be able to make use of some of my results. Due to this I wrote the thesis to place more emphasis on the results of my research so that other projects can use portions of my design or refinements to their system [due to different design considerations such as thermal vs. fast reactor and U-233 vs. U-235 not all of my results can be used].

Table of Contents

Front Matter

Dissertation text

List of Tables

List of Figures

List of Abbreviations

ASRG	Advanced Stirling Radioisotope Generator
DUFF	Demonstration Using Flattop Fissions [small research reactor]
GPHS	General Purpose Heat Source
I_{SP}	Specific Impulse
KRUSTY	Kilowatt Reactor Using Stirling TechnologY [small space reactor design]
LWR	Light Water Reactor
MCNP	Monte Carlo N-Particle [Los Alamos code]
MMRTG	Multi-Mission Radioisotope Thermoelectric Generator
NASA	National Aeronautics and Space Administration
RHU	Radioisotope Heater Unit
RTG	Radioisotope Thermoelectric Generator
SNAP	Systems for Nuclear Auxiliary Power
TRIGA	Training, Research, Isotopes, General Atomic [small research reactor]

Abstract

Deep space probes travel too far from the sun to use solar power and thus are dependent on Nuclear Power. Currently this is in the form of Radioisotope Thermoelectric Generators (RTG) which uses Pu-238. Pu-238 is not currently produced and may soon run out requiring production to be restarted; the only reasonable replacement radioisotope is Am-241. Both of these isotopes are highly toxic and the large masses needed for sufficient power pose nuclear proliferation concerns. The only alternative to radioisotopes is nuclear fission. Previous generations of space reactors have been designed for high power near Earth missions. As a result, previous reactor designs are ill-suited for the deep space missions.

The feasibility of using small reactors of similar weight to current RTG's is covered along with the design criteria for deep space probes. The reactor is designed with no moving parts, using burnable poisons for reactivity control throughout core life. Additionally, the core utilizes conduction for cooling, eliminating the need for pumps and coolant channels. The shielding requirements for the reactor are then calculated. Reactor safety concerns, effects of reactor transients and start-up are covered as well.

The resulting reactor design has a core mass of 27.0 kg containing 8.68 kg of U-233. The use of U-233 reduces the proliferation risks relative to RTG's and has 4 orders of magnitude lower radio-toxicity. The reactor will produce 2,112 W_{TH} at a temperature of 640˚C for a lifetime of 200 years. The reactor will require a shielding mass of 43Kg. Using Stirling technology this should produce 500-800 W_E with an engine/radiator mass of 50-80 kg. This produces a steady specific power of 4.1-5.3 W_E/kg which is the equivalent to 6.0-7.7 W_E/kg-RTG. The reactor design is well suited to the long duration deep space mission with a power supply lifetime significantly longer than any possible

RTG. Due to the steady nature of the generated power and its long life, the specific power generation would exceed current RTG's and match planned advances. In conclusion small low power fission reactors could be used to replace RTG's for future deep space missions.

Chapter 1: Background

Section 1: Regions of interest

To appreciate the need for nuclear power in space, it is necessary to narrow the scope of space from the entire universe to more specific regions. To do this, I divided space into regions by both distance from Earth and the Sun. Distance was chosen as a distinguishing factor since it will strongly affect both the external sources of power available [mainly sunlight] and the duration that power will be needed, due to the time required to reach the destination. In this work, only spacecraft not in contact with bodies are considered. Table 1.1 summarizes representative region of space with distance increasing in roughly a geometric progression. Also included is solar power density which is the largest external energy source in the solar system [1].

Table 1.1: Regions of space [1].

Region	Max Distance [AU]	Time to Reach Max Distance		Sunlight [W/m^2]
		At light speed	At 25 [2] km/sec	
Moons Orbit	0.00257	1.3 Second	4.3 Hours	1,361
Inner solar System	3.3	27 Minutes	7.5 Months	134
Jovian Planets	30.5	4.3 Hours	5.8 Years	1.6
Heliopause	100	14 Hours	19 Years	0.146
Sun Gravity Lens [3]	550	3.2 Days	105 Years	0.005
Jupiter Gravity Lens [4]	6100	35 Days	1,150 Years	0.000 04
Alpha Centauri [in 28,000 years]	187,000	2.97 Years	35,600 Years	1.6x10^{-7} at Halfway
Interstellar	≈5x10^6	≈83 Years	10^6 Years	N/A
Galactic	≫5x10^6	≫83 Years	≫10^6 Years	N/A

Interstellar and galactic targets are shown to represent the limits of travel and not any specific target.

Section 2: Energy sources

To narrow the scope of regions further, it is important to look at the possible sources of energy to provide a comparison to the external sources. While energy cannot be created or destroyed, it can be changed from one form [such as heat] to be used in another form [such as electricity]. All forms of energy can then be grouped by the dominant force used to store the energy. The four fundamental forces are gravity, electromagnetism and the strong and weak nuclear forces.

Gravitational Force: Gravity is the weakest of the four forces. Energy is released by rearranging masses into a lower gravitational energy state. The mass of a typical satellite has a gravity field far too weak to be used as a source of energy. However nearby bodies may possess sufficient mass to exert a considerable force on the spacecraft itself. This force is however applied nearly equally to all parts of the satellite and is thus unable to generate internal energy such as electricity. The uniform force may still be usable for propulsion with evidence by the slingshot effect [1]. As a result gravitational energy will not be considered further.

Weak Nuclear Force: This is the next strongest force and energy can be released by changing the flavor of quarks. This process is responsible for the beta decay of radioactive isotopes [5]. The energy is released as electrons, positrons and gamma rays [and neutrinos but these can be ignored here] which can be converted to heat and used to generate electricity. The gamma rays in particular are difficult to work with, as they are penetrating radiation and require substantial shielding [6]; fortunately a few isotopes undergo beta decay without gamma ray emission [5]. In general the half-life [Log(T½)] of an isotope is inversely related to the decay beta energy. This means that long lived beta decays have low energy [5]. For example, C-14 with a half life of 5715 years, has a beta energy of only 0.0495 MeV [7]. However, it is possible for nuclei to undergo 2 or more

successive beta decays with the first decay of long life controlling the decay rate and the second decay occurring much quicker at higher energy [6]. An example of this is the pair Sr-90, a beta emitter with a 30 year half life and Y-90 with only a 2.65 day life which together produces a useable energy of 1.13 MeV per decay with very little gamma energy [7]. [In practice, Sr-90 is stored as $SrTiO_3$ and only 55% of the strontium is Sr-90 [8] with the rest inert which reduces the initial specific power slightly to 300 W/kg initial or an energy density to 3.2×10^5 MJ/kg [7]]. Sr-90 is significant as it is the only beta pair produced by fission [thus mass produced [9]] with a half-life between 1.02 years [Ru-106 [7]] and 230,000 years [Sn-126 [7]] and as such is the only beta source used in RTG's.

Electromagnetic Force: This force is stronger still and energy is released by rearranging charge configurations into a lower energy states. The elementary unit of charge is 1.6×10^{-19} Coulombs and is present in both electrons [-] and protons [+] and cannot be changed. The distance between the elementary charges however can be changed which affects system potential energy. The magnitude of potential energy is inversely proportional to the distance between the charges. On a macroscopic scale there are a number of devices to store energy [such as capacitors] however the energy density is very poor. At the microscopic scale, the charges can be held at atomic distances [angstroms] as electrons and thus by combining different elements the distances are changed to release energy, resulting in chemical reactions. A common example is liquid hydrogen and oxygen the reaction of which is often used as both propulsion and electricity generation with energy density of only ≈10 MJ/kg [10].

Inter-particle spacing in the nucleus is even smaller on the order of femtometers. When these protons are released from the nucleus they are repelled by electrostatic forces converting large amounts of energy. The two most common examples are alpha decay and fission. In alpha decay two protons quantum tunnel out of the nucleus and are then repelled due to their positive charge. A significant example is Pu-238 with a

half life of 87.7 years and releasing 5.5 MeV per decay [7]. [In practice Pu-238 is stored as PuO_2 and only 84% active for 412 W/kg initial or an energy density of $1.57x10^6$ MJ/kg [8]]

Additionally alpha decay can form chains of alpha decays to release additional energy [5]. An example is Ra-226 which has a half-Life of 1600 years but undergoes 5 alpha decays for 34.2 MeV and a specific power of 252 W/kg initially [7]. However these long alpha decay chains also undergo beta decay as well which can produce significant gamma radiation. Ra-226 for example has 4 beta decays releasing 1.38 MeV as betas and 1.72 MeV in the form of gammas [7]. [This 4.63% gamma emission is comparable to the 9.5% penetrating radiation in fission]

In fission a neutron induces a heavy nucleus to split into two small fragments [11]. Each fragment is positively charged and they separate creating large amounts of kinetic energy [~170 MeV per fission] and additional gammas [8 MeV] and 2-3 neutrons [5 MeV] to continue the chain reaction. In addition the fission fragments tend to be neutron rich leading to additional beta decays adding slightly to the total energy [10 MeV] [11]. An important example is U-233 which releases 191.04 MeV per fission [7], has a bare critical mass of 15.8 kg [12] and an energy density to $7.9x10^7$ MJ/kg.

In practice only weapon designs approach the $7.9x10^7$ MJ/kg while most commercial reactor burn only 4-6% of their fuel [11][13]. However a space reactor may utilize high enriched fuel similar to terrestrial military reactors that burn ≈40% of their high enriched fuel. As a practical matter however the small size of space reactors limits their burn-up even with high enriched fuel [SP-100 was designed to have a 4% burn-up [14]]. As a result 20% burn-up will be considered the limit with likely reactors below this.

Strong Nuclear Force: This is the strongest force and is responsible for binding quarks into nucleons and nucleons together in the nucleus. The main form of energy possible here is the binding of nucleons together known as fusion. The most significant

of these reactions is deuterium and tritium fusing into helium with the release of a neutron. However the half-life of tritium is only 12.3 years [7] which means that long term power production will rely on deuterium-deuterium fusion instead [This is best represented as $5D \rightarrow H+He^3+He^4+2n$ since the resultant triton from DD fusion quickly undergoes fusion a second time]. This releases 24.9 MeV per 5 deuterons with ⅔ of the energy in the form of neutrons [7]. This results in an energy density of $2.4x10^8$ MJ/kg or $8.0x10^7$ MJ/kg if neutron energy is not recovered. [In practice fusion energy has only been created in nuclear weapons to date, as all current fusions systems operate well below breakeven.] In any case the energy density is approximately the same as fission without the neutrons and only 3x higher with the neutrons [and to capture/extract energy from the neutrons, two additional nuclei are needed such as lithium or boron which lowers the effective energy density below that of fission]. A portion of the fusion energy is necessary to sustain the fusion reaction and is not available for the probe to use. An order of magnitude beyond breakeven is therefore needed for this input power to be insignificant to match the output energy density of fission. [Additionally since 66.5% is released as high energy neutron radiation compared to only 9.5% low energy radiation in fission substantially more shielding will be needed [6]] Finally fusion is highly complex and massive [ITER's magnets weigh 6540 Tons] with no significant benefit over fission in energy density.

Non-Force Energy: A final possible form of energy is Antimatter. This has the highest possible energy density at $9.0x10^{10}$ MJ/kg [1140x better than fission] but 100% of the release is in the form of radiation as gammas, high energy electrons and exotic particles [pion's, kaon's and muon's] [15].

Antimatter is currently not feasible in gram quantities [needed to match the energy of kilogram quantities of U-233 or Pu-238] and plans to use much smaller amounts rely on using it as a catalyst for either fission or fusion. As a result neither

antimatter nor fusion will be considered further as both are impractical with current technology within the size limit of an unmanned satellite.

External Energy: This can be divided into natural and artificial sources. By far the largest natural source in the solar system is the sun with a power of 3.85 $x10^{26}$ W [1] dwarfing anything else in the solar system. This power is mainly in the form of visible light with significant infrared and ultra violet light. [An additional 2.3% is emitted in the form of neutrinos but these can be ignored]. The chief disadvantage is that the light spreads out with the radius square with 1361 W/m^2 at 1 Au [Earth's orbit] but is only 50 W/m^2 at Jupiter and <1 W/m^2 at Pluto.

Artificial external sources [beamed power] are more difficult. A very large 1 GW isotropic source will radiate 1361 W/m^2 at a distance of only 240 meters. To reach 1 Au with 1361 W/m^2 and 1 GW with a Gaussian beam [circular beam or (0,0) mode Gaussian [16]] would require tight angular confinement of only 0.00067 arc seconds [this is equal to an accuracy of 3.2 mm at a distance of 1000 km]. Further with the source on earth, which rotates, requires continuous tracking since the beam would very quickly move off target [except for beams aimed directly north or south from the poles]. The beam would also have to contend with atmospheric deflection [a beam source placed on the moon would have slower rotations and no atmosphere but placing the beam on the moon is not feasible at this time]. In addition most beams will spread out faster than geometrically in the vacuum of space; charged beams spread the fastest due to electrostatic repulsion but neutral particle beams still spread from internal pressure and even light will spread due to diffraction. As a result beamed source will not be coincided practical at this time.

For comparison with nuclear energy only solar will be considered for external energy. For comparison purposes solar panels are considered to have an area mass density of 1 kg/m^2 and an efficiency of 22% for 300 W_E/kg at 1 AU [17][18][19]. This

represents current projection for the state of the art solar panels 5-10 years from now. Additionally the efficiency will be assumed to be constant as the panels move further from the sun. [Currently photovoltaic panels have reduced efficiency at low light intensity of <≈ 80 W_{TH}/M^2. This causes solar potential to reduce this faster than simply $1/r^2$. For example of this effect, at Saturn's orbit, panels would generate only 1 W_E/kg instead of 3.3 W_E/kg. However these issues may be resolved in the coming decades [17]]. However, as the panels move closer to the sun a maximum power of ~600 W_E/kg is achievable limited only by overheating the panel [20] [in practice the panels are rotated to reduce sunlight closer to the sun, see section 1.5 for thermodynamic discussion]. Table 1.2 shows specific power at for several distances from the sun. Finally it is assumed that the panels will degrade at only 0.5% per year [an improvement over the current 1-2% per year [17]]. These assumptions may be optimistic but so are projections for other power sources. Additionally sources with radiation [RTG, fission, fusion] must perform significantly better than solar to be of practical value.

Table 1.2: Solar Power drop-off with distance [1].

	Au	W_{TH}/m^2	W_E/kg	Potential for Use
Mercury	0.387	9,087	600	Great
Venus	0.723	2,604	573	Great
Earth	1.000	1,361	300	Great
Mars	1.524	586	129	Great
Ceres	2.770	177	39	Good
Jupiter	5.204	50.3	11	Ok [17]
Saturn	9.582	14.8	3.3	Possible [21]
Uranus	19.201	3.69	0.81	Poor [17]
Neptune	30.047	1.51	0.33	Very Poor
Pluto	39.482	0.87	0.19	Very Poor
GPHS-RTG for reference [22]			5.2	

The GPHS-RTG specific power is using fresh Pu-238 at launch. This decays with time [see Chapter2].

Section 3: Comparing Energy Sources

In order to compare the different energy sources they need to be converted to common units. Power was chosen instead of energy for two reasons: 1-the radioactive isotopes have a characteristic time of decay which is fixed and 2-solar power has no fixed energy limit but a clear power limit [solar continues producing power until the panel degrades or the sun burns out]. This power is plotted as thermal power per kg of fuel [taken to be 0.1 kg/m^2 for solar panels] in Fig 1.1.

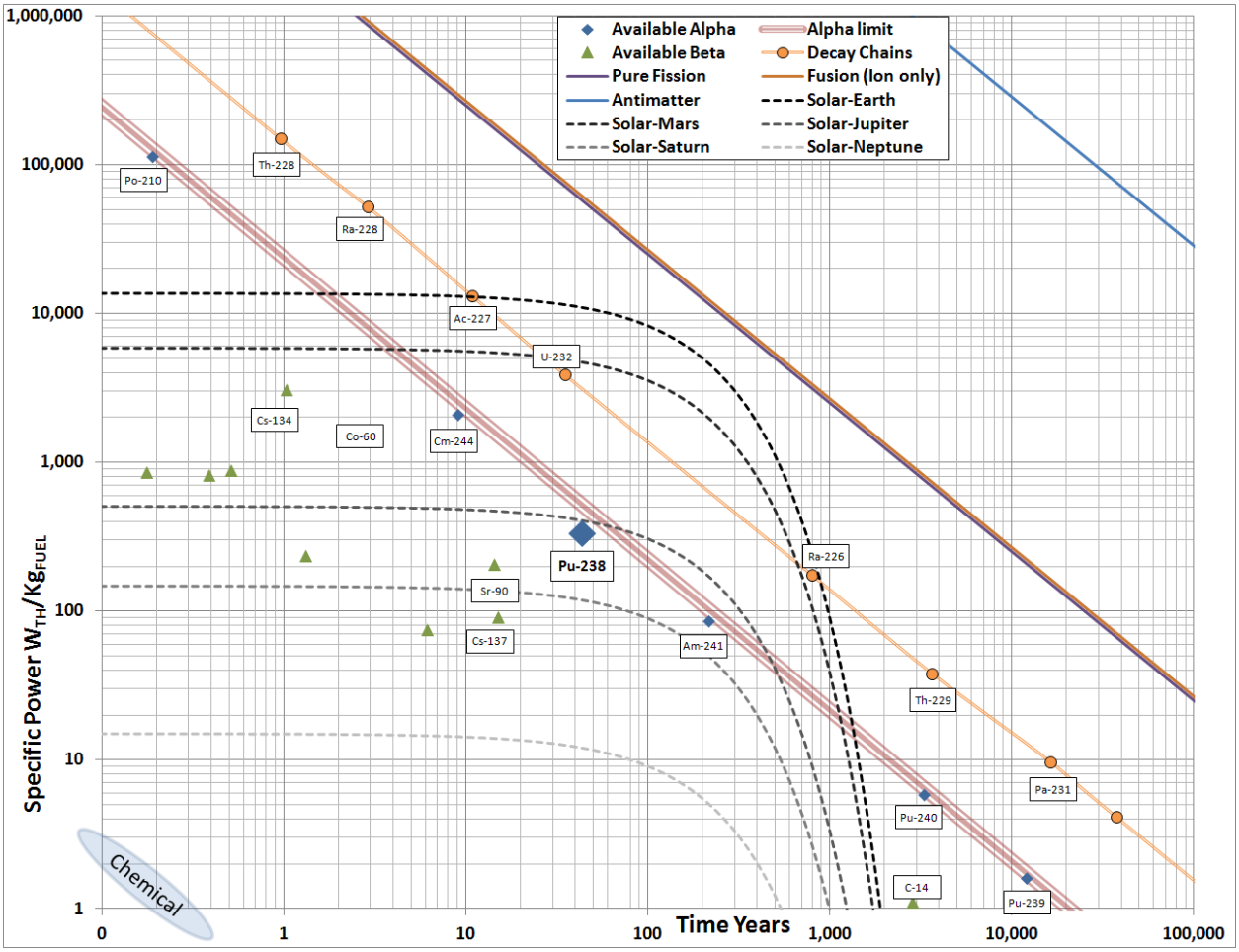

Figure 1.1: Energy source comparison [7][8]**.** This figure plots the relationship between specific power and time. For radioisotopes the time is taken to be ½ of a half-life since power drops drastically beyond this [8], and the power is the average power over the first ½ of a half-life. Solar is plotted with the characteristic degradation [0.5%/year] at several distances from the sun.

In particular solar power at earth orbit outperforms chemical and RTG's except at very short times [0.2 years for Po-210] or very long duration [3,000 years for Pu-240]. Additionally, although ideally fission and fusion appear capable of outperforming solar [28][29], actual and designed reactors have not performed better than solar panels. Even at Mars orbit there is little benefit for nuclear. However by Jupiter orbit solar and Pu-238 in RTG's are nearly equal [Galileo launched in 1989 used the GPHS-RTG while Juno launched in 2011 uses solar power [22]]. While solar may be possible at Saturn in a few decades, for now it is insufficient [Cassini launched 1997 used the GPHS-RTG [21] and the proposed 2020 Titan Saturn system mission would also use Pu-238]. Clearly anything beyond the Jovian planets would not be able to use solar. In this range an internal source of energy will be needed.

The distance from the sun affects the time the power source must last. Trips to the Jovian planets will take several years to a decade and may remain on station a decade longer; missions beyond this require multiple decades to reach. This eliminates shorter lived isotopes from use as a RTG which includes all the beta sources. On the other hand any energy source must maintain sufficient power to keep the spacecraft operating which is taken to be ~25 W_{TH}/kg as a lower limit since adding a thermal efficiency of <20% [as the fuel will be relatively cool] and a nonfuel mass of >5x fuel mass yield less <1 W_E/kg [Pu-239 and Pu-240 are below this limit and as a result no special cooling is needed when they are used in kilogram quantities]. This sets an upper limit for mission duration; 100,000 years with ideal fission or fusion, ~7,000 years for realistic fission [60 GW-Yr/MTHM], 3,650 years for the alpha chain [Th-229] and only 220 years for single alpha decay [Am-241].

While a realistic fission source lasts much less than 100,000 years there is the possibility that the reactor is operated intermittently to conserve power to last longer. Theoretically this could push duration back to ~70,000 years [assuming an average

power of 10% of the 25 W_{TH}/kg]. Likewise a solar panel can remain dormant until reaching a distant star and then reactivate as the satellite approaches the star [30].

To show the possible sources of energy for each region of space, Table 1.1 is expanded with the information above and Figure 1.1 and shown in Table 1.3. Note this shows only possible energy sources. It should be clear that fission is useful only where solar is unavailable and is only in competition with alpha decay.

Table 1.3: Regions of Space and Power

Region	Max Dist [Au]	Time to reach At 25 km/sec	Sunlight [W/m^2]	Form of Power
Moons Orbit	0.00257	4.3 Hours	1,361	Solar is best
Inner Solar System	3.3	7.5 Months	134	Solar is best
Jovian Planets	30.5	5.8 Years	1.6	Solar to Saturn then Alpha or Nuclear
Heliopause	100	19 Years	0.146	Alpha [Pu-238] or Nuclear
Sun Gravity Lens	550	105 Years	0.005	Alpha [Am-241] or Nuclear
Jupiter Gravity Lens	6100	1,150 Years	0.000 04	Alpha Chain or Nuclear
Alpha Centauri [in 28,000 years]	187,000	35,600 Years	$1.6x10^{-7}$ at Halfway	Nuclear transit Solar upon arrival
Interstellar	$5x10^6$	10^6 Years	N/A	Dormant in transit Solar upon arrival
Galactic	$>>5x10^6$	$>>10^6$ Years	N/A	Not feasible

Section 4: Thermal Conversion

Most of the energy consumed aboard a satellite is in the form of electricity. The two most significant exceptions are heating and propulsion. Currently heat is generated from small RHU's which contain Pu-238 producing heat. For example the Cassini-Huygens probe used 117 RHU's [23]. This amounted to 0.315 kg of Pu-238 and 4.68 kg system weight including protective casing. With a fission reactor systems it would be possible to generate heat as an electric load [resistive I^2R] or the waste heat from the heat engine can be utilized. Since neither method would significantly affect the construction of the reactor system, direct heat use will not be coincided further. Propulsion could be a large draw on energy due to the high speed necessary in space travel. However there is no current system providing both propulsion and electric power which the two systems may be considered separately [an electric power system and a separate propulsion system that is one of the electric loads]. Since both heat and propulsion outputs are separate from the power source only electric power needs are considered.

To proceed further it is important to discuss the conversion of heat to electricity in space. Both fission and alpha decay deposit most of the energy directly in the source material [alpha and fission fragments have ranges of ~10 μm] [6] and the source material then heats up. This heat is transferred to a device that converts heat to useful work [thermocouple, thermionic, Stirling engine…] and the waste heat is then radiated into space at a lower temperature. The conversion efficiency depends on the temperature difference between the source and the radiator and is limited by Rankine efficiency [η]. Additionally the power radiated into space can be considered a blackbody problem with power proportional to area times Fin effectiveness [F], emissivity [ε], the Stefan-Boltzmann constant [σ] and temperature [T] to the fourth power. These results are then combined into Equation 1.1.

$$\frac{Electric\ power}{Radiator\ mass} = \frac{\left(\frac{\eta}{1-\eta}\right) * \varepsilon\sigma T_{Radiator}^4 * F}{(Mass/Area)_{Radiator}} \qquad \text{Equation 1.1}$$

To see what this means for the power supply a sample of current power conversion technologies are shown with characteristic efficiencies and cold side temperatures. These are all considered with the following radiator: ε=0.85, F=0.8 and 5 kg/m^2 [which is an improvement over the 12-15 kg/m^{2}currently used for the GPHS-RTG, MMRTG and ASRG [31]]:

1- Thermocouple [SP100]: η~4.1%, T_{Rad}=600°C. 197 W_E/kg [14]
2- Thermocouple [GPHS]: η~5%, T_{Rad}=300°C. 43.8 W_E/kg [22]
3- Thermocouple: η~15%, T_{Rad}=0°C. 7.6 W_E/kg [32]
4- Stirling or Brayton: η~20%, T_{Rad}=100°C. 37.3 W_E/kg [33]
5- Stirling or Brayton: η~35%, T_{Rad}=0°C. 23.1 W_E/kg [33]

This shows that due to the radiator mass alone, power >100 W_E/kg is not feasible. A more detailed analysis was done in by NASA [31] which concluded that for Pu-238 [~500 W_{TH}/kg] systems that a 10 W_E/kg limit is more realistic [31]. Due to this, increasing the heat source power >3000 W_{Th}/ kg_{FUEL} will not significantly decrease system mass [At 30% efficiency in a 10 W_E/kg system the effect of going from 3000 W_{Th}/kg_{FUEL} to ∞W_{Th}/kg_{FUEL} will only decrease overall mass by 1.1%]. Due to the added cost and difficulty of cooling such high density systems, the 3000 W_E/kg_{FUEL} will be considered the upper useful limit for thermal to electric power production in the vacuum of space.

It is natural to ask at this point, how Solar can reach 300 W_E/kg when we found that any thermodynamic system is bounded to <100 W_E/kg. The reason for this is that the panels act as their own radiator, they only have to reject the heat absorbed equally over the whole surface [F=1]. This allows the mass per area to be much lower at ~1 kg/m^2 [17] instead of 5 kg/m^2 since the panels do not need thickness to conduct heat laterally or pipes to transport heat within the panels. Finally since the heat source temperature can be taken as the temperature of the sun [5780°K] [1] the efficiency can

remain high even as the panels heat up beyond 0°C instead of dropping as rapidly as typical thermocouples [1100°C] or Stirling/Brayton [600-850°C].

Solar panel: η~22%, T_{Rad}=112°C. 298 W_E/Kg [Earth orbit] [19]
Solar panel: η~28%, T_{Rad}=150°C. 600 W_E/Kg [Mercury Messenger satellite] [20]

These match the previous statements from section 1.2 that solar will be capable of 300 W_E/kg at earth orbit but limited as the sun is approached to prevent over heating the panels.

Section 5: The Nuclear Window

At this point we have bounded Figure 1.1 to demonstrate the region where nuclear power can be useful. The 5 bounding requirements are:

1- Specific power < 3000 W_{Th}/kg_{FUEL} due to radiator mass
2- Specific power > 25 W_{Th}/kg_{FUEL} for sufficient energy production
3- At least comparable to RTG performance [within a factor of 3]
4- Duration of at least 2 decades for missions to Saturn and beyond
5- Less than 20% burn-up of fission fuel

These are shown in Figure 1.2; the shaded region is the area that nuclear power may be useful which will be discussed further in the next chapter.

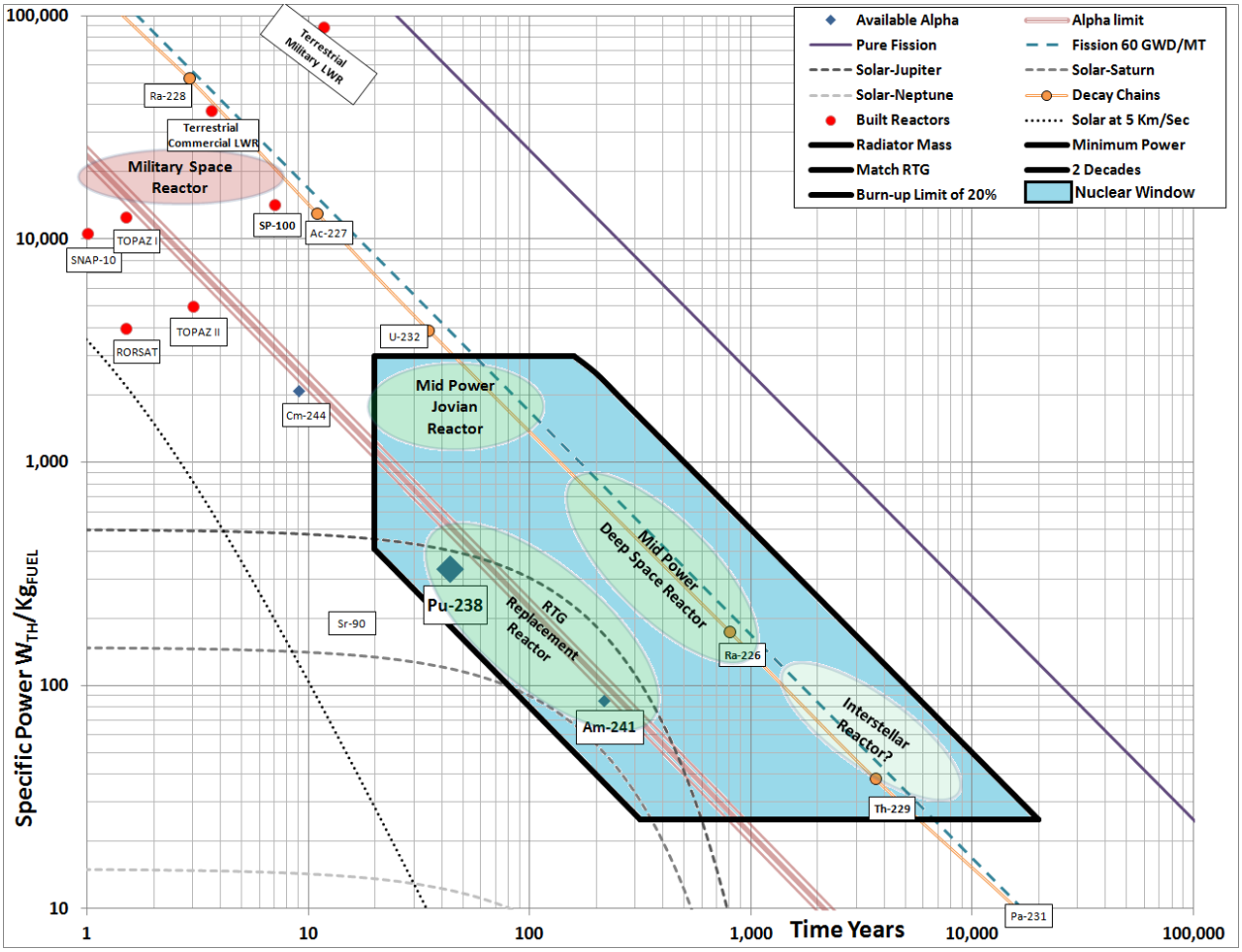

Figure 1.2: The Nuclear Window. This figure is an extension of Figure 1.1 to illustrate the nuclear window

References [Chapter 1]

[1] Marc Kutner, “Astronomy: a Physical Perspective”, Wiley (1987)
[2] B.R. Davis “Gravitational Lens: Deep Space Probe Design” Air Force Institute of Technology (2011)
[3] C. Maccone “The Sun as a Gravitational Lens: A Target for Space Missions Reaching 550 AU to 1000 AU” Power Point (2008)
[4] C. Maccone “A New Belt Beyond Kuiper’s: A Belt of Focal Spheres Between 550 and 17.000 AU for SETI and Science” Acta Astronautica, 69, pp. 939 (2011)
[5] Edward Baum, “Nuclides and Isotopes: Chart of the Nuclides”, Lockheed Martin (2009)
[6] Glenn Knoll, “Radiation Detection and Measurement”, John Wiley & Sons Inc (2000)
[7] National Nuclear Data Center, http://www.nndc.bnl.gov/
[8] M. Ragheb “Ch. 3 Radioisotopes Power Production” (2012), https://dmtpc.mit.edu/twiki/pub/Projects/RadioIsotopeBattery/Radioisotopes_Power_Production.pdf
[9] E.J. Wheelwright “Byproduct Inventories” Pacific Northwest Laboratory (1983), http://www.wmsym.org/archives/1983/V2/21.pdf
[10] David Lide, “CRC Handbook of Chemistry and Physics”, CRC Press (2001)
[11] J.J. Duderstadt and L.J. Hamilton, “Nuclear Reactor Analysis”, John Wiley & Sons Inc (1975)
[12] Van den Berghe “Evaluation of Nuclear Criticality Safety Data and Limits for Actinides in Transport” (2003)
[13] “The Westinghouse PWR Nuclear Power Plant”, Westinghouse (2006)
[14] S.F. Demuth “SP100 Space Reactor Design” Progress in Nuclear Energy, 42, pp.323 (2003)
[15] David Griffiths, “Introduction to Elementary Particles” ,Wiley (2010)
[16] Daniel Zwillinger, “Standard Mathematical Tables and Formulae”, CRC Press (1996)
[17] S.W. Benson “Solar Power for Outer planets Study” Power Point (2007), http://www.lpi.usra.edu/opag/nov_2007_meeting/presentations/solar_power.pdf
[18] IAEA “The Role of Nuclear Power and Nuclear Propulsion in the Peaceful Exploration of Space” (2005)
[19] NASA “Return to Assembly, STS-115” (2006), http://www.nasa.gov/pdf/154433main_sts115_press_kit3.pdf
[20] NASA “Messenger NASA’s Mission to Mercury Launch Press Kit” (2004), http://www.nasa.gov/pdf/168019main_MESSENGER_71504_PressKit.pdf
[21] “Why the Cassini Cannot Use Solar Arrays” Cassini Public Information Jet Propulsion Laboratory (1996)
[22] G.L. Bennett, et al “Mission of Daring: The General-Purpose Heat Source Radioisotope Thermoelectric Generator” IECEC, San Diego, CA (2006)
[23] Department of Energy Facts: Radioisotope Heater Units. U.S. Department of Energy, Office of Space and Defense Power Systems. December 1998.
[24] S.K. Borowski “Nuclear Thermal Propulsion (NTP)” NASA Glenn Research Center, Cleveland, OH (2010)
[25] S.D. Howe and R.C. O’Brien “Recent Activities at the Center for Space Nuclear Research for Developing Nuclear Thermal Rockets” International Astronautics Congress (2010)

[26] R.H. Frisbee “Advanced Space Propulsion for the 21st Century” Journal of Propulsion and Power, 19, pp. 1129 (2003)
[27] G.R. Schmidt, et al “Radioisotope Electric Propulsion (REP): A Near-term Approach to Nuclear Propulsion” Acta Astronautica, 66, pp. 501 (2010)
[28] G.L. Bennett, et al “An Overview of NASA’s Projected Mission Requirements for Space Nuclear Systems” Acta Astronautica, 34, pp. 1 (1994)
[29] G.L. Bennett, et al “Status Report on the U.S. Space Nuclear Program” Acta Astronautica, 38, pp. 551 (1996)
[30] R.L. McNutt, Jr. “Phase II Final Report NASA Institute for Advanced Concepts A Realistic Interstellar Explorer” (2003)
[31] L.S. Mason “Realistic Specific Power Expectations for Advanced Radioisotope Power System” Journal of Propulsion and Power, 23, pp. 1075 (2007)
[32] R.C. O’Brien, et al “Production of Safe Radioisotope Heat Sources by Spark Plasma Sintering” Proceedings of Nuclear and Emerging Technologies for Space, Atlanta, GA (2009)
[33] J.G. Wood, et al “Free-Piston Stirling Power Conversion Unit for Fission Surface Power, Phase I Final Report” NASA (2010)

Chapter 2: Design Specification

In the previous chapter the window of opportunity for nuclear power was shown in Figure 1.2. In this chapter space missions that fall within the window of opportunity will be examined. Additionally a survey of previous power designs for space along with detailed specifications for future reactor designs will be discussed.

Section 1: Detailed Mission Scope

Based on the previous chapter the mission scope extends from the Jovian planets to the outer reaches of our solar system. These missions are however also constrained by mission funding which depends on interest in the objects to be explored. Cost is in large part determined by mass and power of the satellites visiting these regions [1]. All previous spacecraft launched to reach Jupiter are listed in Table 2.1 below.

Table 2.1: Past Satellites reaching Jupiter orbit [1][2].

Spacecraft	Launch Year	Mass [Kg]	Power [W_E]	Power Supply Mass [Kg]	Power Supply Mass Percent
Pioneer 10	1972	258	155	54.4	21%
Pioneer 11	1973	259	155	54.4	21%
Voyager 1	1977	722	475	113	16%
Voyager 2	1977	722	475	113	16%
Galileo	1989	2380	570	111.9	4.7%
Ulysses	1990	370	285	55.8	15%
Cassini	1997	2523	880	169.3	6.7%
New Horizons	2006	478	228	57.9	12%
Juno (solar)	2011	3625	486	340.9	9.4%

Additionally, the time to complete the mission is important. While long term missions [>1000 years] are possible with current technology, improving technology may render them obsolete before they even reach the target. This will limit the nuclear window further. To illustrate this, the window is divided into four mission regions represented by ovals in Figure 1.2:

1- **Interstellar Reactor**: In this region the specific power would be in the range of 25-100 W_{TH}/kg_{FUEL}. As explained above missions lasting longer than 1,000 years are not likely to be launched in the next century or two. As a result this area is left open for the future consideration.
2- **Mid Power Deep Space Reactor**: In this region the specific power would be in the range of 100-1,000 W_{TH}/kg_{FUEL}. The time duration is about 200-1000 years which at 25 km/sec corresponds to 1,000-5,000 Au from the sun. The issue here is that there is little of interest in this region [4]. The Suns magnetic field extends only a few hundred AU and the most distant discovered object is Senda at 90 Au. The furthest proposed realistic missions are to gravitational lens, however the Sun's lens is at 550 Au and the next closest is Jupiter's at 6,100 Au [5].
3- **Mid power Jovian Reactor**: In this region the specific power would be in the range of 1,000-3,000 W_{TH}/kg_{FUEL}. While physically possible, reactors in this range require significant heat transfer, shielding and active reactivity control. The core would be on the order of >20kg [to be critical] which places thermal power at ~40 kW. This corresponds to around 4-10 kW_E [at 10%-25% conversion] and system mass of 400-2000 kg [5-10 W_E/kg] not including shielding [6]. While this is not inconceivable, it is an order of magnitude larger than shown in Table 2.1. A future satellite to Uranus or Neptune could easily suffice on 500 W_E and thus in the interest of cost these larger reactors are not currently necessary [7]. If in the future some need for several kW_E is discovered for these locations, nuclear power should be the first choice.
4- **RTG replacement Reactor**: In this region the specific power would be in the range of 50-500 W_{TH}/kg_{FUEL}. This region is of the most immediate practical interest and is currently being filled by RTG's [8]. Since the power requirements for this mission region are already being met by RTG's [1], it will be demonstrated that nuclear power reactors will not only meet the requirements of RTG's but exceed them is some significant ways. From this point on, reactors will be discussed in the context of a replacement for current RTG systems. Since the comparison will be with RTG's, the characteristics of RTG's and why they were chosen over past reactors will be discussed.

Section 2: Past Reactor and RTG Issues

Past Reactors: There have been several designs for space reactors in the past, 35 of which were launched into orbit and are shown in Table 2.2 [1].

Table 2.2: Past Space Reactor Designs [9][1][10].

Name [# Launched]	Fuel Mass [kg]	Total Mass [kg]	Power [kW_{TH}]	Power [kW_E]	Life [years]	W_E/kg
SNAP-10 [1]	4.3	435	43	0.65	1	1.5
SP100 [0]	140	4518	2,400	100	7	22.1
RORSAT [32]	31	1250	100	3	0.4	2.4
TOPAZ II [2]	27	1061	125	6	3	5.7

These reactors were grouped on Figure 1.2 as military space reactors. They were designed to provide high power back during the Cold War [SP100 was to power the strategic defense initiative lasers and the Soviet RORSAT and TOPAZ reactors were used for radar surveillance] . Since that time, advances in solar power has made these systems obsolete in near Earth orbit and their high power/ short life is not useful for the longer deep space missions [11]. They all have higher mass than any of the power systems in Table 2.1, and the SP100 is larger than even any of the satellites. While the 22 W_E/kg for SP100 is impressive, the mass of 4518 kg is much too large for civil space applications [10]. For this reason, smaller RTG power supplies have been chosen over reactors for past missions. The key lesson learned is that future reactors should be much smaller with masses comparable to RTG's [7][12]. There are however several significant disadvantages of RTG's which are explained below.

Availability: There are only a few isotopes that have the specific power and lifetimes capable of powering deep space missions. This is further narrowed by eliminating the strong gamma sources which are extremely difficult to work with

[gammas are difficult to shield in MCi quantities] and requires significant heavy shielding. This leaves only 4: Pu-238, Am-241, Cm-244 and Sr-90 as possible nuclides.

1- **Pu-238:** The US has not produced any Pu-238 since the end of the Cold War and Russia has also shut down production and has no more Pu-238 to sell [13]. The 2005 US DOE inventory was 39.5 kg of which 15.8 kg was used for the Mars Curiosity Rover and New Horizons probe and an unspecified amount for national security requirements [14]. The Pu-238 used on New Horizons was already 21 years old at launch which lowered power density by ≈15% [15]. There is estimated only enough Pu-238 for one more outer planetary mission before Pu-238 stocks are depleted. Restarting production would take at least 5 years and $200 million [13]. As a result Pu-238 should be considered low availability.
2- **Am-241** is currently not in production and only 16 kg [1.8 kW_{TH}] of separated Am-241 exists in the DOE inventory [1998] [16]. However reprocessing commercial spent nuclear fuel may be used to produce americium in the near future producing ≈½ kg of Am-241 for every ton of spent fuel reprocessed [16]. As a result Am-241 should be considered low availability.
3- **Sr-90** was separated at Hanford during the Cold War with ≈300 kg-SrF_2 capsules as of 1986 [17]. However the production of Sr-90 has ceased so only ~ 150 kg remain with an isotopic composition degraded down to ≈25% [may not be suitable for space purposes]. However, Sr-90 production can be resumed by reprocessing commercial spent nuclear fuel to produce ≈0.4 kg of Sr-90 for every ton of spent fuel reprocessed [18]. Additionally purchases of Sr-90 from other nations do not have the proliferation issues that purchases of actinides have. As a result Sr-90 may be considered available.
4- **Cm-244** is produced in minute quantities only [19]. The largest source of Cm-244 is currently 40 grams [94W] present at Oak Ridge National Lab. However Cm-244 can be produced from reprocessing commercial spent nuclear fuel to produce ≈0.07 kg of Cm-244 for every ton of spent fuel reprocessed. As a result Cm-244 should be considered very low availability.

For comparison 100's of kg of enriched U-235 is produced every year for naval reactor use. Additionally the US has ≈600 kg of high enriched U-233 leftover from the Cold War but no current production [20]. India is currently producing U-233 and has several thorium based reactors such as KAMINI research reactor at Indira Gandhi Center for Atomic Research in Kalpakkam, India operating since 1996 and producing 30 kW_{TH}. The U-233 in the US inventory is currently scheduled for disposal in the time frame of

2015-2017 which could eliminate its availability [21]. Both U-233 and U-235 are far more available than any of the four isotopes.

Useful lifetime: Radio-isotopes decay at a fixed rate which cannot be slowed or stopped. While this is useful from a reliability standpoint it also means that the material cannot be stored for long durations without degrading which limits the useful life. As mentioned in Section 1.5 the heat rejection occurs according to temperature to the 4th power meaning that after one half life the radiator temperature will drop only 16% [for example from 100°C to 41°C, 100°C=373°K*0.5^{¼}=314°K=41°C]. See Figure 2.1 for a flow diagram of ideal heat engine.

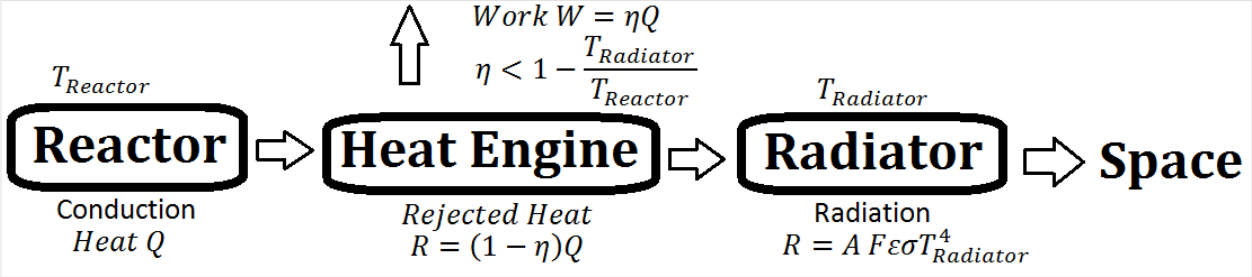

Figure 2.1: Heat flow overview diagram. This figure is an illustration of the overall heat transfer in an idealized system.

At the same time, power drops by a factor of two which will reduce the temperature difference across the heat engine by ≈50% [assuming simple resistive model] which greatly exceeds the drop in radiator temperature resulting a drop in efficiency which compounds the drop in thermal power. For example the Voyager RTG's in 2011 [34 years or 0.4 $T_{½}$] [2] reduced to 57% of initial electrical power despite still having 76% of initial thermal power. Despite the large reduction in RTG specific power [nearly 10% in the first 3 years for Pu-238 space RTG's] the listed specific power is usually the initial specific power [perhaps to make it seem as high as possible]. For

comparison with reactors which have a more steady power the average specific power should be used. Six examples are listed for the GPHS-RTG below:

1- Initial/Listed Specific Power: 5.20 W_E/kg [25]
2- Average Specific Power [0-5 Years]: 4.83 W_E/kg [25]
3- Average Specific Power [0-20 Years]: 4.27 W_E/kg [25]
4- Average Specific Power [0-30 Years]: ≈4.0 W_E/kg
5- Average Specific Power [0-44 Years]: ≈3.6 W_E/kg
6- Average Specific Power [20-44 Years]: ≈3.0 W_E/kg

This limits RTG's to approximately one half of a half-life or less for more dynamic conversion [the ASRG is designed for only 17 years or ⅛$T_{½}$ [22]]. This means that the 20 year life requirement actually requires a half-life of at least 40 years due to the non-constant power and prevents the shorter lived Sr-90 and Cm-244 from fulfilling this role, see Table 2.3.

Proliferation: The alpha emitting actinides are all fissile isotopes making them proliferation concerns. The critical mass of Pu-238 is actually less than that for pure Pu-239 [23]. Table 2.3 below lists the basic criticality parameters of the radio-nuclides.

Both Pu-238 and Am-241 have a heat per critical mass of less than 5 kW_{TH} meaning any satellite needing higher power than this would require more than one critical mass [note that greater than one critical mass can remain subcritical based on geometry or poison loading]. The Cassini probe for example contained ≈4 critical masses of Pu-238 in its 3 GPHS-RTG's [24][25]. Additionally Am-241 has a low enough spontaneous fission rate that a gun type device could be used instead of more complex implosion devices [16].

The only arguments against considering Pu-238 a proliferation issue are the relatively high spontaneous fission rate in Pu-238 and the high heat production [28]. The heat can complicate the construction but as seen in RTG's it can be removed. The spontaneous fission [SF] rate would require an implosion device. It also affects the predetonation probabilities. Even a predetonation fizzle could still be several kilotons of

TNT equivalent and due to the very high radio-toxicity of Pu-238 cause significant fallout [29]. As a result any use of Pu-238 or Am-241 in quantities approaching their critical masses should be considered a proliferation issue.

Table 2.3: Isotopes properties with Critical Mass [CM] for commercially available oxides compared to weapon material [23][26][27].

	$T_{½}$ [Yrs]	W_{TH}/kg	CM [kg]	W_{TH}/CM	γ [ppm]	SF/CM [WGPu≡1]
Pu-238	87.7	348	9.49	3,750	1.7	31.8
Am-241	433	85.7	57.6	5,431	11.6	0.087
U-235	$7x10^{8}$	$4.7x10^{-5}$	46.7	0.002	27,300	$7x10^{-7}$
Pu-239	24,110	1.6	9.99	16	9.8	0.0003
WGPu	24,110	2.5	10.5	26.5	9.7	1

[WGPu is taken to be 93.8% Pu-239, 5.8% Pu-240, 0.35% Pu-241, 0.022% Pu-242 and 0.012% Pu-238, which is the lower limit for practical weapon production]

Activity Hazard: The greatest risk to the RTG is during launch when radioactivity is the highest. For example NASA estimates [24] that the likelihood of a plutonium release very early in the Cassini launch was 1 in 1,100 near Cape Canaveral and 1 in 476 late in the launch over the ocean [compared to 1 in 13 million during the Earth swing-by]. The effluent limit for Pu-238 is $2x10^{-8}$ μCi/ml [US effluent limits are controlled by regulation 10 CFR 20 [26]] which is the same as Pu-239 [and Am-241]. The much shorter half-life of Pu-238 results in the radio-toxicity of Pu-238 being 276 times higher on a mass basis than Pu-239. The 8.1 kg of Pu-238 in a GPHS corresponds to the same radio-toxicity as 2.23 tons of Pu-239 [6,936 km^3 water or $6.94x10^{9}$ km^3 air] [26][27] and as a result any release would be significant. NASA calculated that if Cassini were to reenter Earth's atmosphere during the swing-by [while very unlikely] an estimated 5,000 additional cancer death could occur within the next 50 years [24]. Over all the radio-toxicity of RTG's is significant and should be reduced if possible.

Section 3: Design Specs

From the aforementioned considerations, it is now possible to lay out design requirements for a RTG replacement reactor. In general the reactor design should match current RTG's in all aspects and offer improvements in one or more of the following six important areas.

Mass: The mass of the system should be as light as possible with 50-150 kg as an expected range for the entire system. With the radiator, support assembly and heat engine taking ≈½ the mass of the system [6] this means the mass of the reactor and shield combined should be 25-75 kg.

Power: The power of the system should be as high as possible however 500 W_E should be sufficient [the largest probe power supply from Table 2.1: Cassini had 880 W_E at launch but this decayed to 600-700 W_E while in mission around Saturn [30]]. The power should be capable of remaining steady as needed or in temporary reduced mode during portions of the mission.

Time: The system should be capable of maintaining power for >20 years with 100 years as an initial goal. To meet this goal reliability becomes an important issue so the need for moving parts should be minimized [12]. Additionally little to no active control and instrumentation should be needed over the life of the reactor.

Activity Hazard: There should be significant improvement in this area. The reactor should be clean and shut down during launch and maintain orders of magnitude lower Radio-Toxicity than a comparable RTG for the first few years after launch [due to possible swing-by orbits].

Proliferation: The reactor should be designed with less than one critical mass of fissile material in a non-metallic form [preferably chemically bonded to a moderator] to greatly reduce proliferation risk [2 or more devices would needed to obtained sufficient material for a bomb and chemical processing would likewise be needed]. The reactor

should always be subcritical on fast prompt neutrons alone. Additionally the reactor should be non-spherical to make any implosion attempt impractical.

Cost and Availability: The reactor should be designed to use only currently available materials [for example Cm-247 is potentially an excellent fuel [23] but it can only be produced in sub gram quantities]. Given the expensive nature of space systems [the GPHS-RTG cost estimate for New Horizons was $65-90 million [15]] the high cost of less common materials such as beryllium or lithium would not be prohibitive. In particular the system will be designed to be compatible with the Stirling engines already designed for the ASRG for cost and simplicity reasons [22].

Section 4: Is it possible?

A number of design goals were just set and the question now becomes: is it possible to build such a reactor? The answer turns out to be yes, but to demonstrate this, the next few chapters cover specific issues and details of how the design specs can be met.

Chapter 3 covers the neutronics of reactors to determine if it is possible to construct a reactor capable of achieving criticality within the weight limits at sufficient temperature to generate electrical power.

Chapter 4 covers the thermal analysis to determine if the reactor could be cooled without moving parts through conduction alone for reliability.

Chapter 5 covers the core lifetime to determine whether the reactor could maintain criticality through decades of burn-up.

Chapter 6 covers shielding to determine the mass of shielding that would be necessary due to the high energy gamma and neutrons from the reactor.

Chapter 7 covers safety to determine the proliferation risks and ensure that there is low radio-toxicity particularly early in the mission where accidents affecting the earth can occur.

Chapter 8 covers transients to determine the stability of the reactor during transients such as power changes and startup.

References [Chapter 2]

[1] IAEA “The Role of Nuclear Power and Nuclear Propulsion in the Peaceful Exploration of Space” (2005)

[2] R.R. Furlong and E.J. Wahlquist “U.S. Space Missions Using Radioisotope Power Systems” Nuclear News, pp. 26 (1999)

[3] B.R. Davis “Gravitational Lens: Deep Space Probe Design” Air Force Institute of Technology (2011)

[4] Marc Kutner, “Astronomy: a Physical Perspective”, Wiley (1987)

[5] C. Maccone “A New Belt Beyond Kuiper’s: A Belt of Focal Spheres Between 550 and 17.000 AU for SETI and Science” Acta Astronautica, 69, pp. 939 (2011)

[6] L.S. Mason “Realistic Specific Power Expectations for Advanced Radioisotope Power System” Journal of Propulsion and Power, 23, pp. 1075 (2007)

[7] D.I. Poston, et al “A Simple, Low-Power Fission Reactor for Space Exploration Power Systems” Proceedings of Nuclear and Emerging Technologies for Space, Albuquerque, NM (2013)

[8] D. Poston “The Demonstration Using Flattop Fissions (DUFF) Experiment” Los Alamos National Laboratory (2012)

[9] G. Schmidt “SNAP Overview”, ANS DCN: SP-100-XT-002 (2011), http://anstd.ans.org/NETS2011/Documents/Presentations/Opening%20Dinner%20SNAP%2010A%20Schmidt.pdf

[10] S.F. Demuth “SP100 Space Reactor Design” Progress in Nuclear Energy, 42, pp.323 (2003)

[11] George Scmidt, “Nuclear Systems for Space Propulsion and Power”, NASA Glenn Presentation (2010)

[12] D.I. Poston, et al “The DUFF Experiment-What Was Learned?” Proceedings of Nuclear and Emerging Technologies for Space, Albuquerque, NM (2013)

[13] RADIOISOTOPE POWER SYSTEMS – SPACE BATTERIES. U.S. Department of Energy, INL. (2005), http://nuclear.inl.gov/spacenuclear/docs/final72005faqs.pdf

[14] Radioisotope Power Systems: An Imperative for Maintaining U.S. Leadership in Space Exploration http://www.nap.edu/catalog/12653.html

[15] Final Report of the New Horizons II, NASA Review Panel (2005)

[16] D. Albright and K. Kramer “Neptunium 237 and Americium: World Inventories and Proliferation Concerns” (2005)

[17] E.J. Wheelwright “Byproduct Inventories” Pacific Northwest Laboratory (1983), http://www.wmsym.org/archives/1983/V2/21.pdf

[18] N. Kocherove, M. Lammer, and O. Schwerer “Handbook of Nuclear Data for Safeguards” Nuclear Data Section, IAEA (1997)

[19] M. Ragheb “Ch. 3 Radioisotopes Power Production” (2012), https://dmtpc.mit.edu/twiki/pub/Projects/RadioIsotopeBattery/Radioisotopes_Power_Production.pdf

[20] C.W. Forsberg and L.C. Lewis “Uses for Uranium-233: What Should be kept for Future Needs?” (1999)

[21] J.W. Krueger “U-233 Disposition Project Update” (2011), http://www.oakridge.doe.gov/em/ssab/Minutes/FY2011/Presentations/U-233ProjectUpdate.pdf
[22] R.K. Shaltens and W.A. Wong “Advanced Stirling Technology Development at NASA Glenn Research Center” NASA (2007)
[23] Van den Berghe “Evaluation of Nuclear Criticality Safety Data and Limits for Actinides in Transport” (2003)
[24] NASA, “Final Environmental Impact Statement for the Cassini Mission” (1995), http://saturn.jpl.nasa.gov/spacecraft/safety/safetyeis/
[25] G.L. Bennett, et al “Mission of Daring: The General-Purpose Heat Source Radioisotope Thermoelectric Generator” IECEC, San Diego, CA (2006)
[26] U.S. Nuclear Regulatory Commission Regulations: Title 10, Code of Federal Regulations (2012)
[27] National Nuclear Data Center, http://www.nndc.bnl.gov/
[28] J.C. Mark and E. Lyman “Explosive Properties of Reactor-Grade Plutonium” Science and Global Security, 17, pp.170-185 (2009)
[29] T.E. Liolios “The Effects of Nuclear Terrorism: Fizzles” EUROPSIS
[30] “Why the Cassini Cannot Use Solar Arrays” Cassini Public Information Jet Propulsion Laboratory (1996)

Chapter 3: Neutronics

In this chapter the neutronics of reactors is explored to see if a reactor can go critical within the 25-75 kg weight limits at sufficient temperature [650-850°C] to generate electrical power [the temperature limits defined in Chapter 4]. This is explored for several reactor designs which end up being rather comparable. Further, reactor stability is assessed for sensitivity to power changes and poison build-up.

Section 1: Material Selection

The first step of this analysis was to look at the possible materials from which the reactor could be built and then to down select materials.

Fuel: The first fuel selection criterion is that the fuel must be thermally fissile. This was evaluated by running MCNP over all nuclides in the ENDF file [1] to see which ones are thermally critical. This narrowed material selection down to 22 actinides. The next requirement was that the material must be stable over the mission duration. At a minimum this means there should be less than 20% decay over 100 years [max burn-up from Chapter 1], which is the goal for reactor life [from chapter 2]. This corresponds to a half life of at least 232 Years. All nuclides meeting these two requirements are listed in Table 3.1. The next selection criterion is the material availability. U-235 is the only naturally occurring nuclide on the list with the other isotopes requiring transmutation [2]. To look at the availability of the materials, the number of (n,γ) captures necessary to create the material from naturally occurring sources is listed also in Table 3.1.

U-233 and Pu-239 require only a single capture reaction and stockpiles of 100's of kg exist for both of them. Np-236 only requires 3 reactions however the (n,2n) reaction from Np-237 has two significant effects: 1-Significantly smaller quantities exist due to low production efficiency of the fast fluxes necessary and 2-the Np-236 will be mixed with Np-237 requiring Isotope separation for extraction [3]. The Curium and Californium isotopes require a large number of captures and isotope separation and as a result only gram quantities exist. As a result of this only U-233, U-235 and Pu-239 are considered possible fuels.

Table 3.1: Possible Reactor Fuels sorted by Nuclide Mass [4][5][1][6].

Isotope	$\nu\Sigma_F/\Sigma_T$	σ_F [barns]	$T_{½}$ [kYr]	CM [Kg]	# (n,γ) Reactions
U-233	2.3	533	159	15.8	1
U-235	2.1	585	703,960	46.7	0
Np-236	3.0	3,021	153	6.79	3*
Pu-239	2.1	751	24	9.99	1
Cm-245	3.1	2,151	8.5	9.11	7
Cm-247	2.5	112	15,601	6.94	9
Cf-249	3.0	1,640	0.35	5.91	11
Cf-251	2.7	5,326	0.90	4.46	13
PU-238 for reference			0.088	9.49	3

* Np-236 cannot be made with (n,γ) reactions alone. First Np-237 is made via two (n,γ) reactions and then a (n,2n) reaction from a fast flux is necessary to produce Np-236

The fuels will be embedded in a zirconium alloy fuel form [discussed later] for proliferation resistance. This ensures the fuel is chemically mixed with the moderator preventing direct use as a weapon. [This requirement is for non-state actors upon theft of the material will have time constraints due to enforcement pursuit. The delay caused by needing to chemically dissolve the reactor and reform metallic fuel may be significant]

Moderator: Because the reactor is designed as a thermal reactor, a moderator [Moderating Ratio >>1] must be used to thermalize neutrons. The fuel time requirement of a half-life of >232 years will still apply. Moderator's availability is not an issue since all moderators are naturally occurring elements [2]. The moderator requirement will be that the isotope is in naturally occurring elemental form or isotope separation is available [H, He, Li and B only]. This leaves only 12 possible moderators which are listed in Table 3.2.

Table 3.2: Possible Moderators sorted by Moderator Ratio [7][5][1].

Moderator	ξ	σ_s [Barns]	σ_a [Barns]	Ratio $\xi\sigma_s/\sigma_a$	Density [10^{22}/cm^3]	Mod. Power $\xi\Sigma_S$ [cm^{-1}]
He-4	0.425	1.34	0	∞*	1.88**	0.011
H-2	0.725	7.64	5.2×10^{-4}	10,678	5.93***	0.328
O-Element	0.120	4.23	1.9×10^{-4}	2,672	4.29**	0.022
C-Element	0.158	5.55	0.0035	250	11.4***	0.100
H-1	1.000	82.0	0.333	247	5.93***	4.862
Be-9	0.207	7.63	0.0076	207	12.4	0.195
B-11	0.171	5.77	0.0055	180	13.1	0.129
F-Element	0.102	4.02	0.0096	43	4.77**	0.019
Li-7	0.260	1.40	0.045	8.0	4.63	0.017
Ne-Element	0.097	2.63	0.039	6.5	3.63**	0.009
Mg-Element	0.081	3.71	0.063	4.8	4.36	0.013
P-Element	0.063	3.31	0.17	1.2	3.54	0.007

* In practice He-4 will have trace amounts of He-3 which reduces the moderating ratio; it is 76 in naturally occurring helium.

** The atomic densities for gasses are given for liquids at the boiling point at atmospheric pressure.

*** The density for hydrogen is given for hydrogen in solid LiH. It would be 4.89 in U-$ZrH_{1.65}$. For carbon the density of graphite is used, not diamond which would be impractical

The bottom four have moderating ratios <10 which makes them unsuitable moderators in a small reactor [Na-23 which is often used in fast reactors has a moderating ratio of 0.52 [7]]. The small size of the reactor places a premium on slowing down power [$\xi\sigma_s$] and atomic density which should be as large as possible. The product

of these two is moderating power [$\xi\Sigma_S$] which is the best measure of moderator effectiveness in a small reactor [7].

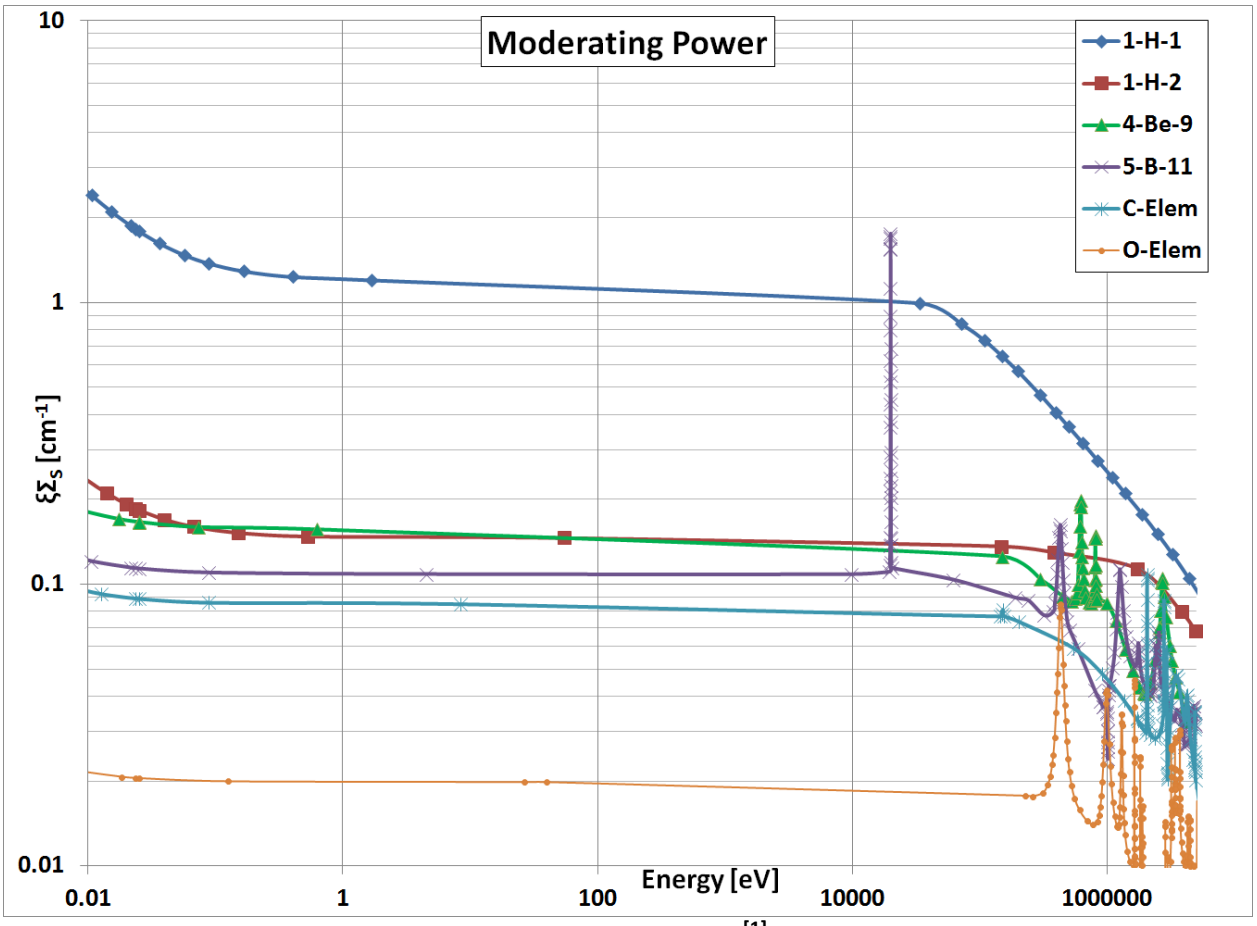

Figure 3.1: Moderator Power from 0.01 eV to 10 MeV [1]. This figure is a graph of moderating power verse neutron energy in a log-log plot.

There is an order of magnitude gap in moderator power between H-1 [$\xi\Sigma_S$=4.86 cm^{-1}] and the next highest nuclide H-2 [$\xi\Sigma_S$=0.33 cm^{-1}] which has otherwise similar physical and chemical properties. In initial MCNP simulations this corresponded to an order of magnitude in reactor mass when using U-233 and as a result deuterium should not be considered an effective moderator in small reactors [25-75 Kg]. While atomic densities for other elements can reach twice that of hydrogen, [e.g. beryllium, boron and carbon], the 50 fold difference in slowing down power means that no other moderator performs close to hydrogen in moderating power. The core will have a radius

of ≈10 cm (≈25 kg and ≈6g/cm^3) and ≈$\mathbf{e}^{17}$ reduction in neutron energy [ln(2MeV/0.1eV)] [7] to thermalize which requires the moderating power to be ≈1.7cm^{-1} [17 decrements in energy in 10 cm]. For completeness the moderating power [for H-1 and the 4 closest elements and oxygen] is shown in Figure 3.1 for energies from 0.01eV to 5 MeV. From Figure 3.1 it should be clear that H-1 is by an order of magnitude better moderator [with H-2 and Be-9 in a distant 2nd place]. As a result, for this work hydrogen was selected as the moderator for the small reactors.

While hydrogen is a great moderator it is not a solid at reactor temperatures [650-850°C] [2]. This requires a survey of high temperature hydrogen compounds. Several lightweight, high density sources of hydrogen are listed below:

1- Water — Critical point 374°C at 220 atmospheres of pressure [8]
2- Polyethylene — Decomposes to CH_4 at 411°C [9]
3- BeH_2 — Decomposes at 250°C [10]
4- $LiBH_4$ — Decomposes at 380°C [11]

If the system was to be pressurized then a pressure vessel would be needed. This would introduce a possible failure mode as well as increase the mass of the system. Due to the high temperature of the reactor [650°C] material creep would be a significant limit on reactor lifetime [See chapter 5]. As a result, a source of hydrogen that does not require high pressures is desired [Pressure ~<10 atmospheres]. Hydrogen compounds were compiled by hydrogen content per mass and then the effect of high temperatures were considered. These compounds either boiled [For example H_2, H_2O, NH_3, CH_4 and light hydrocarbons [8]], hydrogen disassociated [BeH_2, UH_3, $LiAlH_4$ and polyethylene and heavy hydrocarbons [12][13]], were heavy per hydrogen content [CsH SrH_2], had high neutron absorption cross sections [CdH [2]] or a combination of these. Only LiH [14] and interstitial metal hydrides [of which only U-$ZrH_{1.65}$ [15] was found to be practical] were found to retain hydrogen at the desired temperatures and pressure with high hydrogen densities. As a result of this only LiH and U-$ZrH_{1.65}$ were considered as possible moderators.

LiH is a salt that had the best hydrogen retention at low pressure of any of the compounds considered. The partial pressure of hydrogen in LiH is <10 atmospheres up to a temperature of 1120°C and only $8.6x10^{-3}$ atmospheres at melting [688°C] [14]. As a moderator, it will require Li-7 since Li-6 is a poison but kilogram quantities of Li-7 are available [1]. LiH has a large temperature coefficient of expansion of $253x10^{-6}$/°C at 650°C [14] [For comparison, this is smaller than water 2330 $x10^{-6}$/°C at 280°C and 15 MPa, but much larger than UO_2 at 1500°C found in LWR's]. Additionally LiH melts at 688°C and expands in volume by 16%. LiH has a low density of 0.707 g/cm^3 at 650°C making it very lightweight for the amount of hydrogen retained which is useful to keep mass low [14]. Above 600°C LiH is will not retain any radiation damage and is quite soft [ultimate tensile strength is down to 2.4 ksi by 425°C and below 350 psi by 475°C]. LiH is chemically very reactive and will explode in water and slowly reacts with air [14] but neither of these are significant issues in the vacuum of space.

U-$ZrH_{1.65}$ is a commercially produced reactor fuel that contains significant hydrogen with the fuel. 1.65 hydrogen atoms is the highest loading per zirconium atom possible while remaining stable [δ phase $ZrH_{1.65}$] [15]. Additionally uranium loading can be as high as 45 weight%. The hydrogen retention is not as high as in LiH with partial pressures of 1, 2, 3, 5 and 10 atmospheres at 770, 825, 845, 880 and 930°C respectively [15]. The temperature coefficient of expansion is $63x10^{-6}$/°C at 650°C and does not melt until >1100°C [after it off gasses the hydrogen] [16]. Six SNAP reactors used U-$ZrH_{1.65}$ with a centerline fuel temperature at 850°C [15]. U-$ZrH_{1.65}$ has a high density of 8.02 g/cm^3 at 650°C but the mass includes 45% Uranium making the effective hydride density a more reasonable 4.4 g/cm^3 [still much larger than LiH]. The effect of radiation on $ZrH_{1.65}$ is well characterized and the SNAP reactors showed no significant effects to their peak burn-up of 2.1 GWD/MTHM [see Chapter 5].

Table 3.3: Possible Reflectors sorted by Σ_{TR-S} [7][5][1].

Moderator	σ_s [Barns]	σ_a [Barns]	$1-\mu_0$	Ratio σ_s/σ_a	Density [10^{22}/cm^3]	Σ_{TR-S} [cm^{-1}]
H-1	82.0	0.333	0.333	247	5.93***	1.62
Be-9	7.63	0.0076	0.926	1,004	12.4	0.874
B-11	5.77	0.0055	0.939	1,049	13.1	0.710
C-Element	5.55	0.0035	0.944	1,586	11.4	0.596
H-2	7.64	5.2×10^{-4}	0.667	14,721	5.93***	0.302
F- Element	4.02	0.0096	0.965	419	4.77**	0.185
O-Element	4.23	1.9×10^{-4}	0.958	22,274	4.29**	0.174
He-4	1.34	0	0.833	∞*	1.88**	0.021

* 179 in elemental He. */**/*** See table 3.2

Reflector: The reflector has similar availability and material requirements as the moderator. The two key differences are: 1-the reflector does not need to slow the neutron down [ξ is of secondary importance] and 2-the average scattering angle is now significant since the neutrons need to change direction in reflection [need $(1-\mu_0)$ large, where μ_0 is the average cosine of the scattering angle with $\mu_0 \approx 2/3A$ with A=atomic mass [7]]. The determination of suitable reflectors will proceed similarly to the determination of moderators with $(1-\mu_0)$ substituted for ξ. The ratio of σ_s/σ_a was used to ensure the reflector is not highly absorbing with only 8 materials having $\sigma_s/\sigma_a>100$ which are listed in Table 3.3.

The small size of the reactor places a premium on cross section [σ_s], reflection angle [$1-\mu_0$] and atomic density which are combined to make reflecting power [$(1-\mu_0)\Sigma_s$]. This parameter should be as large as possible. Thus the reflection power will nearly equal the transport cross section since $\sigma_a/\sigma_s<0.01$. As a result reflector power is labeled Σ_{TR-S}. This is shown in Equation 3.1. Next Σ_{TR-S} is plotted for the 8 reflectors vs. energy in Figure 3.2 for energies from 0.1eV to 5 MeV.

$$\boldsymbol{\Sigma_{TR} = \Sigma_T - \mu_0\Sigma_S = \Sigma_S\left(1-\mu_0+\frac{\sigma_a}{\sigma_S}\right) \approx \Sigma_S(1-\mu_0) = \Sigma_{TR-S}} \qquad \text{Equation 3.1}$$

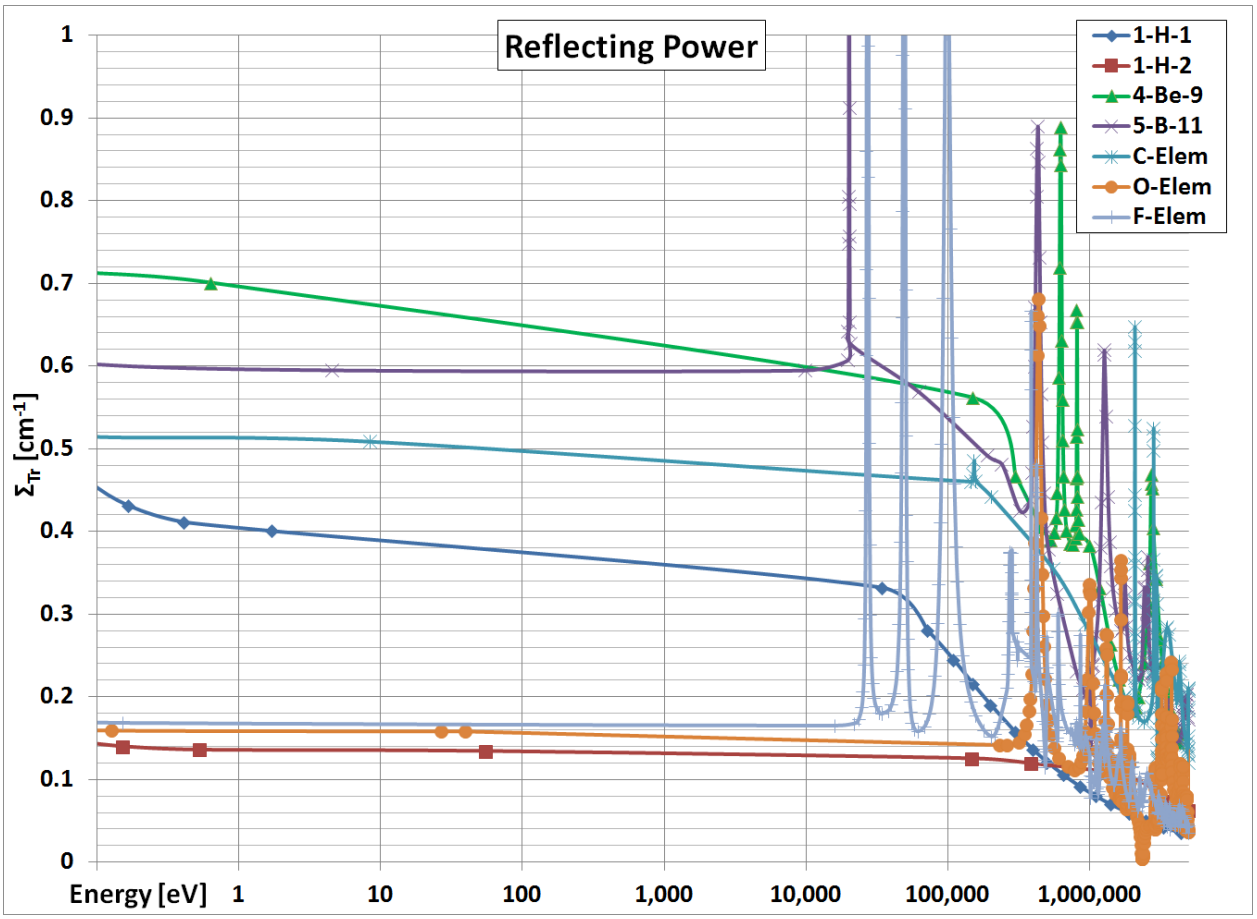

Figure 3.2: Reflecting Power from 0.1 eV to 5 MeV [1]. This figure is a graph of reflecting power verse neutron energy in a linear-log plot.

From Figure 3.2 there are four reflectors that stand out: hydrogen, beryllium, boron and carbon. Beryllium has the highest reflecting power. Boron is next [≈85% of beryllium] but has two significant drawbacks: 1-isotopic enrichment is needed to remove B-10 which is a strong poison [B-11 is commercially available] which is costly and 2-the thermal conductivity is an order of magnitude less than beryllium [8] [the importance of which is discussed in chapter 4]. Next is carbon [73% of beryllium] but it has lower thermal conductivity, 23% higher density resulting in higher mass [8] and is a less effective moderator. Finally hydrogen [57% of beryllium] has the duel use of being both a reflector and a great moderator but has two disadvantages: 1- Hydrogen has no resonance region greatly reducing reflecting power at the high energy of the fission

spectrum [0.2-5 MeV] and 2- Low thermal conductivity of LiH which was the only high temperature form of hydrogen without fuel [the reflector should defect neutrons back to the fuel not away from it]. As a result beryllium was selected as the reflector material for small reactors.

Beryllium is a light weight metal [1.85 g/cm^3 [8]] with high thermal conductivity [95.2 W/m°K at 700°C [17]] and a melting point [1,287°C [8]] well above reactor temperatures. Beryllium is rigid at 700°C, the tensile strength is 23.2 ksi and the bulk modulus is 37.5x10^3 ksi, and as a result the beryllium reflector can also provide structural support [17]. Beryllium is currently used in many aerospace and nuclear applications and due to its ability to tolerate radiation damage [covered in more detail in Chapter 5] and has high transparency for X-Rays and gamma rays [1].

Section 2: Many Similar Systems

With the materials that the reactor is to be constructed a reduced trade space of the [3 fuels, 2 moderator materials and 1 reflector] the next task is to determine the construction of the reactor.

Methods: A method to model the neutronics of the system is needed. A Monte Carlo method were chosen for two reasons: 1- The small size of the reactor means the whole reactor is within a few mean free paths of a boundary and as a result diffusive methods should not be used. 2- The small size of the reactor means that a smaller number of particles are needed to sample all the features of the core, thereby allowing for faster computations. The Monte Carlo code chosen for the neutronics analysis is MCNPX which is widely used and has been extensively tested [18].

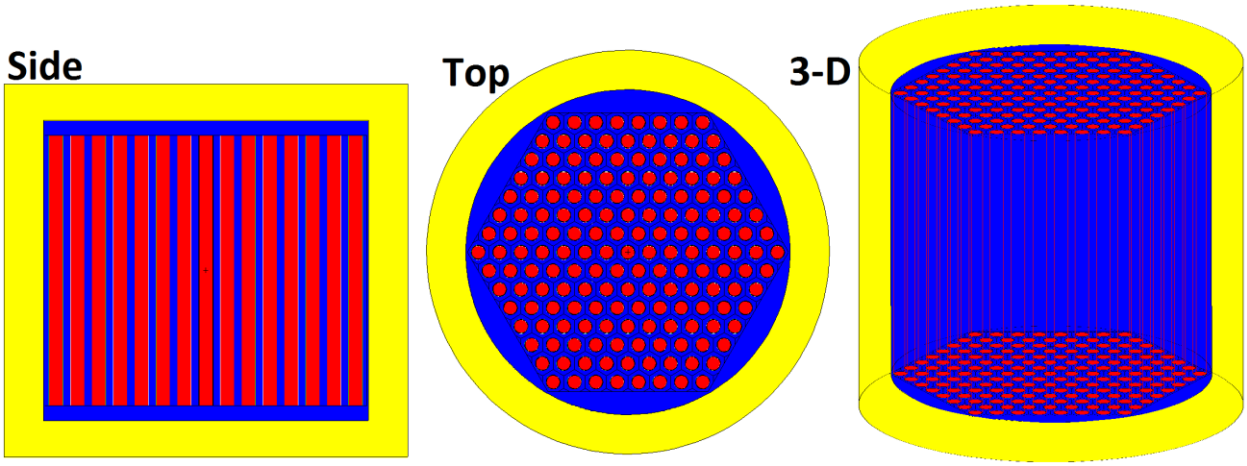

Figure 3.3: Example Reactor top, side and 3-D view cross sections. This is a representative reactor [Model B from Figure 3.5]. The reactor is cylindrical in construction with a hexagonal array of homogenous U-233 $ZrH_{1.65}$ fuel pins [Red] surrounded by the LiH moderator [Blue] with an outer beryllium reflector [Yellow]. A thin steel cladding surrounded each pin [Green] but is too thin to be visible in the figure above. The figure above represents final optimized configuration.

A wide array of reactor shapes and compositions were explored to determine the lowest mass configuration. The goal here was to minimize the mass of a reactor while

maintaining criticality. To illustrate the methodology, the design of one example model will be discussed [see Figure 3.3 and 3.4]

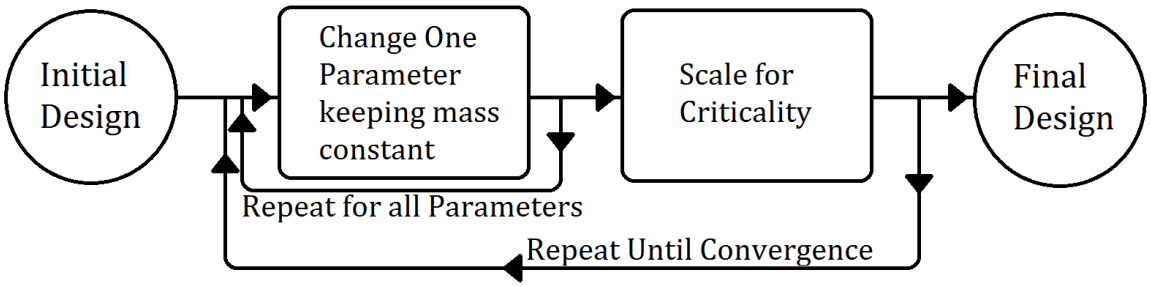

Figure 3.4: Optimization Flow Chart. This is a representation of the method used to optimize the reactor design for mass while maintain criticality.

To optimize this system [as low of a mass as possible while maintaining criticality] a large number of MCNP runs were required as there are a large number of parameters to adjust. Among these were:

1- Fuel number of pins, diameter, length
2- Moderator pin separation, top and side thickness
3- Reflector top and side thickness

To automate the large number of MCNP runs, a Matlab routine was created to run through the combinations [after several were validated manually]. For the model, one parameter at a time was adjusted; the resulting system [kept at constant mass by scaling the parameters] was run through MCNP and the system reactivity was then used to evaluate the effect. A quadratic polynomial of reactivity for each parameter was created and the resultant peak reactivity point was used to set the parameter. The Matlab routine then cycled though the set of parameters for the system to converge [the system was considered converged when all parameters change by <1% from one cycle to the next, minimum of 2 cycles]. Between each cycle of parameters the whole system was scaled to maintain criticality [+/- 0.1%] by adjusting the system size. The system is optimized when the mass could no longer be reduced. This method is depicted schematically in Figure 3.4.

On occasion some parameters had to be fixed manually. For example the number of fuel pins increased without bound. As a result the number of pins was fixed at 169 [8 pins hex array] to limit complexity in Fig 3.3 example. Additionally all shapes were fixed with a flat top and bottom for heat transfer to the heat engine. Complex shapes were avoided with most components rectangular, hexagonal cylindrical or spherical.

For the given example, the reactor mass was determined to be 25.1 kg with an outer radius of 12.82 cm and a height of 23.68 cm. The fuel pins used U-233 and had a radius of 4.38 mm and were 17.15 cm long. The reflector was 2.50 cm thick on the side and 2.31 thick on top/bottom and 0.96 cm of moderator between the rods and reflector on the top and bottom.

Masses: With the exception of the fuel type [discussed in the next section] most of the optimized systems investigated resulted in very similar masses. Six examples are shown in Figure 3.5.

In general the spherical systems had slightly lower mass, since the sphere optimizes volume to surface area [19], but the effect was only a few percentage points difference from the cylindrical designs [compare Model C and E masses; 3% difference]. Due to proliferation issues associated with spherical designs, they were excluded from further consideration. Likewise metal fuel showed no benefit compared to hydride fuels but resulted in significantly larger fuel mass [compare Model A and B; similar total mass but A requires 2.56x more U-233 than B]. The associated proliferation issues of higher fuel mass and no chemically bonded moderator meant metallic fuels were also unacceptable and thus were excluded from consideration as well.

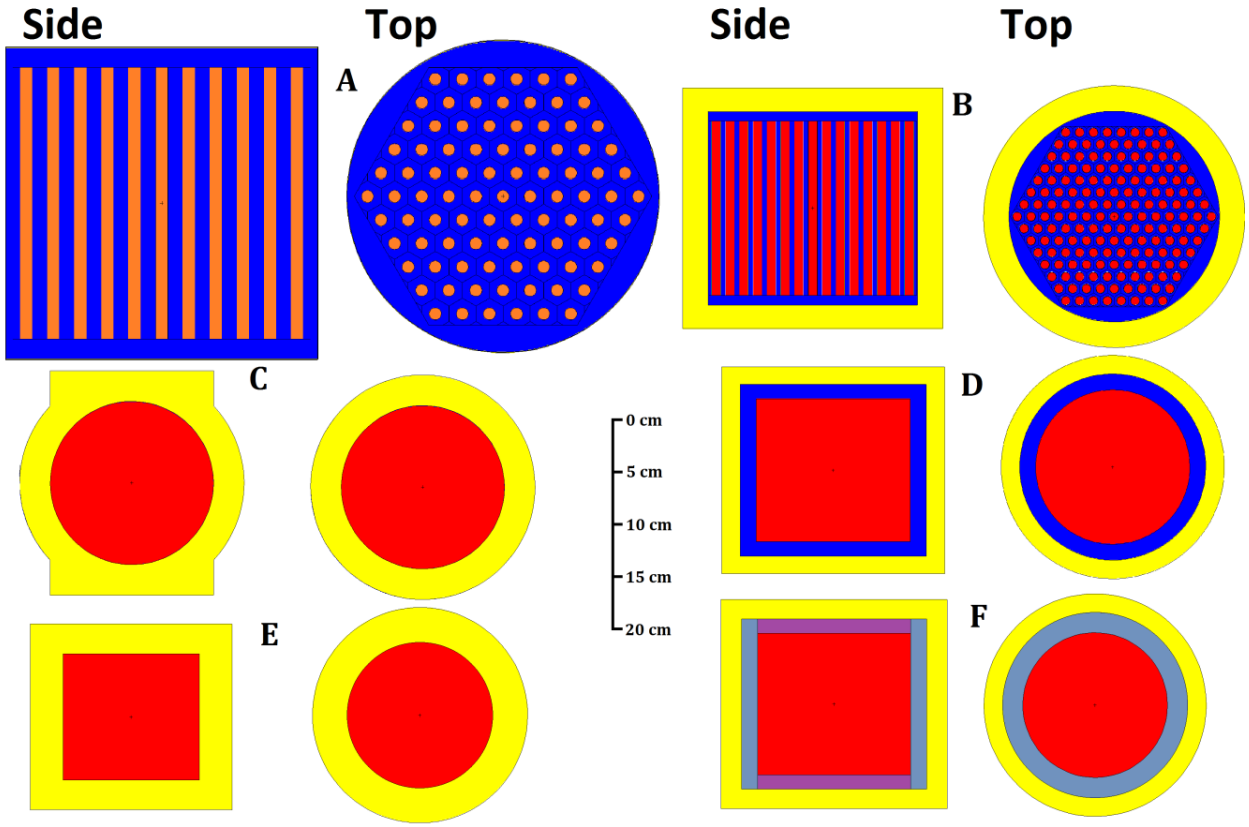

Figure 3.5: Several optimized reactors, top and side cut views. U-233 $ZrH_{1.65}$ fuel pins [Red], LiH moderator [Blue], beryllium reflector [Yellow], U-233 metal [Orange], Be/LiH plates [Purple and light blue] and steel [Green]. The steel is too thin to be visible in the figure above.

Table 3.4: Several optimized reactors masses by design [kg].

Reactor	Total	U-233	$ZrH_{1.65}$	LiH	Be	Steel
A	25.6	15.5	-	7.58	-	2.55
B	25.1	6.05	7.40	3.22	7.79	0.64
C	25.0	7.88	9.62	-	7.51	-
D	26.2	8.73	10.7	1.24	5.54	-
E	25.8	7.67	9.38	-	8.70	-
F	27.0	8.69	10.61	1.13	6.59	-

Fuel Selection: The one parameter that had considerable effect on system mass was the fuel selection. To illustrate the effect of fuel selection the critical mass parameters for one representative model [model D from fig 3.5] is presented in Table

3.5. All three fuels are shown as well as a chosen selection of lower enrichment possibilities.

First it should be noted that Pu-239 as a fuel for a thermal reactor requires greater than 1 bare critical mass. This is due to Pu-239 being a better fast fuel [in weapons] than a thermal fuel [reactors] [4]. For proliferation reasons Pu-239 was therefore removed as a possible fuel [Pu-239 reactors also have a higher mass than U-233, a substantially shorter life and have a fission resonance peak at 0.2-0.4eV which is 2600-4900°C] [1].

Table 3.5: Several optimized reactors masses by fuel [kg].

Fuel	Radius [cm]	Total Mass	Fuel Mass	Critical Mass [6]	% Critical Mass
Pu-239	12.19	**37.95**	12.66	9.99	127%
U-233	10.77	**26.18**	8.73	15.8	55%
U-235	14.07	**58.35**	19.46	46.7	42%
20% U-235 LEU	19.97	**166.8**	55.64	746	7.5%
12% U-233 LEU	17.12	**105.2**	35.08	681	5.2%
32% U-233 MEU	14.06	**58.19**	19.41	122	16%

The parameters shown above are for the type D reactor in figure 3.4. The total mass and fuel mass are from this optimization study. Critical masses are the bare critical masses. For comparative purposes the moderator and cladding thicknesses are fixed at their U-233 value.

Second U-233 and U-235 have similar performance relative to their critical masses and proliferation but U-233 reactors are substantially lighter. For low enriched fuel [20%U-235 or 12% U-233 [20]], U-233 has both a lower mass and is a smaller fraction of the critical mass. At a moderate enrichment of 32% U-233 will perform as well as 100% enriched U-235 in terms of reactor mass and has a much larger critical mass [20] [122 kg vs. 46.7 for U-235].

Finally, low enriched fuels are not an attractive option. U-233 LEU requires a mass of 105 kg which is above the goal of 25-75 Kg [from Chapter 2 which includes

shielding]. Moderate enrichments can be used to reduce proliferation risk at a cost of increased mass. However, since the reactor fuel mass is already well below the critical mass the additional effects of a further decrease are less significant. As a result only high enriched fuels are considered. For these reasons U-233 is selected as the fuel of choice and will be the only fuel considered further.

No Standout. After modeling dozens of systems there was no clear optimum configuration. In part, this is due to the fact that all the reactors used the same fuel, moderator and reflector [U-233 in $ZrH_{1.65}$, LiH and Be] and that hydrogen has similar reflective properties as beryllium. For the optimized designs, the amount of U-233 varied from 5 to 10 kg but the total reactor mass remained at around 25 kg.

Many of the follow on studies was done for only a selected subset of the models [some were not used beyond critical mass calculations as they were relatively heavy]. For some of the analysis in later chapters, only Model F of figure 3.4 is used [or slight variations]. This does not mean that model F is the only possible design but rather is a representative model that was selected for further refinement. A key driver for the selection of Model F was the heat transfer analysis of Chapter 4.

Section 3: Transients and stability

The next step involved determining the transient parameters such as delayed neutrons, the temperature coefficient of reactivity, and the power coefficient of reactivity. These are then used to examine the stability of the reactor system. The temperature and power coefficients of reactivity should be negative for stability and the delayed neutron fraction represents the margin to prompt criticality, which should be avoided in reactors [7].

Delayed Neutrons: The thermal delayed neutron fraction for U-233 is smaller than U-235 and is comparable to Pu-239 [7]. This is shown in Table 3.6. The smaller fraction of delayed neutrons will reduce the size of allowed transients to ensure reactivity stays below prompt super-critical. MCNP was used to evaluate the effective delayed fraction since the energy spectrum of delayed neutrons is slightly lower than prompt neutrons. The effective delayed fraction was (0.312±0.028)% which limits reactivity transients to less than this amount [for later calculations the delayed neutron fraction is taken to be 0.2674% ΔK/K≡1$ reactivity].

Table 3.6: Neutrons per thermal fission and delayed fraction [4].

Fuel	Total Neutron /Fission	Delayed Neutron /Fission	Delayed fraction	λ_{EFF} [sec^{-1}]
U-233	2.49	0.0067	0.27%	0.075
U-235	2.43	0.0166	0.68%	0.088
Pu-239	2.88	0.0065	0.23%	0.072

Temperature: Temperature and power interact to change reactivity [power will change the temperature gradient] but these will be divided into two nearly separate effects. The temperature coefficient of reactivity [α_T] is the change in reactivity that

occurs as the entire reactor changes temperature at zero power. Power reactivity represents the effect of an increase of power on reactivity at a fixed heat sink temperature.

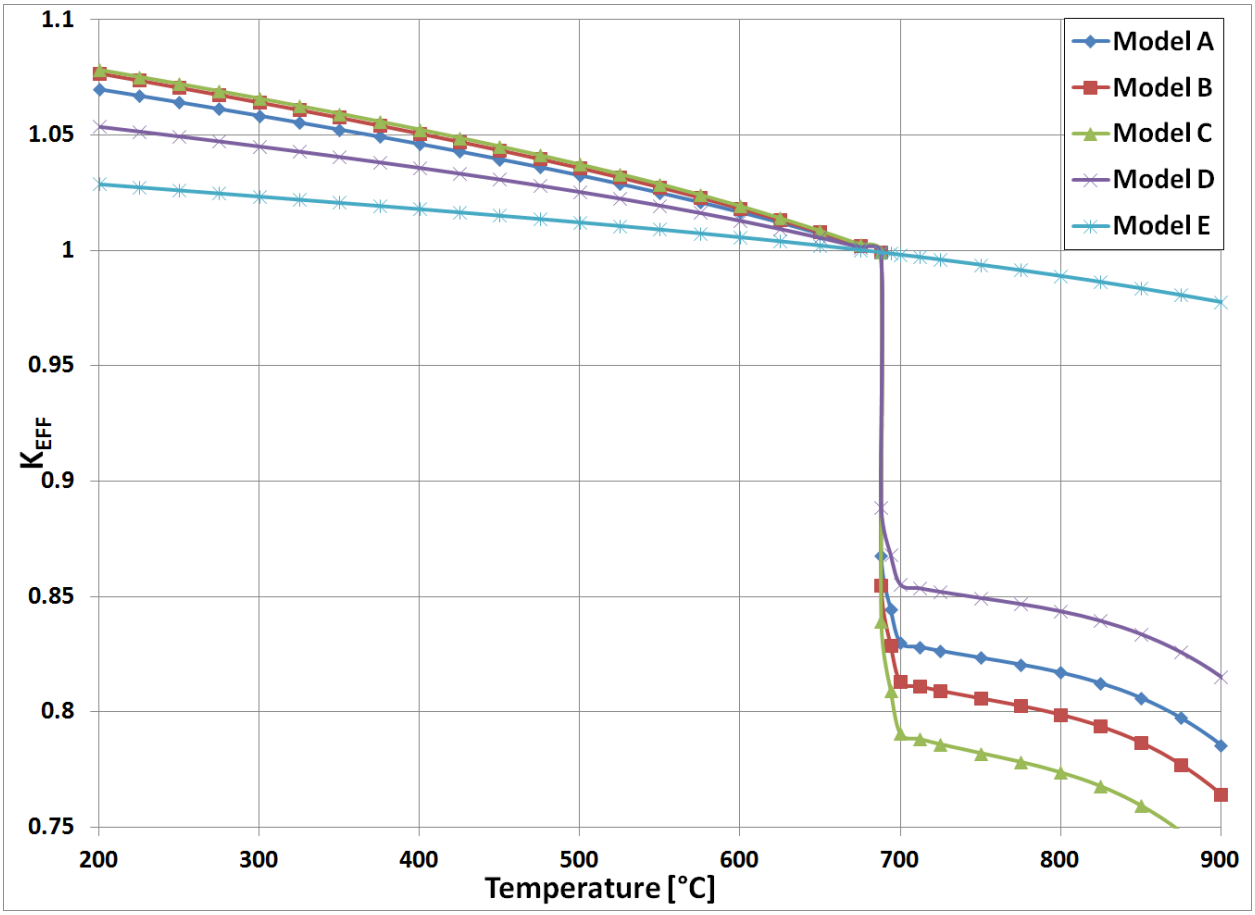

Figure 3.6: Effect of temperature on reactivity. This is a plot of core reactivity verse temperature. The model lettering here does not correspond with Figure 3.4 above. To compare with Figure 3.5, Figure 3.6 [C,A,D,E] match with figure 3.4 [B,D,F,E] respectively. Model B here is not shown in figure 3.5.

As the temperature changes there will be two main effects:

1-the density of the system will change. In these systems, the rise in temperature will cause the materials to expand. The model systems used were designed to fit together at 688°C [the melting temperature of LiH] and be exactly critical. For temperatures below this the reflector and fuel are allowed to contract with the LiH

filling in the space between them with some void formation [LiH has a larger thermal coefficient of expansion than the fuel or reflector]. At higher temperatures the fuel and reflector expand, but the melting of the LiH will cause the reflector to expand axially along the centerline to accommodate the increased LiH volume.

2-The thermal neutron energy will change affecting the effective cross section of reactor materials [Doppler effect]. This is modeled in MCNP [using the TMP and MT commands [21]] to reflect the change in reactivity with temperature.

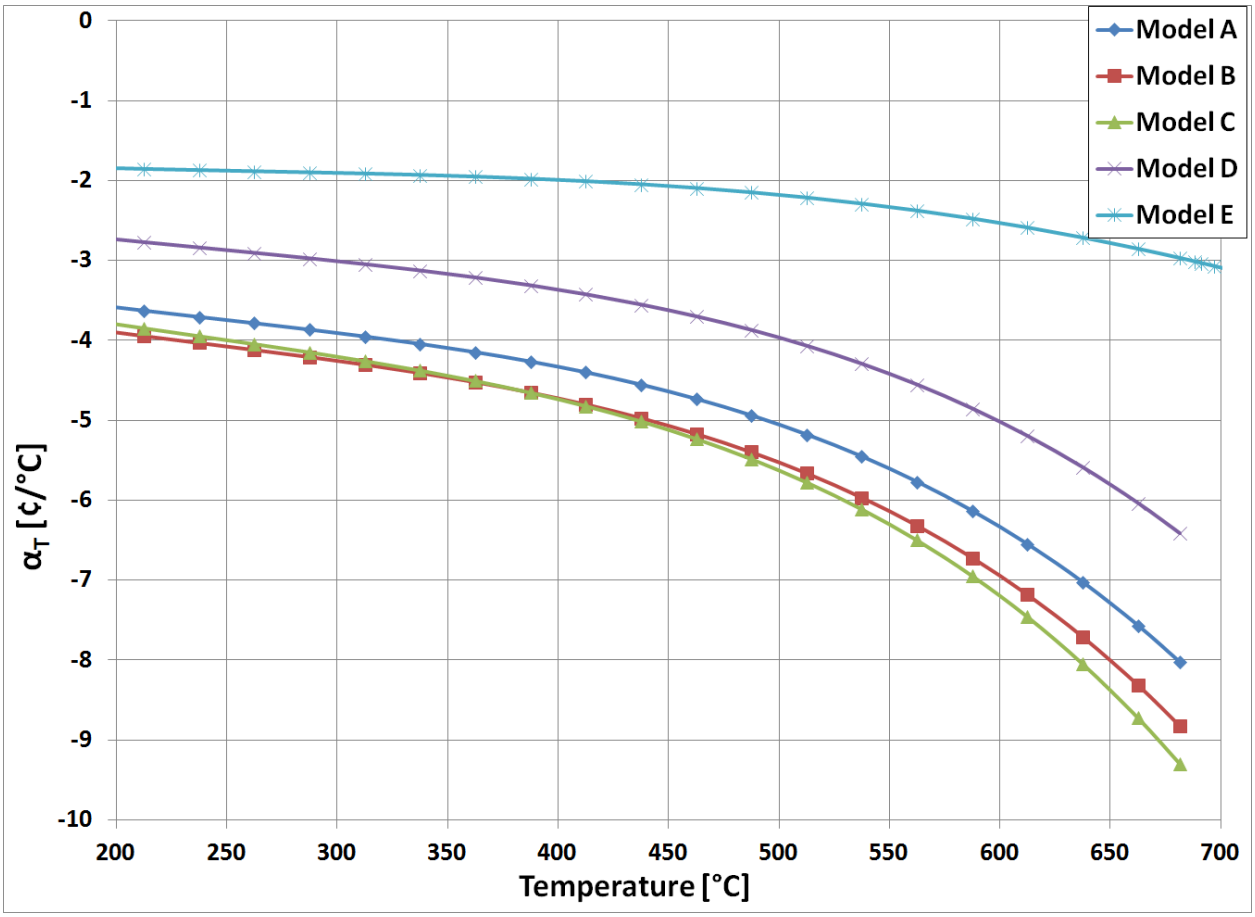

Figure 3.7: Temperature coefficient of reactivity. This is a plot of core temperature coefficient of reactivity verse temperature [the slope of Figure 3.6]. The model lettering here does not correspond with Figure 3.4 above. To compare with Figure 3.5, Figure 3.6 [C,A,D,E] match with figure 3.4 [B,D,F,E] respectively. Model B here is not shown in figure 3.5.

Several of the models were run in MCNP at many temperatures and the resultant reactivity is plotted as a function of temperature in Figure 3.6. The slope of the line is the temperature coefficient of reactivity [α_T] and is shown in Figure 3.7. Model E of Figure 3.5 does not use LiH and as a result there is no sharp drop in reactivity at the melting point of LiH, additionally α_T is smaller since there is less expansion in the fuel and reflector than in LiH.

For reference reactor, α_T is -6.42¢/°C or -1.71×10^{-4} ΔK/K-°C at 680°C which is close to the value found in most commercial LWR. The drop in reactivity at 688°C is 46.1$ or 0.123 ΔK/K [46¢ or 12×10^{-4} ΔK/K for each 1% of the LiH melting].

Power Change: Power reactivity will be the effect of an increase of power with a fixed heat sink temperature. To determine the power reactivity, the temperature gradient across the core is needed. This is described in Chapter 4 and will not be repeated here. MCNP was run with both the flat temperature profile and the full power temperature profile [simplified as several small step changes in temperature for MCNP] with the difference being the change in reactivity. The result was a change of 0.0077 ΔK/K or 2.89$ of reactivity [2.89¢/% power] at 640°C. This equates to a temperature change of 37.2°C between zero and full power [which matches expectations, the Be heats up ≈0-20°C, the LiH heats up ≈6-36°C and the fuel heats up ≈25-100°C]. This means that for the reactor that is critical at 677.2°C at zero power will be critical at 640°C at full power.

Xenon and Samarium: Associated with power changes in reactors is the buildup of the fission products Xe-135 and Sm-149 whose large cross sections can change the reactivity of the core leading to large swings in temperature [7]. However, the low power level that our core operates at and the large fission cross sections of the U-233 fuel lower the flux of the core well below that of commercial reactors [22]. This means that I-

135 [$T_{½}$=6.58 Hr], Xe-135 [$T_{½}$=9.17 Hr] and Pm-149[$T_{½}$=2.21 Days] decay times [2] are much smaller than the absorption lifetimes of Xe-135 and Sm-149.

MCNP was run using the BURN module in an attempt to observe the effect of Xe-135 but the effect was smaller than the margin of error in the Monte Carlo code [the effect of Sm-149 is however visible and will be addressed in Chapter 5]. As a result analytical analysis [7] is used to estimate the magnitude of the effect. First, the thermal flux is approximated by Equation 3.2 which can be used in Equation 3.3 to approximate the steady state change in reactivity from Xe-135 build-up.

$$\boldsymbol{\phi_{TH} \approx \left(\frac{P}{M}\right)_{Fuel} m_{Fuel} / \sigma_F E_{Fiss}} \qquad \text{Equation 3.2}$$

$$\boldsymbol{\Delta\rho_{SS}^{Xe} \approx -\frac{\sigma_A^{Xe}(\gamma^{Xe}+\gamma^{I})\phi_{TH}}{\upsilon(\sigma_A^{Xe}\phi_{TH}+\lambda^{Xe})}} \qquad \text{Equation 3.3}$$

The transient effect of Xe-135 is complex since both Xe-135 and its precursor I-135 decay. In this case the buildup of xenon after a power down will only occur if Equation 3.4 is met

$$\boldsymbol{\phi_{TH} > \frac{\gamma^{Xe}\lambda^{Xe}}{\gamma^{I}\sigma_A^{Xe}}} \qquad \text{Equation 3.4}$$

The results are summarized in Table 3.7. The reactivity swing will be ~½¢ which corresponds to temperature change of 1/15th of a °C which is negligible. Additionally equation 3.4 is not satisfied so that no transient Xe-135 reactivity swing occurs.

Table 3.7: Xenon reactivity magnitude [7].

	$(P/M)_{FUEL}$ [KW/Kg]	ϕ_{TH} [1/cm^2-s]	$\Delta\rho_{SS}^{Xe}$	$\frac{\gamma^{Xe}\lambda^{Xe}}{\gamma^{I}\sigma_A^{Xe}}$
Space	0.2	4.79x10^9	-0.55¢	2.27x10^{12}
LWR [22]	38	2.77x10^{13}	-3.08$	2.91x10^{11}

Since samarium does not decay [Stable → λ^{Sm}=0], Equation 3.4 for samarium is considerably simpler [ϕ_{TH} >0] and is always met. As a result the transient swings will need to be included. The magnitude of this will be reactivity effect of all the Pm-149 changing to Sm-149 [see Equation 3.5]. For the space reactor this is 1.40x10^{-7}ΔK/K or 0.0052¢ reactivity which is insignificant.

$$\boldsymbol{\Delta\rho_{Tr}^{Sm} \approx -\frac{\sigma_A^{Sm}\gamma^{Pm}\phi_{TH}}{\upsilon\lambda^{Pm}}} \qquad \text{Equation 3.5}$$

Likewise the equation corresponding to Equation 3.3 is considerably simpler Equation 3.6. The steady state reactivity is constant. The 1.095$ of reactivity is significant and must be accounted for. It is possible to preload the core with equilibrium Sm-149 which will be discussed in Chapter 5 [2.1g of elemental samarium per kg U-233].

$$\boldsymbol{\Delta\rho_{SS}^{Sm} \approx -\frac{\gamma^{Pm}}{\upsilon} = 0.00311\frac{\Delta K}{K} = 1.095\$} \qquad \text{Equation 3.6}$$

The final question is how long will it take for Equilibrium Sm-149 to build up. The characteristic time is given by equation 3.7 [assuming equilibrium Pm-149 exists which takes a ~5 half-lives or ~11 days].

$$\boldsymbol{\tau^{Sm} = (\sigma_A^{Sm}\phi_{TH})^{-1}} \qquad \text{Equation 3.7}$$

This buildup time is 165.5 years. Because this borders on the lifetime of the core, the question of preloading the core with equilibrium Sm-149 is addressed in Chapter 5 which covers core life.

Section 4: Summary

The core can be made to go critical within the weight limit and with the selection of chosen materials [U-233 in $ZrH_{1.65}$, LiH and Be] the weight would be ≈25 kg. The core can posses a strong negative temperature and power coefficients of reactivity for stability and xenon and samarium will have insignificant transient effects.

References [Chapter 3]

[1] National Nuclear Data Center, http://www.nndc.bnl.gov/
[2] Edward Baum, “Nuclides and Isotopes: Chart of the Nuclides”, Lockheed Martin (2009)
[3] D. Albright and K. Kramer “Neptunium 237 and Americium: World Inventories and Proliferation Concerns” (2005)
[4] N. Kocherove, M. Lammer, and O. Schwerer “Handbook of Nuclear Data for Safeguards” Nuclear Data Section, IAEA (1997)
[5] Neutron Scattering Lengths and Cross Sections, NIST Data, ATI (2001)
[6] Van den Berghe “Evaluation of Nuclear Criticality Safety Data and Limits for Actinides in Transport” (2003)
[7] J.J. Duderstadt and L.J. Hamilton, “Nuclear Reactor Analysis”, John Wiley & Sons Inc (1975)
[8] David Lide, “CRC Handbook of Chemistry and Physics”, CRC Press (2001)
[9] Y. Tsuchiya and K. Sumi “Thermal Decomposition Products of Polyethylene” reprinted from Journal of Polymer Science, 6, (1968), National Research Council of Canada (1968)
[10] G.J. Brendel, E.M. Marleet, and L.M. Niebylski “Crystalline Beryllium Hydride” Inorganic Chemistry, 17, pp. 3589 (1978)
[11] Kamienski, “Lithium and Lithium Compounds” Kirk-Othmer Encyclopedia of Chemical Technology (2004)
[12] Zaluska, L. Zaluski, and J.O. Ström-Olsen “Lithium-beryllium Hydrides: the Lightest Reversible Metal Hydrides” Journal of Alloys and Compounds, 307, pp. 157 (2000)
[13] P.E. Barry, et al “Reaction of LiH and BeH2” Journal of Nuclear Materials, 173, pp. 142 (1990)
[14] R.L. Smith and J.W. Miser “Compilation of the Properties of Lithium Hydride” Lewis Research Center, Cleveland, OH (1962)
[15] D. Olander, et al “Uranium-Zirconium Hydride Fuel Properties” Nuclear Engineering and Design, 239, pp. 1406 (2009)
[16] S. Yamanaka, et al “Thermal Properties of Zirconium Hydride” Journal of Nuclear Materials, 294, p. 94 (2001)
[17] “Beryllium Properties”, Advanced Energy Technology Group (2012) http://aries.ucsd.edu/LIB/PROPS/PANOS/be.html
[18] R. Brewer “Criticality Calculations with MCNP5TM: A Primer” (2009)
[19] Michael Greenburg, “Advanced Engineering Mathematics”, Prentice Hall (1998)
[20] C.W. Forsberg, et al “Definition of Weapons-Usable Uranium-233” (1998)
[21] Denise Pelowitz, “MCNP User Manual”, Los Alamos (2008)
[22] “The Westinghouse PWR Nuclear Power Plant”, Westinghouse (2006)

Chapter 4: Thermal Analysis

In this chapter, the heat transfer within the reactor is explored to determine if the design reactor can be operated within the thermal limits without moving parts. In this regard cooling is to be achieved by thermal conduction instead of moving parts to improve reliability.

Section 1: Thermal Limits

Fuel Thermal Properties: The thermal conductivity [k] of U-ZrH_{2-X} has been measured to be 18±1 W/m°K [1][2] for a wide range of uranium and hydrogen loadings [3]. For $U_{[45w\%]}$-$ZrH_{1.65}$ the theoretical predicted thermal conductivity is $\approx 17.6-3.1\times10^{-3}(T_{[°C]}-650)$ W/m°K [2] over the range of reactor temperatures [500-930°C]. The thermal coefficient of expansion is $7.4\times10^{-6}\times(1+0.002T_{[°K]})$ $°K^{-1}$ at reactor temperatures [1] and a heat capacity $32.85+0.0362\ T_{[°C]}-1.24\times10^{6}/\ T^{2}_{[°K]}$ J/mole-°K at reactor temperatures [2].

A temperature limit for the fuel has to be set to prevent significant hydrogen out gassing, which would otherwise irreparably damage the core. In the range of reactor temperatures [500-930°C], the hydrogen partial pressure is $1.25\times10^{-5}\ e^{0.0146\ T[°C]}$ atmospheres [1]. To prevent hydrogen migration in a core operating for ~100 years the central temperature should be kept under 770°C [1 atm partial pressure] in steady state reactor operation. For short duration transients [minutes to hours] the temperature may briefly exceed this limit up to 930°C at which the hydrogen pressure is expected to reach 10 Atm and may damage the vessel [see Chapter 5]. It should be noted that the SNAP reactors operated with a centerline temperature of 850°C [3 Atm] [1] but had a pressurized core and reactor vessel [4]. If the mission duration ranges between 10-30

years, then a higher temperature of 850-930°C may be permissible, particularly if a cladding is used to limit hydrogen migration.

LiH Thermal Properties: The thermal conductivity of LiH has been measured for both crystals and amorphous compacts from 0-600 °C and this has been extrapolated to the melting temperature at 688°C [5]. In addition, the thermal conductivity of liquid LiH has been measured [~½ that of solid LiH]. The best fit line for thermal conductivity is $3.97-2.3x10^{-3}(T_{[°C]}-650)$ W/m°K [5] over the range of reactor temperatures for solid compacts [500-688°C]. The thermal coefficient of expansion is $84.5x10^{-6}$ $+0.14(T_{[°C]}-650)$ $°K^{-1}$ at reactor temperatures and a heat capacity $60.67+0.0482$ $(T_{[°C]}-650)$ J/mole-°K at reactor temperatures [5].

The temperature limit for the LiH will be the melting point at 688.7°C [6]. While there will be expansion room for partial melting [10%], complete melting of the LiH will rupture the core. This is used to set a hard temperature limit on the reactor.

Beryllium Thermal Properties: The thermal conductivity of beryllium is excellent and is well characterized over the entire reactor range [7]. This thermal conductivity is $2.36x10^{-10}(T_{[°C]}-650)^4-1.37$ $x10^{-7}(T_{[°C]}-650)^3$ + 1.70 $x10^{-5}(T_{[°C]}-650)^2$ - 4.26 $x10^{-2}(T_{[°C]}-650)$ + 97.3 W/m°K [7]. This is 25x better than LiH and 5x better than U-$ZrH_{1.65}$ making beryllium the preferred heat transfer conduit. The thermal coefficient of expansion is $16.5x10^{-6}$ $(1+ 3.62x10^{-4}(T_{[°C]}-650)$ $-1.81x10^{-7}(T_{[°C]}-650)^2)$ $°K^{-1}$ at reactor temperatures [400-730°C] and a heat capacity $26.82+0.00799(T_{[°C]}-650)-5.85x10^{-6}(T_{[°C]}-650)$ J/mole-°K at reactor temperatures [7].

The melting point is well above reactor temperature [1287°C] [6] and the beryllium is the outer layer of the core and as such will be the coolest component. At high temperatures beryllium retains significant structural strength, at 700°C the tensile strength is 160 MPa which is well above the pressure requirements and capable of

maintaining ≈20 MPa of hydrogen pressure [see Chapter 5, Equation 5.1]. However the long term radiation damage would result in significant migration and damage as a result the lower pressure limit of the fuel will be maintained. As a result no temperature limit for beryllium is needed.

Section 2: Simple Model

Before the core is modeled numerically by computer it is instructive to look at simpler analytical models. The heat from the fission in the core [Q] will be conducted out through any moderator and reflector to the heat engine where a portion will be converted to electricity [W] and the remainder will be rejected [R] to the radiator, which radiates the heat into space. See Figure 4.1.

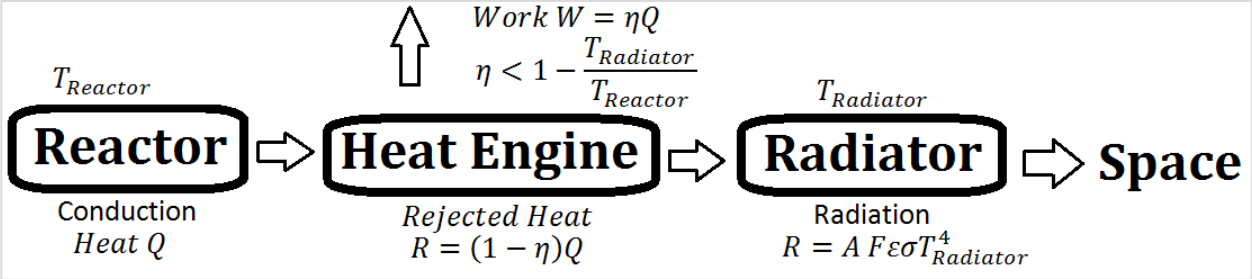

Figure 4.1: Heat flow overview diagram. This figure is an illustration of the overall heat transfer in an idealized system. [Same as Figure 2.1]

Simple Spherical Systems: The first step in the model is to look at the steady state heat conduction in the core. For the sake of simplicity and clarity the reactor is modeled as a sphere of U-$ZrH_{1.65}$ [Core] surrounded by spherical layers of LiH and beryllium. For this model all thermal conductivities are fixed at their 650°C values and are constant. The power [heat q] in the core is assumed to be a bare critical profile and deposited locally as shown below in equation 4.1 [8] and Figure 4.2 [9].

$$q_{(r)} \propto \frac{1}{r}\sin\frac{r\pi}{R} \qquad Equation\ 4.1$$

Heat transfer then follows the conduction equation [Equation 4.2]

$$-k\nabla^2 T = q \qquad Equation\ 4.2$$

with Q being the integrated core power. [Equation 4.3]

$$Q = \iiint q\ dV \qquad Equation\ 4.3$$

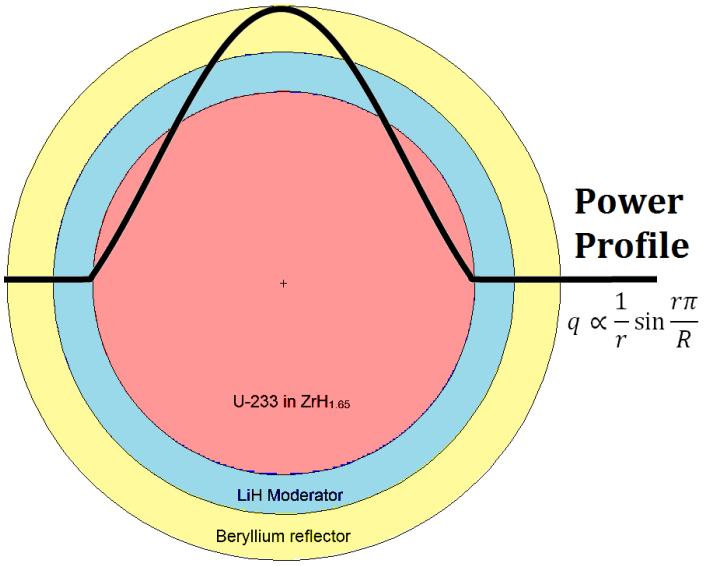

Figure 4.2: Spherical core profile [8]. This is an illustration of the cross section and power profile for an idealized spherical reactor.

These are solved to obtain the temperature rise across the core which is shown in Equation 4.4 with electric power at 500 W and R≈8.4 cm [the spherical version of the reference model, 19.8 Kg of U-ZrH1.65 and a density of 8.0 g/cm^3 [1]].

$$\Delta T = \frac{Q}{4\pi kR} = \frac{P_{ELectric}}{\eta\ 4\pi kR} \approx \frac{27°\text{C}}{\eta} \qquad Equation\ 4.4$$

Equation 4.4 thus sets a limit on thermal efficiency: with a maximum fuel temperature of 770°C and maintaining a heat source temperature of 688°C leaves a maximum temperature rise across the core of 82°C. This sets the minimum thermal efficiency of 33%. This is a conservative estimate since the actual power profile will not be the bare critical profile, the moderator and reflector will push the flux to the outer edge and some heat will be deposited by neutrons and gammas away from the fission point [8]. The temperature feedback will also change power distribution. A best case estimate would be a flat power profile [$q_{(r)}$=constant]. For this case the system is resolved which results in equation 4.5

$$\Delta T = \frac{Q}{8\pi kR} = \frac{\Delta T_{Eqn\ 4.4}}{2} \approx \frac{13.5°\text{C}}{\eta} \qquad Equation\ 4.5$$

For this best case estimate the thermal efficiency would only need to be 16.5%. Averaging these two results to a thermal efficiency of ≈25% will be appropriate for this simple spherical system [the later computer models resulted in a minimum efficiency of 23.0%]. Likewise thermal efficiencies based on an 850°C and 930°C central temperatures would be 13% and 8.5% respectively.

Next the temperature rise across the LiH and beryllium were examined. In this case, there is no significant heat production in these regions [q≈0] and the problem is now a simple diffusion problem which has been solved many times [10]. The resultant temperature drop is shown in equation 4.6.

$$\Delta T = \frac{P_{ELectric}}{\eta \ 4\pi k} \cdot \frac{R_{Outer} - R_{Inner}}{R_{Outer} \times R_{Inner}} \qquad Equation\ 4.6$$

This can be evaluated using the spherical thicknesses LiH [1.53cm] and beryllium [2.13 cm] and their 650°C thermal conductivities. This is shown in equations 4.7.

$$\Delta T_{Be} \approx \frac{0.73°\mathrm{C}}{\eta} \ and \ \Delta T_{LiH} \approx \frac{18.4°\mathrm{C}}{\eta} \qquad Equations\ 4.7$$

The temperature rise across the beryllium is insignificant, only 2.9°C at 25% efficiency. The temperature rise across the LiH is however significant. At 25% efficiency, the rise would be 74°C. The LiH temperature limit is 688°C, which limits the temperature rise to <35°C which would require a thermal efficiency of >53%, which is rather unreasonable. This can be addressed by 3 approaches:

1- Lower the outlet temperature below 650°C. The temperature would need to be lowered to ≈600°C at a reasonable efficiency of 25%.
2- Make the LiH thinner. Thickness would be reduced to <0.73 cm which may make the LiH ineffective at moderation.
3- Increase the thermal conductivity. This can be accomplished by including beryllium plates as a parallel heat transfer path. Only 4% beryllium by volume [10% by weight] would be needed to increase the effective thermal conductivity [the thickness of the outer beryllium can be reduced slightly to keep the mass nearly the same.]

Option 3 is preferable to option 2 since it is desirable to retain the LiH to keep the system more thermal. In the spherical model, the LiH is reduced only 4% by option 3 but reduced ≈53% by using option 2.

Picking between option 1 and 3 is left to the more detailed computerized analysis in Section 3. For now however it appears that the analysis of the thermal conductivity in the core has reached its limit. The temperature at the Core-LiH interface will be ≈688°C [actually ≈678°C to allow a 10°C margin] with a central temperature <770°C requiring a minimum efficiency of ≈25%. The heat source temperature is then controlled by the temperature drop across the LiH which must be reduced to keep the heat source temperature to ≈650°C. At this point the efficiency of the heat engine, which is the topic of the rest of this section, is needed to proceed further.

Heat Engine Efficiency: The efficiency of heat engine will depend on three things: 1-the temperature of the heat source, 2-the temperature at which heat is rejected at and 3-the type of heat engine used. The temperature of the heat source is controlled by the thermal limit of core materials [688°C] and conduction in the core.

The temperature at which heat is rejected at the radiator is now discussed. The two equations for the heat rejected [R] are shown in equation 4.8 [11].

$$R = P_{ELectric}\frac{1-\eta}{\eta} = Area \cdot \varepsilon\sigma T^4 \cdot F \qquad \text{Equations 4.8}$$

Equation 4.8 can be solved for system efficiency in terms of the other parameters. For this the values of ε [0.85], Fin effectiveness F [0.8] and mass per area [5 kg/m^2] introduced earlier in section 1.5 are used [11]. The electric power required is at least 500 W and the radiator mass should be less than 50 kg which limits the radiator Area to 10 m^2. The solution is given in equation 4.9.

$$\eta \geq \frac{1}{1 + 7.7 \times 10^{-10} T_{[°K]}^4} \qquad \text{Equations 4.9}$$

Equation 4.9 along with the efficiency limit from core conductivity sets the minimum bounds for efficiency, plotted in figure 4.3.

The final design step is the selection of the heat engine. While there are a large number of heat engine designs, only 4 will be considered here [12]:

1- Thermionic
2- Thermoelectric
3- Stirling
4- Brayton.

These 4 have been selected based on maturity of the technology [12], scalability to small size [eliminates Rankine cycle] and resistance to ionizing radiation [13] [eliminates solid state and photovoltaic devices]. All heat engines are limited to Carnot efficiency but each engine design has further limitations.

Thermionic converters have been used on the Topaz space reactors with overall efficiency of ≈5% with the hot junction at 1600°C [14]. There are thermionic designs reaching 12-20% efficiency but all require high temperatures with typical ranges of 1200-1800°C [15][16]. The lower temperature of the core [≈650°C] means that thermionic conversion is not applicable to this reactor.

Thermocouples have been used successfully in several space missions both nuclear and RTG. To date thermocouples have had lower efficiency than conventional heat engines but are easily scaled to small size and have no moving parts [12]. The efficiency of thermocouples is modeled using the material properties to obtain a dimensionless figure of merit "Z" [which is the ratio electrical to thermal conductivity multiplied by the Seebeck coefficient squared [17]]. This thermal efficiency is shown in Equation 4.10. The figures of merit for current Si-Ge is Z=0.7-0.9 [650-900°C] [17] and the current goal NASA research on thermocouples is to improve this to Z≈2 at 900°C [12] [to match Stirling/Brayton a Z≈10 would be needed].

$$\eta_{Thermocouple} \leq \eta_{Carnot} * \frac{\sqrt{Z+1}-1}{\sqrt{Z+1}+T_C/T_H} \qquad Equation\ 4.10$$

Stirling and Brayton engines both use the expansion of a working gas and have similar efficiencies. While both can reach Carnot efficiency at very low specific power, the practical requirement of high specific power [≥10 W_E/Kg] reduces the efficiency. The Curzon-Ahlborn efficiency shown in Equation 4.11 [18] is not a limit but rather an expression for expected efficiency at full power based on the tradeoff between efficiency and power. Due to the small size of this reactor the efficiencies will be reduced somewhat below the Curzon-Ahlborn efficiency [19]. Between 650°C to 30°C, the Curzon-Ahlborn efficiency is 43% while early Stirling prototypes only reached 36% [12].

$$\eta_{\text{Curzon-Ahlborn}} \equiv 1 - \sqrt{T_C/T_H} \qquad Equation\ 4.11$$

The choice of Stirling over Brayton is not based on any physical limitation but rather based on current NASA designs. The Stirling development is more mature with more current funding and development [12]. In either case the efficiencies are similar so the choice between them has little effect on the reactor design.

The current [2007] Stirling engines designs are for a hot temperature of 650-850°C and a cold temperature of 60-90°C [19]. The mass is ≈19-23 kg [with radiator] with 500 W_{TH} and 143-160 W_E for an efficiency of 28-32% [19]. While 4 current 650°C ASRG [8 total Stirling engines 250 W_{TH} each] have a mass [≈84 kg without Pu-238 but with radiator] slightly above the 25-75 kg goal it is the expectation that this limit can be met using two 1000 W_{TH} Stirling engines with reduced system mass [≈50 kg for the 500 W_E, base on a 10 W_E/kg heat engine [11]].

To compare thermocouple with Stirling, Figure 4.3 combines all of the efficiency results on a single graph. In Figure 4.3, the three bounding requirements are:

1- Radiator mass
2- Temperature rise across the core
3- Curzon-Ahlborn efficiency.

From the figure the Z=0.8 Si-Ge thermocouples cannot both provide high specific power and keep the core below 770°C, even with advanced Z=2 thermocouples the thermocouple window is very small. As a result Stirling engine was chosen in this work. For now the efficiency of the Stirling engines will be considered 25% which fixes the thermal heat at 2KW. If advances in thermocouple materials extend the figure of merit to Z=5-10 and are radiation hardened then thermocouples should be reconsidered for the heat engine.

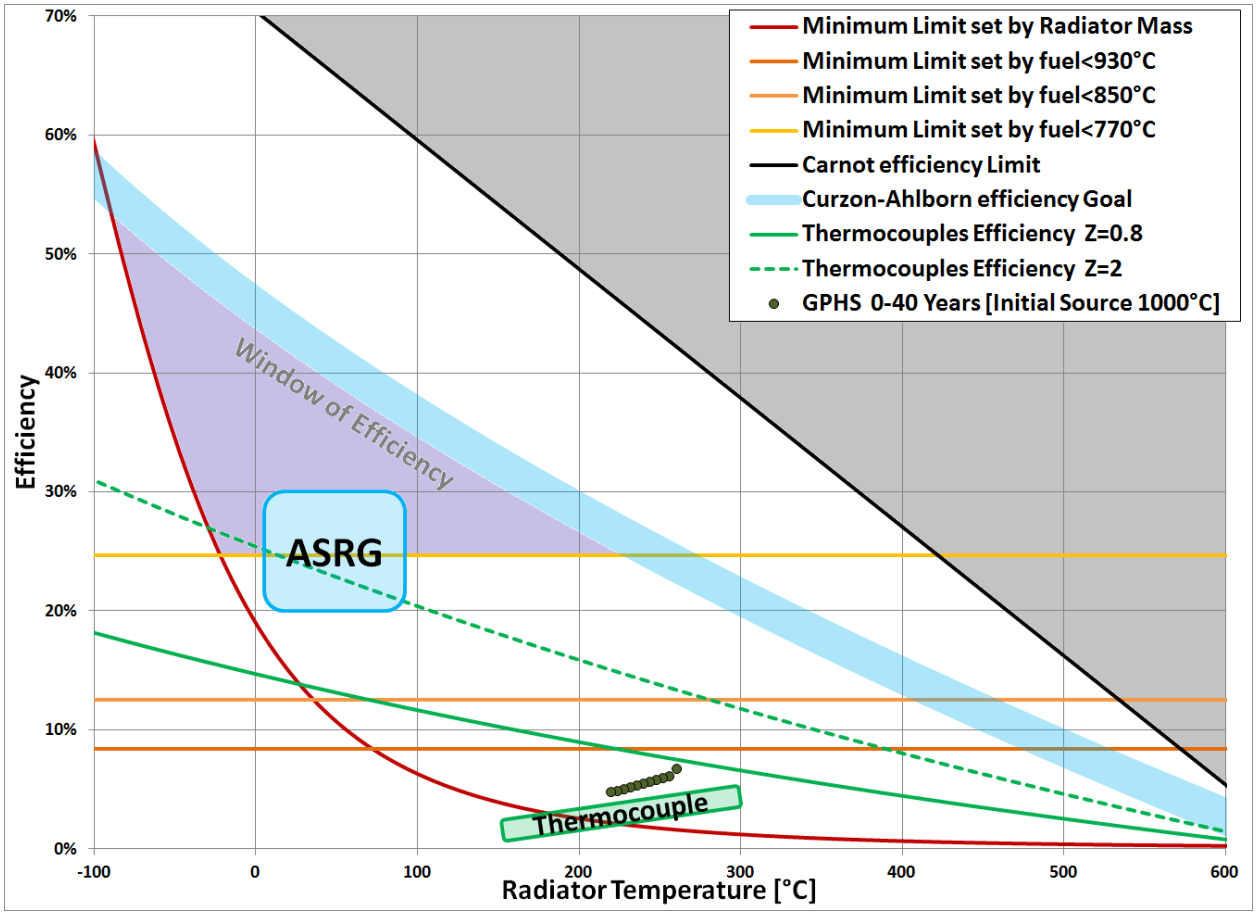

Figure 4.3: Efficiency requirements with source temperature at 650°C. This plots the bounding requirements for heat engine efficiency. The GPHS points are at a hotter temperature of 1000°C [20].

Section 3: Detailed analysis

Because for efficient operation the heat engine requires a high core temperature, approaching the established upper limit, it is desirable to refine the model. The 1-D spherical model will be abandoned and in its place a 3-D cylindrical model is used [See Figure 4.4]. This will better approximate the actual cylindrical design but will not significantly affect the scaling shown in Figure 4.3.

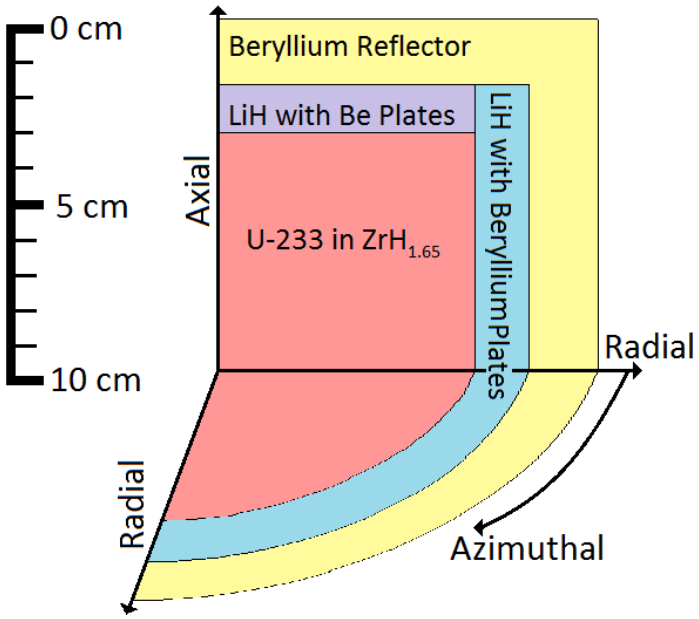

Figure 4.4: Cylindrical Model. The Beryllium plates in the LiH are not shown. The two colors for LiH represent different Beryllium plate density in the LiH.

Method: The two important attributes addressed by the model include: 1-spacial heat generation profile [Core neutronics model] and 2-the thermal diffusion of heat to the sink. A Matlab program was written to perform the thermal diffusion portion to generate a temperature profile. The program starts with a bare critical heat profile which was input to the thermal diffusion portion which in turn determines the temperatures profile. This was then input to MCNP which then calculates the heat generation profile which is then fed back into the thermal diffusion module. This was iteratively repeated until the temperature stabilized. See Figure 4.5.

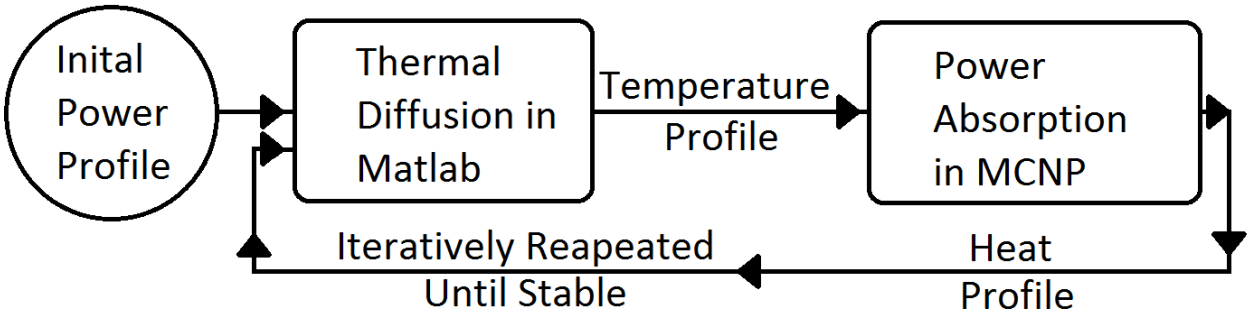

Figure 4.5: Thermal Model Flow Chart. This figure is an illustration of the thermal model to determine the temperature profile of the reactor.

For the heat generation in MCNP, tallies were used to collect both the local fission heating [21] [from fission fragments and beta decay] and two additional tallies to capture the neutron and gamma heating in the moderator and reflector. The local heating profile was flattened by two effects: 1-an extrapolated boundary due to transport considerations [8] and 2—increased power near the edge where the moderator and reflector increase the flux profile. Most of the gamma heating and much of the neutron heating occurred in the fuel material but had a flatter profile than the direct heating profile. The neutron and gamma heating in the moderator and reflector is also included in the model and accounted for only 0.4% of the total energy. [The reactivity effect of the heat sink and heat pipes were measured but found to be insignificant]

To model the thermal diffusion, the core was broken into 151 radial and axial slices but only 36 azimuthal slices [there is little azimuthal heat flow]. This meant that the cells were smaller than 1 mm and a uniform temperature could be assumed within the cell. This was then used to determine the thermal conductivity of the cell material and the temperature difference to the adjacent cell determined the heat flow. Any imbalance of heat flow resulted in the cell heating or cooling, which determined a temperature change using the material heat capacity. Between each MCNP run, the diffusion code would run the equivalent of 1 hour in 1 second steps to reach thermal equilibrium. There were two heat sinks:

1- The axial endpoints were thermal conductors and were fixed at 650°C where the heat would travel to the heat engines
2- In the radial direction heat could be lost by thermal radiation.

Radiated heat losses require the reactor to be run at a higher power and central temperature. As a consequence, it is desirable to limit this heat loss. Using equation 4.8 with the emissivity of beryllium at 650°C [ε=0.18] [22] and F=1 the heat radiated over the 478.8 cm^2 area would be ≈355 W_{TH} [0.74 W_{TH}/cm^2]. This would be added to the 2000 W_{TH} conducted to the heat engine and the core would need to generate 2360 W_{TH} of heat. This can be reduced by the use of a thin polished coating around the radial edge. For safety reasons it is desirable for the radiated emission to be capable of removing the core's decay heat if the heat engines are not in use. The decay heat for U-233 is 5.32% of full power meaning the radiated heat should be 112.4W [23]. This corresponds to an emissivity of ε=0.057 which is in the range of polished metal coating [at 650°C: Gold-ε=0.03, Silver-ε=0.03, Al-ε=0.06, Zinc-ε=0.04] [22]. The choice of the polished finish is not considered further since the thin layer will not significantly affect mass or the neutronics of the system.

One side of the reactor is adjacent to the shielding which will reduce the radiated heat from that side. This was modeled as the emissivity between a cylinder and a flat wall with the emissivity of the wall at ε≈0.8 [22] [Unpolished oxidized surface of lead/tungsten] which lowered the effective emissivity on that side to ε=0.0564 [a decrease of ≈1%]. The result of the model showed that only 0.18W of heat flowed azimuthally from the shielded side and affected the temperature by <0.01°C. As a result the model was then simplified by ignoring the azimuthal direction for a 2-D model to speed up calculations [see Figure 4.4].

First Results: The first runs were with the model D reactor from Fig 3.5. The calculated results matched the simple spherical model with a few exceptions. The first

thermal profile is shown in Figure 4.6. From this the requirement to keep the core temperature rise <82°C [770°C-688°C] resulted in an efficiency requirement of >23.0%. The temperature rise across the LiH was large [≈100°C] as expected and the beryllium rise across the end plates was <5°C.

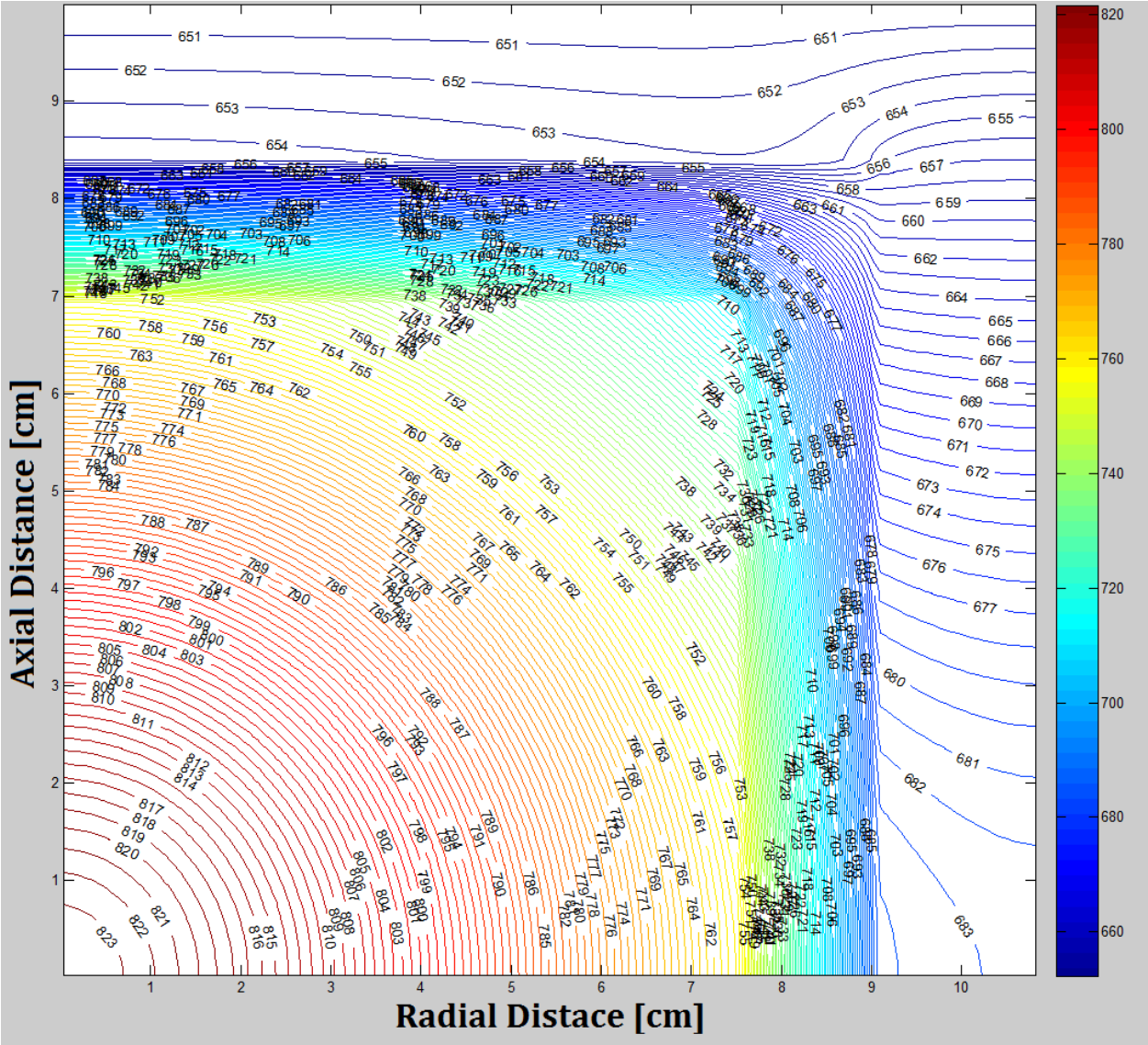

Figure 4.6: Model D thermal Profile. Only the ¼ core is shown [see Figure 4.4]. This contour graph has the temperature contour lines are separated by 1°C.

The main difference with the spherical model was that half the heat flow into the beryllium had to flow axially through the outer radial reflector to reach the endplate reflector. The long distance heat flow [8.37cm] resulted in a thermal temperature rise

of ≈29°C from the centerline to the end plate. This is too large of a temperature rise since the combined LiH and beryllium rise is desired to be <38°C [688°C-650°C] and the LiH temperature rise is already an issue. To reduce this there are two methods: 1-Increase outer reflector thermal conductivity [thicker and/or shorter or 2-decrease heat flow. The system was adjusted to be somewhat shorter and thicker but mass and reactivity constrained how far option 1 could be used. Option 2 could be used but the total heat flow of the system is constant. Thus this option requires shunting radial heat flow from the core to axial heat flow. To do this the thermal conductivity between the core and the endplate beryllium would need to be increased. This is accomplished by using beryllium plates to conduct heat between the core and the endplates.

The inclusion of these beryllium plates into the design of model D of figure 3.5 required repeating the neutronics of Chapter 3 and the final new design is that labeled model F. In going from D to F several different models [based on number and thickness of plates] were tried with varying success. The first attempts included blocks of beryllium connecting the core to the base plate which reduced the temperature rise across the beryllium outer radial reflector but this still resulted in the LiH reaching >688°C around the axial centerline. Next additional beryllium blocks were used to decrease the axial centerline temperatures. The final effort along this line is shown in Figure 4.7. While all the core thermal limits were met over 50% of the LiH was displaced and that which remained was pushed to the corner of the core where it would have little effect on reactivity. In effect, the neutronics of the core behaved like the Figure 3.5 model E reactor with very little moderation.

Refinement: The main issue with the large block approach was that large blocks of LiH would cause the LiH temperature to bulge [Figure 4.8] on the core and exceed the thermal limits. To eliminate this, thin plates of beryllium were sandwiched in the LiH. This would allow LiH to be used around the entire core for neutronics reasons. The

effective thermal conductivity [K] of the parallel plates would be between that of LiH and beryllium. Additionally the thermal conductivity is directional; see equation 4.12-13 and figure 4.8.

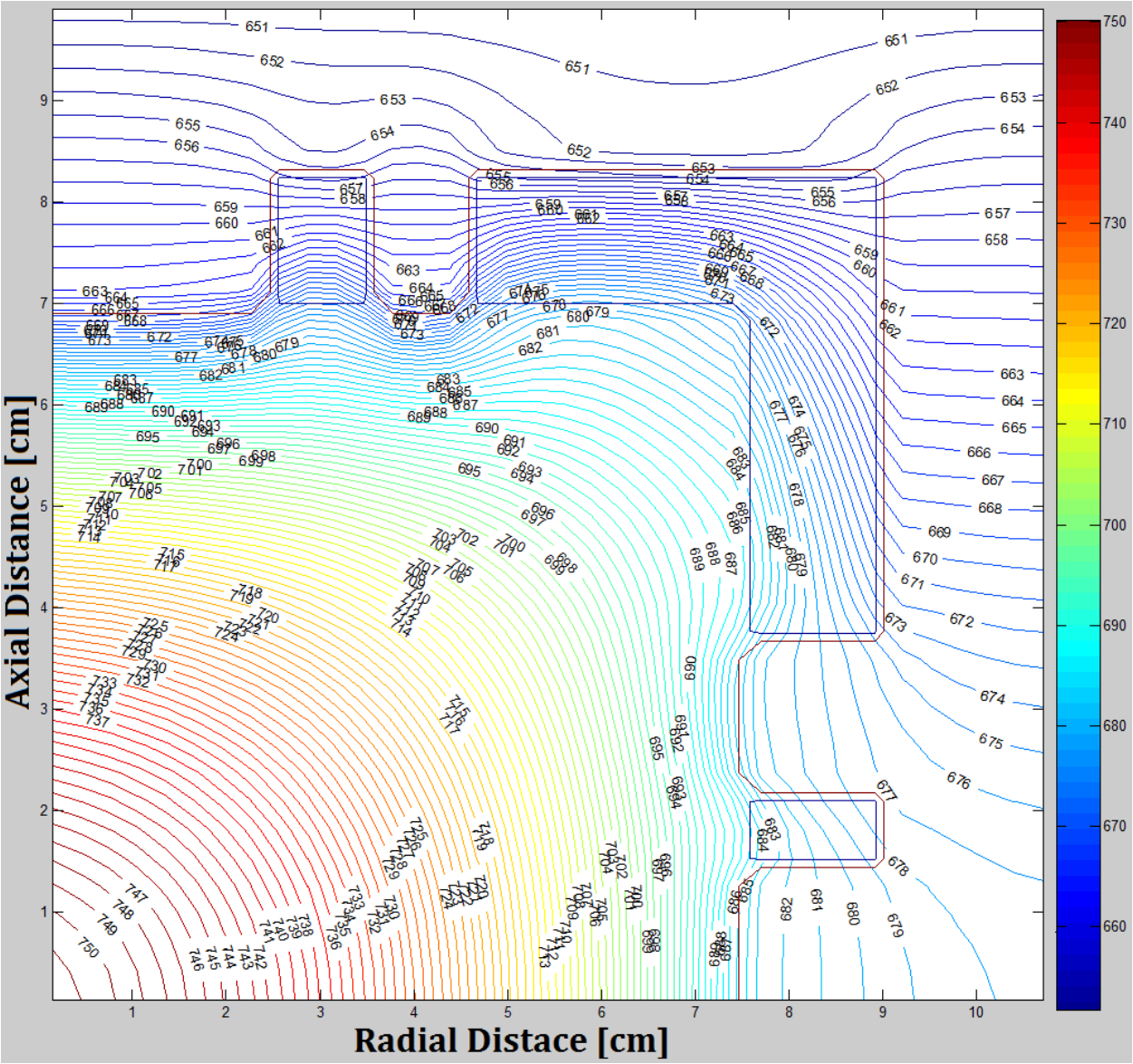

Figure 4.7: An early reactor model to improve the conductivity issue. Only the ¼ core is shown [see Figure 4.4]. This contour graph has the temperature contour lines are separated by 1°C. The blue blocks are the remaining LiH.

The thermal conductivity is higher parallel to the plates [2 dimensions] than perpendicular to them [the third dimension]. Since the need for thermal conductivity in the azimuthal direction is lowest this should be the perpendicular direction with the

increased thermal conductivity in the axial and radial directions. The 3-D thermal program in Matlab was updated to allow different thermal conductivities in the three directions while the 2-D simplification used only the parallel thermal conductivity. F_{Be} is the fraction of area using beryllium.

$$K_{\parallel} = K_{\mathrm{Be}}F_{\mathrm{Be}} + K_{\mathrm{LiH}}(1 - F_{\mathrm{Be}}) \qquad Equation\ 4.12$$

$$K_{\perp} = \frac{K_{\mathrm{Be}}K_{\mathrm{LIH}}}{K_{\mathrm{LIH}}F_{\mathrm{Be}} + K_{\mathrm{Be}}(1 - F_{\mathrm{Be}})} \qquad Equation\ 4.13$$

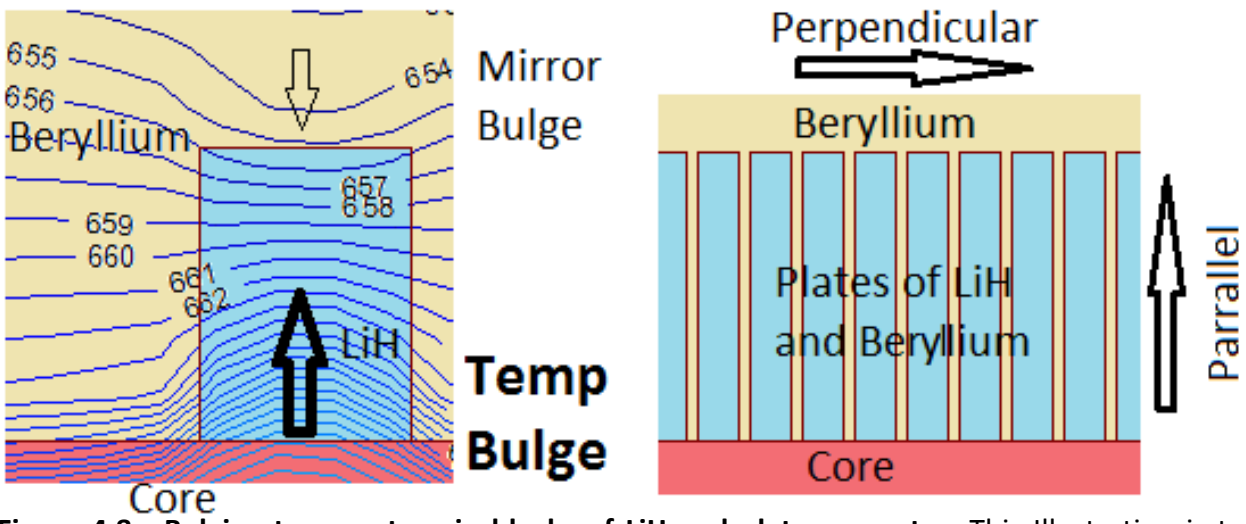

Figure 4.8: Bulging temperature in blocks of LiH and plate geometry. This Illustration is to show the temperature bulge found in monolithic LiH blocks and how it is reduced by this layers of beryllium and LiH.

The final step of reducing the temperature rise across the outer radial reflector was more difficult. Reducing the heat flow in the radial direction could only be accomplished by increasing the heat flow in the axial direction. This is accomplished by increasing the ratio of Be-LiH for the axial heat flow. However, this decreases the overall amount of LiH and reduces moderation. To combat this, more LiH and less Beryllium is used in the radial direction but this has the effect of increasing the temperature rise across the LiH and raising the temperature of the LiH. A large variety of ratios between LiH and beryllium were modeled with the ratio varied between 1-50%.

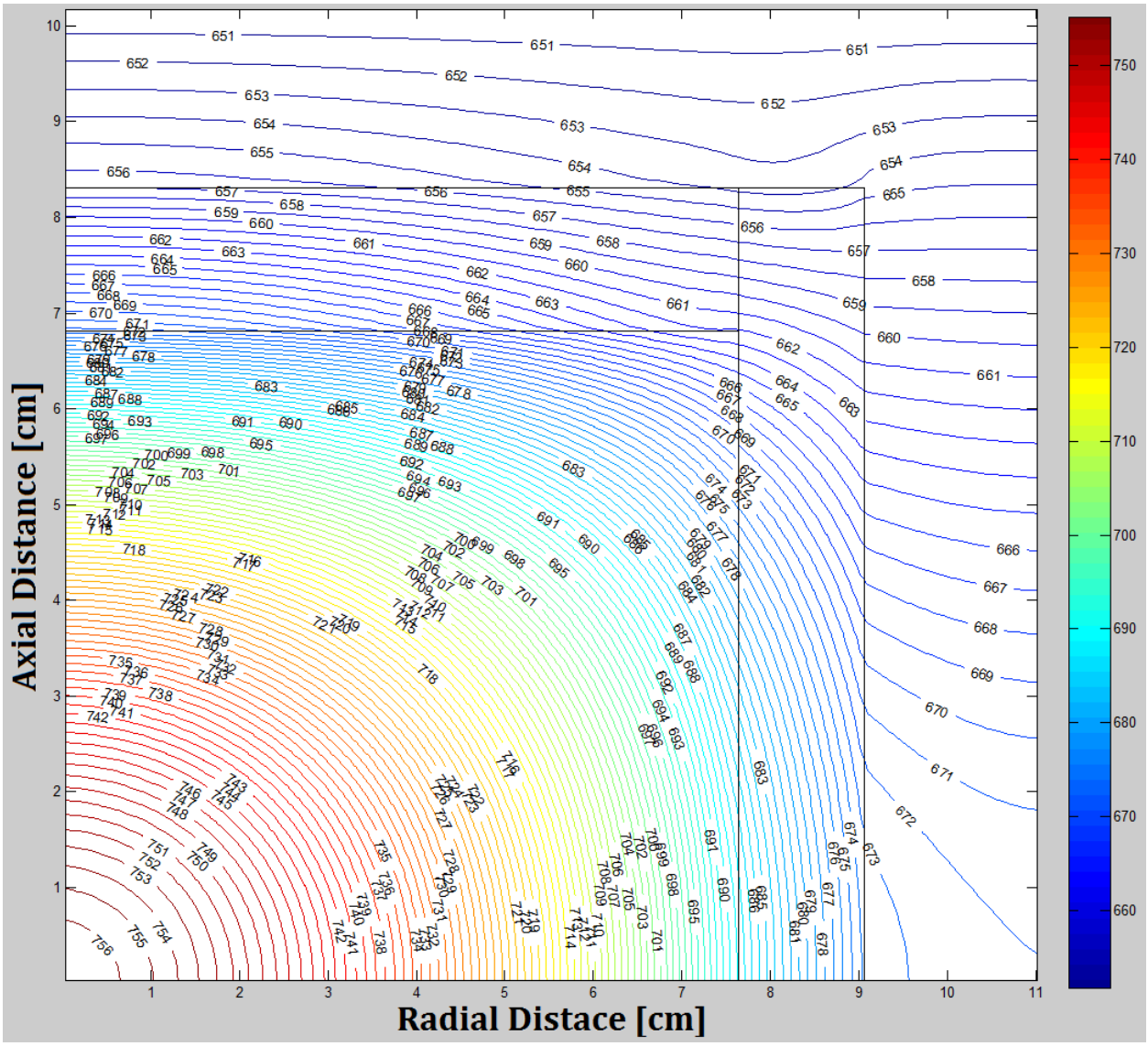

Figure 4.9: Model F Thermal Profile. 650°C Sink Temperature. Only the ¼ core is shown [see Figure 4.4]. This contour graph has the temperature contour lines are separated by 1°C.

Since the hottest LiH occurs along the axial centerline, the ratios that minimized this temperature for a given total amount of LiH were found to occur when the temperature rise across the LiH equaled the temperature rise along the outer radial reflector. Setting these temperatures equal meant that the thermal conductivity of the radial LiH-Be plates should have the same thermal conductivity as the fuel in the core. This set the radial Be/LiH ratio at 15% [14.37% but 15% is used]. The axial Be/LiH ratio was then varied to set the maximum LiH temperature at the limiting temperature of

688°C. This occurred with a 31% Be/LiH ratio. The resultant temperature distribution is shown in Figure 4.9.

Operating the reactor at its limiting temperature is not desirable. However since reducing the LiH temperature by 5-10°C further requires the near elimination of LiH. The increased use of beryllium plates is not practical. To create a margin it was be necessary to reduce the outlet temperature to the heat engine. To create a 10% margin [3.8°C] and an additional 5°C margin to allow for temperature variation over core lifetime [See chapter 5] it would be necessary to reduce the outlet temperature by 8.8°C [Actually only 8.78°C since thermal conductivity improves at lower temperatures]. As a result the outlet temperature is set to 640°C instead of 650°C. This temperature drop is well within the operating range of the ASRG [which has a range of ≈580-650°C to allow for the Pu-238 source to cool over the lifetime].

The effect on overall system efficiency is insignificant. Figure 4.3 can be replotted with the 640°C source temperature but the effect is insignificant.

Reduced Power: It is desirable to allow the core to operate at reduced power to extend core life or allow standby operation. As will be shown in chapter 5, the core is designed to operate for 200 years at full power so this option is not entirely necessary. However it is not difficult to show that this option is possible. The temperature gradients are all reduced at reduced power so that with fixed heat sink temperatures all the thermal limits would be trivially met. However the negative power coefficient of reactivity results in added reactivity at lower power which results in the core heating up. The balance between the rising heat sink temperatures and lowering temperature gradients will determine whether reduced power is possible. While there are many possible reduced power modes [90%, 73%, 28% for example] for simplicity and illustration only two will be shown: 1- ½ power mode and 2- Standby mode [Standby is not zero power].

½ power mode: In theory there are 2 methods by which the core could operate at ½ power: 1-use only 1 of the 2 ASRG at full power and 2-use both ASRG at half capacity. The first option attempted was to use only 1 of the 2 ASRG at full power. In this case, the heat from the half of the core with the non operating ASRG would need to flow through the half of the reactor with the operating ASRG. This effectively doubles the heat flow at half power on the operating side and raised the temperature gradients to near their original value and temperatures are close to their original values. The non-operating side however increases significantly in temperature and exceeds the temperature limits. As a result, this mode of operation should be avoided.

The second option of both ASRG operating at half power [24] [Current space Stirling engines are not designed to change loads since decay heat is fixed [18]] is the better of the two options. Figure 4.10 shows the temperature profile at half power. In this case the LiH remains at nearly the same temperature as full power with the core much cooler and the Beryllium hotter. Since the side radiated power is slightly higher at the higher temperature actual core power is at 53% full power to deliver 50% full power to the heat sink. The efficiency of the ASRG will change slightly due to the decreased flow rate and the hotter inlet temperature of 660°C [instead of 640°C] and the electrical output will be ≈250W.

Standby mode: When the ASRG are both off, the power will not go to zero. The negative temperature coefficient of reactivity will prevent the core from cooling down and as a result the core will remain at operating temperature. As a result there will still be thermal radiation as well as some heat flow conducted through the ASRG. To model the Standby power, the limiting case of no heat leakage to the ASRG is assumed. The thermal radiation losses will increase to ≈140 W due to the higher temperature of the beryllium reflector. The resultant temperature profile is shown in figure 4.11.

From both a neutronics and thermal perspective reduced power is possible if core life needs to be extended [discussed further in chapter 5].

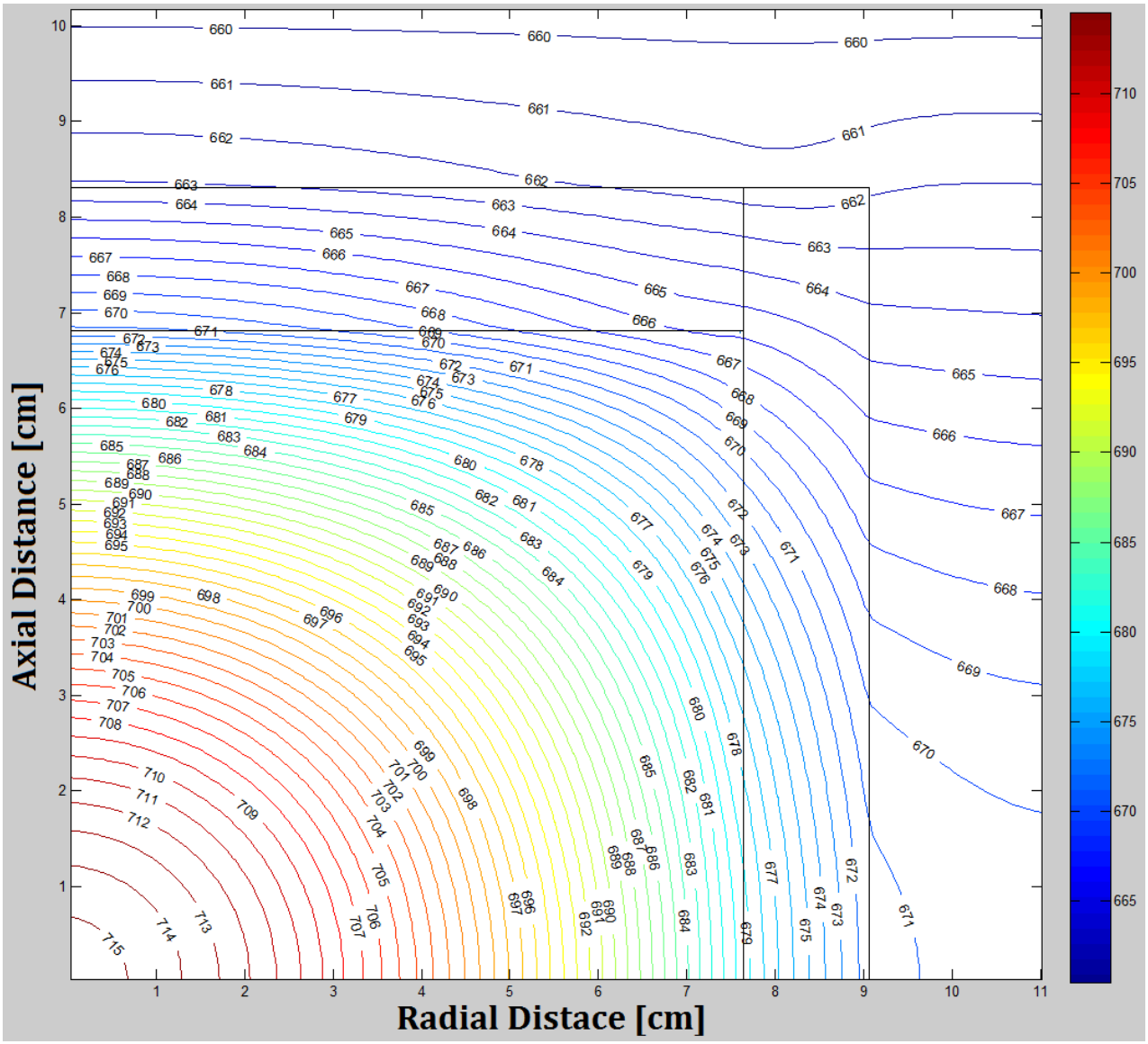

Figure 4.10: Model F Thermal Profile at ½ Power. 640°C Sink Temperature. Only the ¼ core is shown [see Figure 4.4]. This contour graph has the temperature contour lines are separated by 1°C.

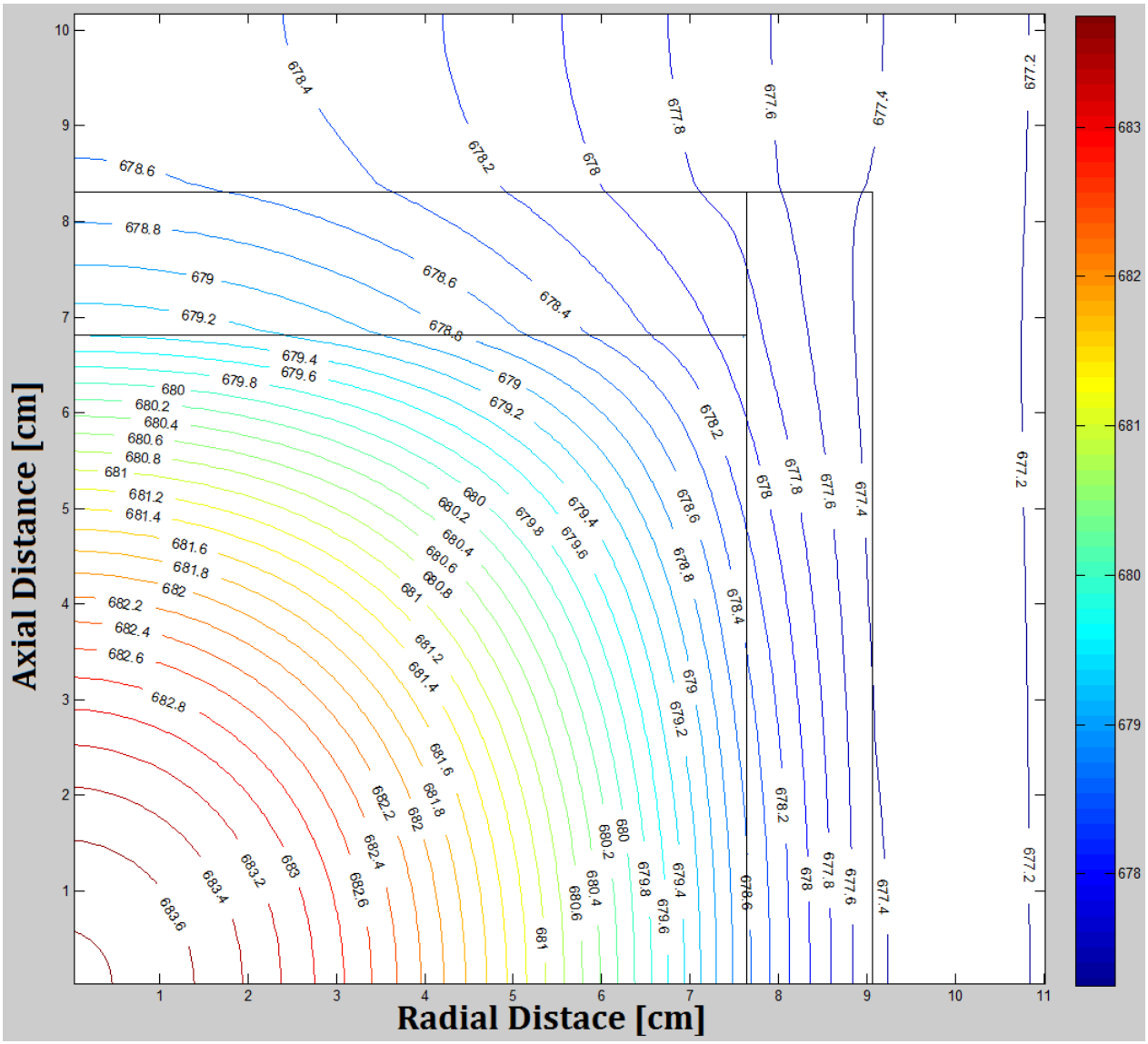

Figure 4.11: Model F Thermal Profile at standby power. 640°C Sink Temperature. Only the ¼ core is shown [see Figure 4.4]. This contour graph has the temperature contour lines are separated by 1°C.

Section 4: Future Possibilities

The thermo model [Model F of figure 3.5] allows the thermal limits of the core to be met with an acceptable margin. This is however not the only possibility. Similar to Chapter 3, there are a range of possible designs and variations. Some of these are covered in this section.

Higher efficiency of 30-40%: The 25% thermo efficiency is based on the design of the ASRG. The design of the ASRG is however not optimized for a reactor design. Looking at figure 4.3 there is room for improvement. This would come primarily from two effects: 1-the larger size of the reactor and 2-the more stable temperature. The current ASRG [ASC-E] is designed for 75 W_E with a smaller Pu-238 source [19]. The larger 250 W_E for this reactor design would allow improvements in efficiency and operation closer to the Curzon-Ahlborn efficiency. Since the Pu-238 source decays, the power and thus the heat source temperature will decrease considerably over the life of the ASRG [18]. In contrast the reactor can maintain a very stable temperature and power over core life [Chapter 5] allowing the Stirling engine to be finer tuned to the temperature and power increasing possible efficiency. As a result it may be practical in the near term to increase efficiency to the range of 30-40% [see Figure 4.3]. Additionally the mass may be reduced to the ≈50 kg range [11].

This higher efficiency can be utilized in one of two ways: 1-maintain the current 500 W_E output but use less thermal power [1250-1670 W_{TH}] to extend core life and allow a large thermal margin or 2- allow electric power to increase to 600-800 W_E with the same thermal power.

No LiH: The LiH was the limiting component in the thermal analysis. The main use of the LiH was to provide more hydrogen to improve the temperature coefficient of reactivity [which helps for core lifetime] but LiH is not absolutely necessary in the

reactor [the Hydrogen in the fuel provides some moderation]. If the LiH was removed the temperature to the Heat engine could be raised. For this Model E from Figure 3.5 is considered [the core design without LiH]. The next limiting component was the $ZrH_{1.65}$ with a limit of 770°C, allowing the sink temperature to be raised until the central temperature reaches this limit allows the sink temperature to be raised from 640°C to only 670°C; the 30°C raise is fairly insignificant. The 770°C limit is however not a strict limit. If a shorter duration mission is called for then the temperature limit can be raised. Using the 10 atmosphere pressure limit temperature of 930°C as the central temperature limit the sink temperature can be raised to 827°C. This would be a significant improvement in temperature with Curzon-Ahlborn efficiency of 46%. The ASRG program has already developed higher temperature Stirling designs; this is a similar temperature to the ASC-2 [850°C] which operates with 32% efficiency [19].

Alternatively the 640°C sink temperature could be kept and the power could be raised until the central temperature reaches the limit. In this case the similar reactor design could provide ≈1300W_E instead of the lower 500W_E or a thermocouple design of 9.6% efficiency [Z=0.6] could be used to remove all moving parts.

These thermal profiles of the two options of higher power or temperature are shown in figure 4.12. Choosing between these two ways to use the reactor would depend whether the additional power could be used. While the reactor would be the same mass a larger heat engine and radiator would be needed.

While it would be possible to operate at higher temperatures or power, doing so reduces core life to much less than the 100 year goal and thus will not be considered the base line model.

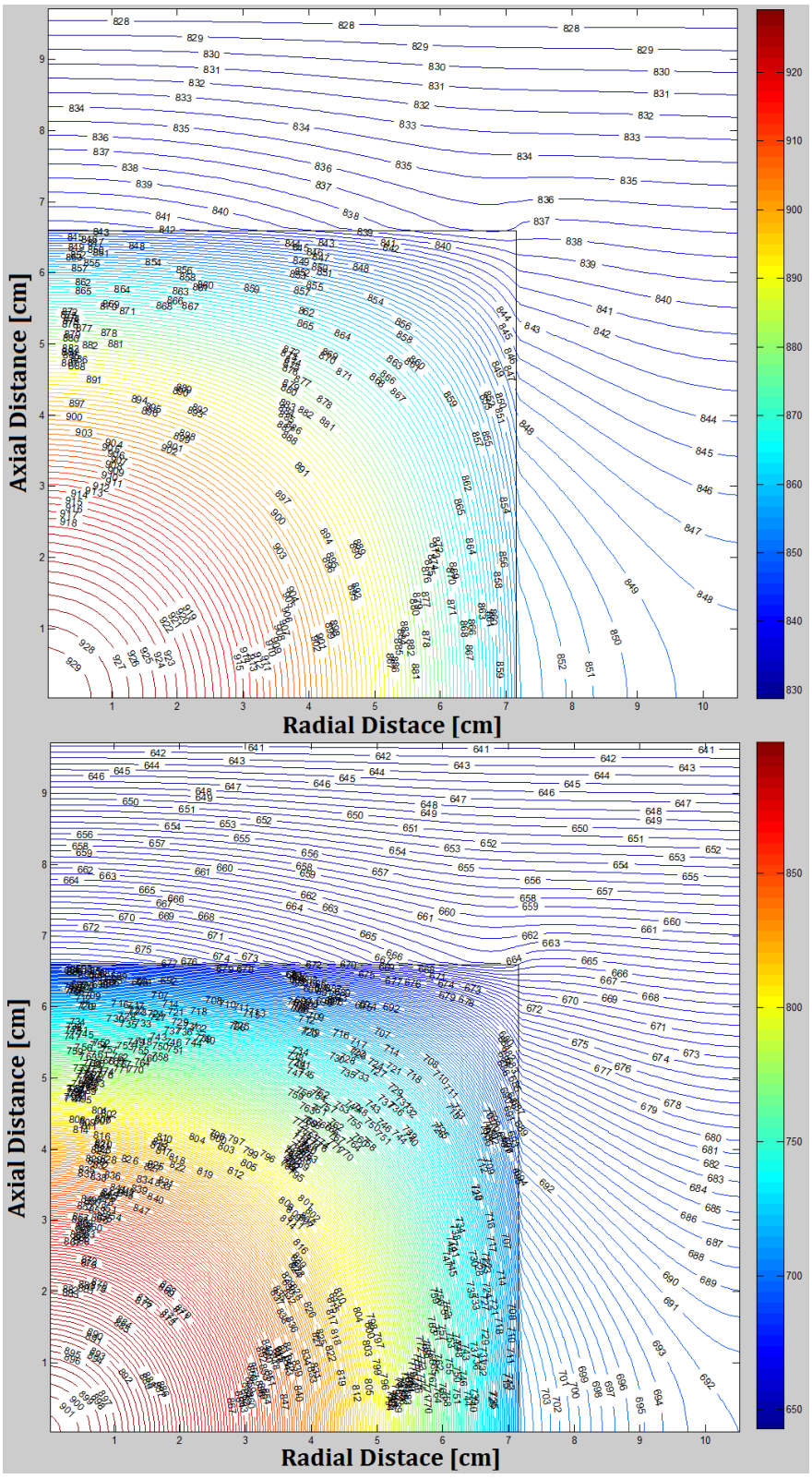

Figure 4.12: Model E Thermal Profiles. Only the ¼ core is shown [see Figure 4.4]. This contour graph has the temperature contour lines are separated by 1°C. The top figure is the hotter sink temperature [827°C] and the right figure is the higher power, cooler sink [640°C].

Convection: The reactor represents the limit of power that can be reached using thermal conduction. However convection [or Heat pipes] could be used to significantly increase heat flow. This was not used for four main reasons:

1- Reduced reliability of pumps to operate a steady flow for a 100 year lifetime [25]
2- Increased system mass due to the inclusion of coolant channels in the core and pump,
3- No need for the higher heat flow as $500W_E$ should be sufficient [see Chapter 2]
4- Moving fluids can cause erosion in radiation environments and neutronics instability.

However if a need for higher power in the future is found [The mid-power Jovian reactor from figure 1.2] then a moving fluid for heat transfer should be considered.

Section 5: Summary

In this chapter the thermal design of the reactor was analyzed. The reactor could be kept below any temperature limit using conduction alone without the need for coolant pumps. The use of dynamic heat engines will be needed with the Stirling engine chosen. An efficiency of only 25% is sufficient to meet all design goals and higher efficiency of 30-40% may be practical in the near future.

References [Chapter 4]

[1] D. Olander, et al "Uranium-Zirconium Hydride Fuel Properties" Nuclear Engineering and Design, 239, pp. 1406 (2009)

[2] S. Yamanaka, et al "Thermal Properties of Zirconium Hydride" Journal of Nuclear Materials, 294, p. 94 (2001)

[3] "Safety Evaluation Report on High-Uranium Content, Low-Enriched Uranium-Zirconium Hydrid Fuels for TRIGA Reactors" U.S. Nuclear Regulatory Commission (1987)

[4] G. Schmidt "SNAP Overview", ANS DCN: SP-100-XT-002 (2011), http://anstd.ans.org/NETS2011/Documents/Presentations/Opening%20Dinner%20SNAP%2010A%20Schmidt.pdf

[5] R.L. Smith and J.W. Miser "Compilation of the Properties of Lithium Hydride" Lewis Research Center, Cleveland, OH (1962)

[6] David Lide, "CRC Handbook of Chemistry and Physics", CRC Press (2001)

[7] "Beryllium Properties", Advanced Energy Technology Group (2012) http://aries.ucsd.edu/LIB/PROPS/PANOS/be.html

[8] J.J. Duderstadt and L.J. Hamilton, "Nuclear Reactor Analysis", John Wiley & Sons Inc (1975)

[9] Michael Greenburg, "Advanced Engineering Mathematics", Prentice Hall (1998)

[10] Daniel Zwillinger, "Standard Mathematical Tables and Formulae", CRC Press (1996)

[11] L.S. Mason "Realistic Specific Power Expectations for Advanced Radioisotope Power System" Journal of Propulsion and Power, 23, pp. 1075 (2007)

[12] D.J. Anderson, et al "An Overview and Status of NASA's Radioisotope Power Conversion Technology NRA" NASA Glenn Research Center, American Institute of Aeronautics and Astronautics (2005 year)

[13] George Messenger, "The effect of radiation on Electronic Systems", VNR (1986)

[14] IAEA "The Role of Nuclear Power and Nuclear Propulsion in the Peaceful Exploration of Space" (2005)

[15] F.N. Huffman, et al "High Efficiency Thermionic Converter Studies" NASA Lewis Research Center, for NASA (1976)

[16] Thermionic Energy Conversion, NEEP 602 Lecture 9, University of Wisconsin (2000)

[17] X.W. Wang, et al "Enhanced Thermoelectric Figure of Merit in Nanostructured n-type Silicon Germanium Bulk Alloy" Applied Physics Letters, 93, p. 193121 (2008)

[18] J.G. Wood, et al "Free-Piston Stirling Power Conversion Unit for Fission Surface Power, Phase I Final Report" NASA (2010)

[19] R.K. Shaltens and W.A. Wong "Advanced Stirling Technology Development at NASA Glenn Research Center" NASA (2007)

[20] G.L. Bennett, et al "Mission of Daring: The General-Purpose Heat Source Radioisotope Thermoelectric Generator" IECEC, San Diego, CA (2006)

[21] Denise Pelowitz, "MCNP User Manual", Los Alamos (2008)

[22] Table of Total Emissivity (2011), http://www.monarchserver.com/TableofEmissivity.pdf

[23] National Nuclear Data Center, http://www.nndc.bnl.gov/

[24] D. Thimsen, "Stirling Engine Assessment", EPRI (2002), http://www.engr.colostate.edu/~marchese/mech337-10/epri.pdf

[25] M.S. El-Genk, Space Safety Regulations and Standards, “Chapter 26 Safety Guidelines for Space Nuclear Reactor Power and Propulsion Systems” pp. 319 (2010)

Chapter 5: Core Life

In this chapter, core life is discussed. The issue is whether the reactor can maintain criticality through the design core life and what core lifetimes are possible. Additionally approaches to increase core life are considered.

Section 1: End of Life Mechanisms

To consider the end of core life, first the end of life mechanisms must be examined. This chapter will only consider slow and gradual causes of core aging. Catastrophic end of core life such as crashes will be considered in Chapter 7.

Temperature Drop: The core is a critical system with a negative temperature feedback. Any slow gradual change to the reactor will affect the core reactivity. The core will then change temperature to return to criticality. The core life is then the time that the core temperature remains in the desired temperature range [1]. For example consider a hypothetical process that causes the core to lose a constant 1$ of reactivity per year. To compensate, the temperature will drop to add 1$ of reactivity. For the reference reactor this comes to an initial drop of 15.6°C for the first year and then 16.5°C for the second year and so on. In one decade the total temperature drop to add 10$ of reactivity is 201.2°C. This would reduce operating temperature from 640°C to 438.8°C, which would limit the ability of the system to operate the heat engine and produce power.

There is not a temperature at which the system switches off. Figure 5.1 uses the thermal efficiencies from chapter 4 and plots the temperature drop and efficiencies for this hypothetical case.

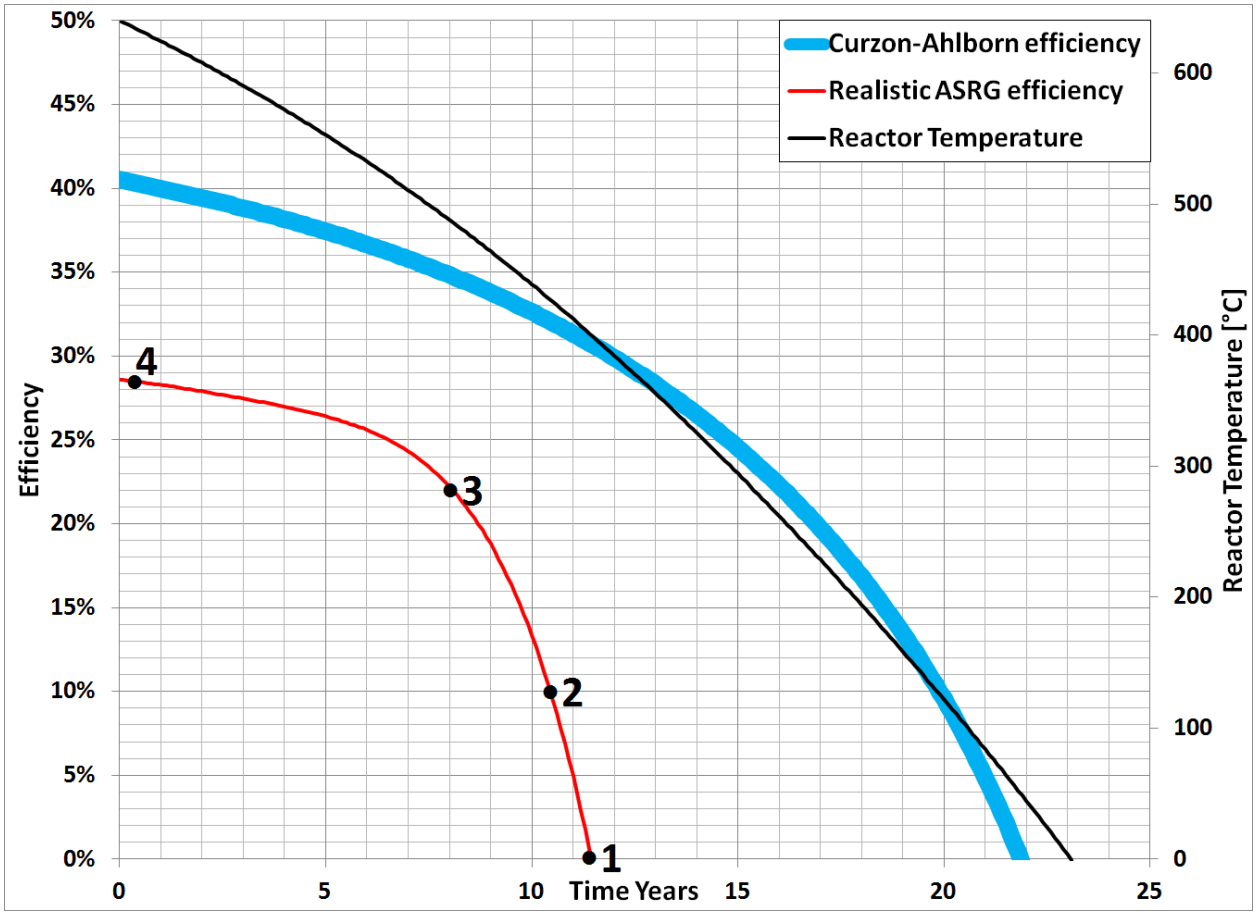

Figure 5.1: Core aging Example. This graph is for a hypothetical 1$ reactivity drop per year. T_{SINK}=50°C and the realistic Stirling design is designed for 600°C with a 200°C temperature band,

From the figure several end of life points can be picked:

1- Cooled reactor where temperature drops to the point thermal efficiency is zero [11.5 years in this example],
2- minimum power necessary to operate the probe [~10% or 10.5 years],
3- the knee where efficiency drops [≈8 years] or
4- Narrow band of high efficiency with a small temperature drop [for example, <5°Cwhich is ⅓ year in this example].

As it will turn out the core can be designed so that condition 4 can be met for 100's of years so that a very narrow definition of core life will be used. The reason for this is that there are processes that could raise temperature as well. The core only has a narrow margin of which temperature can be raised [see Chapter 4] but has a large range of which temperature can be dropped. For most of this chapter core life will mean that

the core remains at its initial temperature ±5°C. Since this temperature band is small the temperature coefficient of reactivity can be considered nearly constant and changes in reactivity can be listed in terms the associated temperature change. The changes are divided up as to whether they are proportional to power [fuel and poison burn-up, radiation damage] or independent of power [alpha decay of the fuel, Hydrogen migration] as that will affect the ability of the reactor to extend life by reducing power.

Finally there are several processes occurring in the core at the same time. The sum change in reactivity due to all of them at once will need to be considered. First we will look at most of the changes separately and then use computer models to consider them all at once.

Fuel Burn-up: The first and most obvious way in which the core reactivity will change is the consumption of fuel. While this will be considered in more detail in Section 2, a simple calculation here will be used to illustrate the magnitude of this effect. Consider the ideal burn-up of 1% of the core fuel in the reference reactor. This amounts to 0.0869Kg of U-233 [2], which is 2.24×10^{23} atoms consumed. Of these ≈92% of the atoms will be fissioned releasing 6.28×10^{12}J of energy. This is the equivalent to 94.26 years at full power [2112W_{TH}]. Running MCNP for the reference core with 1% of the U-233 atoms removed causes a reactivity drop of 0.991$ which corresponds to 15.4°C or 0.164°C/Year.

This effect is quite small, even with the ±5°C band the core life would be 30 years and if the knee definition of end of life [#3 from Figure 5.1] was used the core would last 760 years at full power.

However this simple picture is complicated by fission product build-up and neutron capture in the fuel. The magnitudes of the effect of these complications are estimated below based on their thermal cross sections relative to U-233, which has a 531b fission cross section:

1- Fission produces the poisons Xe-135 and Sm-149 [See Chapter 3, Xenon and Samarium section]. The Xe-135 is insignificant and the Sm-149 drops temperature initially at 0.103°C/Year [to a maximum of 17°C with τ=165 Years].
2- The other fission products have an average cross section of ~50b and 2 are produced per fission which increases absorption by ~100b [1]. The reactivity effect would be ~17% the size of fuel burn-up or ~0.029°C/Year.
3- The capture produces U-234 which has a capture cross section of 106b [3]. The reactivity effect would be ~0.0026°C/Year.
4- The U-234 captures to U-235 which increases the reactivity -this would be a 2nd order effect and mostly negligible.
5- Hydrogen, Li-7 and Be-9 all capture neutrons but have cross sections <1b and this effect can be neglected [2].
6- Other higher order effects [for example U-236 and H-2 production and fission product (n,2n) reactions].

These factors together add up to ≈0.297°C/Year which would limit core life to 17 years. This is still simplified as a thermal system. There is a large number of resonance absorbing fission products. Additionally, the regions of the core with the highest power will have the highest burn-up, thus most fuel loss and poison build-up will occur in the most reactive regions of the core. To include all these effects requires a computer model. This was done using the BURN routine in MCNP which can track the actinides and up to 210 fission products in each individual cell [4] and burn the core in small steps at low power. The core was also divided into 25 radial, axial and azimuthal slices so that each region would burn at the proper rate. For stability reasons the time steps were logarithmically sized. The first time steps were set to hours. When the burn-up reached 10 years the steps were then constant at 1 year each. MCNP will only compute the neutronics changes of the fuel. The resultant effect of the effect on reactivity due to burn-up is shown in Figure 5.2.

From Figure 5.2 the best fit line through the MCNP data is has an actual initial drop of ≈0.3112°C/Year which would limit core life to ≈16 years.

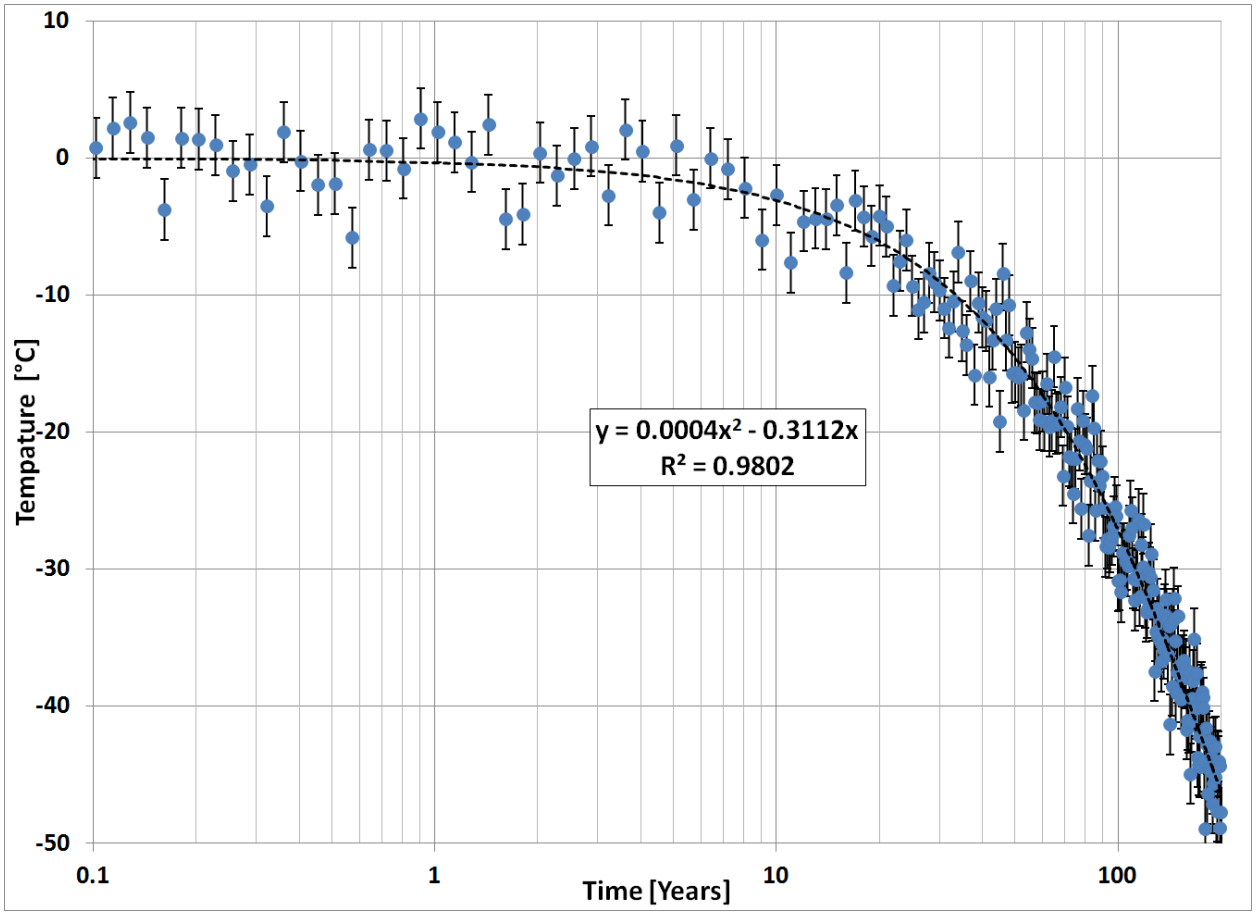

Figure 5.2: Poison Free core Burn-Up without physical changes. This graph is the MCNP calculated temperature drop for the reactor at full power. The scatter and error bars on the data are reflective of the Monte Carlo procedure that is used to generate the data. The actual temperature drop line would be smooth. The quadratic fit is not meant to imply that the rate is quadratic but merely that it is well approximated over this interval

Poison Burn-up: While it would seen that the core life is only ≈16 years, which is less than the 100 year goal, the effects of burn-up can be countered with the used of burnable poisons. If the core is initially loaded with burnable poisons then they would add positive reactivity as they are consumed, which would raise temperature. This option is evaluated in Section 2.

Hydrogen Migration: Any physical changes to the core will also affect the reactivity of the core. The driving force for movement of materials is pressure. The minimization of pressure was the reason the for the fuel thermal limits set in chapter 4.

The hydrogen pressure depends on the temperature of the fuel and the local concentration of hydrogen. In the reference core's region of interest, the partial pressure of hydrogen in ZrH_X at temperature T can be approximated as a linear function of X and T [the Log of pressure] $P=10^{(6.00X+0.00833T-16.49)}$ Atmospheres [5]. Since the center of the core is hotter, the hydrogen will migrate to the edge, which is cooler. This raises the H-Zr ratio which raises the pressure at the outer edge and lowers the partial pressure at the center. A new equilibrium will be reached when the hydrogen partial pressure is the same throughout the core. The diffusivity of hydrogen in $ZrH_{1.65}$ is ~$10^{-5}cm^2/s$ [5]. This means the characteristic diffusion time is ~80 Days [The actual diffusion time will be faster when under irradiation]. This is much shorter than the expected life time of the core and as a result equilibrium will be reached.

To examine this effect, the spherical model temperature from Section 4.2 is used with the updated central temperature of 747°C and outer temperature of 678°C from the computerized model of Section 4.3. Microsoft Excel was the used to solve the system using the Goal Seek function to keep the total hydrogen content constant and the partial pressure constant throughout the core. The resultant pressure was 0.194 Atm and the H-Zr ratio is shown in figure 5.3.

This distribution was then modeled in MCNP to examine the reactivity effect. The resulting drop in reactivity is 0.65$ which correspond to a change in temperature of 10.1°C, which is significant. However this is a onetime change in reactivity and would not vary over core life. As a result the core can be constructed with the equilibrium concentrations built in [or closely approximated by step functions].

The hydrogen diffusion in the LiH and through the beryllium is also considered but is insignificant. The diffusion in the LiH will occur in minutes due the LiH being near its melting point and would quickly reach equilibrium [6]. The permeability of hydrogen through beryllium is very low even at 650°C [P≈1.05μg/(cm-Year-√Atm)] [7] and as a

result the total hydrogen loss through the reflector over 100 years will be ≈30mg [≈0.005°C over the 100 year frame].

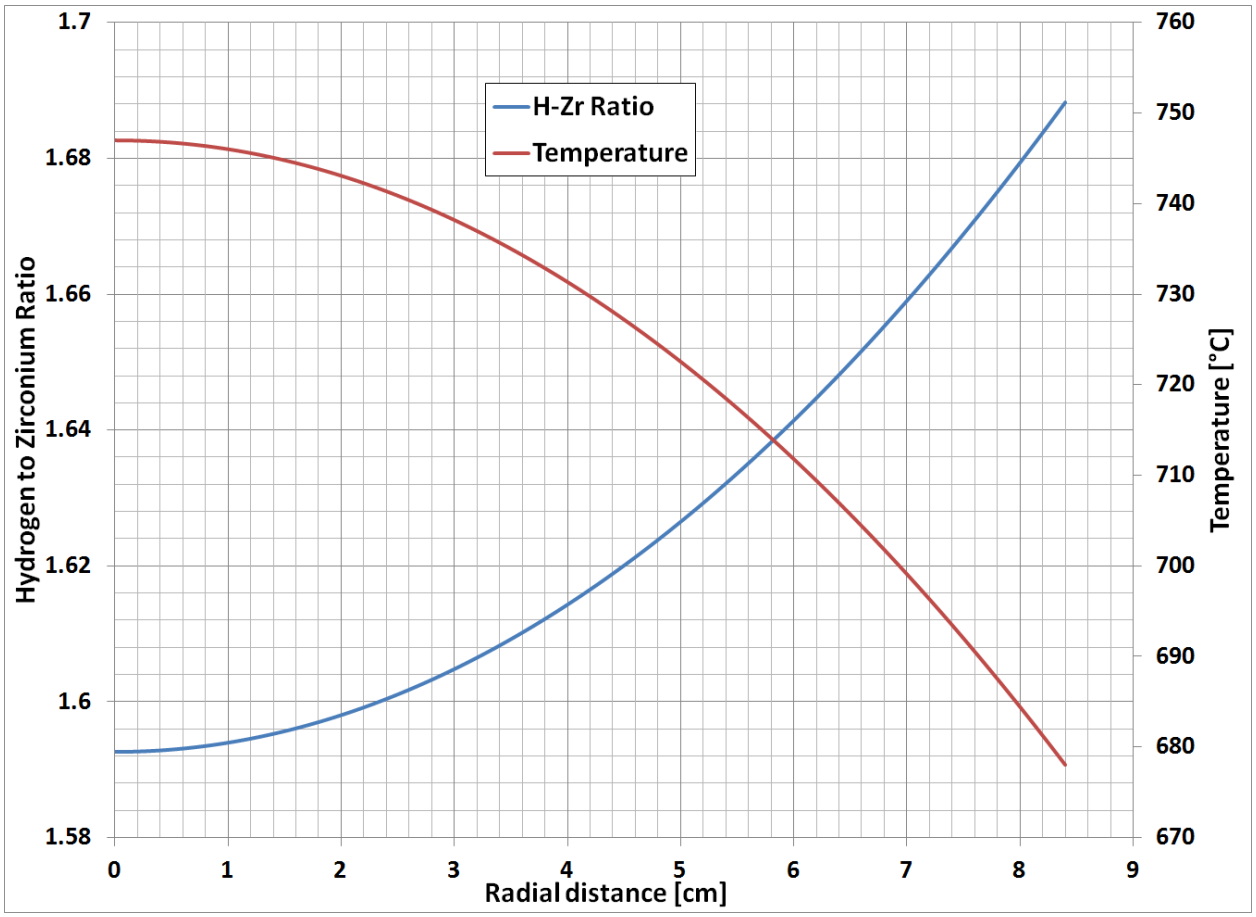

Figure 5.3: Hydrogen Migration in simplified Core. This graph is the Excel calculated hydrogen distribution through the core based on the temperature profile.

As a result Core temperature changes due to hydrogen migration will be considered insignificant so long as the core is not damaged.

Pressure Damage: If the core were to expand then the reactivity of the core would decrease. The initial Hydrogen partial pressure in the core is ≈0.2Atm, which is quite small. However as the fuel burns fission product gasses and Helium will build-up in the core and cause pressure to increase. This leads to two issues: 1-Possible Rupture and 2-Material Creep.

To consider possible rupture in the Beryllium reflector, the reflector is considered a cylindrical pressure vessel and the fission product gasses buildup in the core is modeled as an ideal gas at the hottest core temperature of 770°C. The tensile strength [σ_{Be}] of the beryllium at reactor temperature is 160 MPa [8] and an ideal beryllium pressure vessel would rupture at ≈194 Atm of pressure [with a 50% design margin, See Equation 5.1].

$$Pressure \approx \frac{Mass_{Be} * \sigma_{Be}}{6\pi * \rho_{Be} * R^3} \approx 290.7\text{Atm} \qquad \text{Equation 5.1}$$

However well before this point, creep [creep is the tendency of a solid material to move slowly or deform permanently under the influence of stresses] will occur since the beryllium is at ≈60% of its melting temperature. To limit creep, the stress in the pressure vessel should be much less than the shear modulus [Since diffusion creep is much less than dislocation creep]. Due to this, the pressure limit is reduced by an order of magnitude to a pressure of 20 Atm. To find the fission product pressure, the fission yields of U-233 are examined from the ENDF data since some fission products will form solids and other will be volatile gasses. Each fission produces on average 0.589 Fission product gasses [Br, Kr, Rb, Te, I, Xe and Cs] [2]. However most of the fission products remain in solution in the fuel. In hydride fuels only ~1.6×10^{-4} of the fission product gasses would be released from the fuel due primarily to recoil [5]. At the 20 Atm limit, the volume of this gas would be 0.313cm^3 in 200 years. Since the core is designed with expansion space for the core to swell due to radiation damage [~2.4% or 60.2cm^3] and thermal expansion, this gas pressure would be insignificant for the 200 year period

Radiation damage: The final method of core degradation is due to radiation damage. This damage is caused by the radiation and will be proportional to energy deposition. This will primarily affect the fuel core as most fission fragments and beta

particles will not reach the outer layers of the reactor. As a result most of the damage will occur in the U-$ZrH_{1.65}$ fuel.

The LiH will quickly anneal out any radiation damage and experiments have observed that LiH will not retain any damage at temperatures >600°C [9]. The beryllium will receive the least amount of radiation damage and will also anneal a large fraction of the damage due to the low rate of damage and the hot temperature of the beryllium. Based on beryllium irradiation in test reactors, the fast neutron flux will cause the most damage and that swelling and other radiation effects will be insignificant at fast neutron fluencies of $<6.5x10^{19}$ n/cm^2 at >1 Mev [10]. MCNP tallies show that the average neutron flux >1 MeV in the beryllium reflector is $1.71x10^{-4}$ n/cm^2/fission. As a result the radiation damage in the reflector is insignificant for ≈160 Years

The radiation damage in the fuel will be quite significant. The fission fragments will deposit the bulk of the fission energy here and the resulting fission products will build up here causing swelling and chemical changes. These effects have been measured for both TRIGA and SNAP reactors, but these are measured at much higher specific power [11]. To better assess this, low specific power fuel testing would need to be done. For now, it will be assumed that the radiation damage in the fuel at low burn-up rate will be similar to that observed in other ZrH_X fuels at higher burn-up rates. In other ZrH_X fuels the radiation damage causes swelling in two stages [5]: 1-offset swelling that occurs early in core life and 2-nearly linear swelling due to the buildup of fission products and gasses on the fuel. Using MCNP the reactivity effect of swelling is 2.154$ per 1% swell [which is 33.56°C/%].

The offset swelling is highly temperature dependent and was found to be nonexistent at ~700°C, but will grow to be quite large at temperatures of 760°C [5]. From Chapter 4 the fuel temperature ranged from 678°C to 747°C with an average temperature of 690.6°C. The offset swelling that occurs early in core life saturates at a burn-up of ~$1.0x10^{-3}$ fissions per initial metal atom [5], which is the equivalent to a burn-

up of 0.412% of the fuel or 38.8 years of burn-up. To find the total swelling, the swelling as a function of temperature is integrated over to core volume using the temperature distribution for Chapter 4. The total offset swelling will reach 0.859%, which would cause a temperature drop of 28.8°C, which is quite significant. The offset swelling is nearly linear for these 38.8 years so the temperature drop rate will be considered constant at 0.743°C/year.

The linear swelling rate due to fission product buildup is larger in hydride fuels than in oxide fuels. Other ZrH_X fuels swell at ≈3% swell per % fissions per initial metal atom [5]. In 200 years the core burns 2.12% of the U-233 or 0.515% of the initial metal atoms. Thus the swell would be 1.55% over the entire 200 years which corresponds to a temperature drop of 0.259°C/year.

This radiation damage is well characterized over 200, years which is only a burn-up of 17.8 GWD/MTHM. Several hydride fuels have been tested to well over this burn-up [12]. The core is designed to accommodate this small amount of swelling of the fuel into the LiH, which is near its melting point and quite soft.

Higher Order: Each of these core limiting effects are viewed in isolation from the others. So long as each effect is individually small such an approach is appropriate. However, as the core ages each mechanism will affect the others and the higher order effects will become dominant. For example while hydrogen migration out of the reactor is insignificant early in core life [≈0.005°C over the 100 year frame] due to the low permeability of beryllium. The radiation damage and pressure effects could cause cracks or other migration pathways later in life that allow the hydrogen to escape at a much higher rate [13]. Since it is not possible at this time to evaluate these higher order effects, the evaluation of core life will be limited to 200 years.

Total: The sum of each of these effects are added together to show the rate of temperature drop in Figure 5.4. For reference the approximate temperature drop from a hypothetical RTG is shown for both Pu-238 and Am-241 fuel for comparison [14]. As one can see the life of the core will depend on the temperature drop that is allowed. Maintaining a strict ±5°C band limits core life to ≈8 years. Using the knee approach and the same temperature drop as the ASRG [15] would allow a core life of ≈90 Years. At this point the next step is to look to extend the life of the core by using neutron poisons.

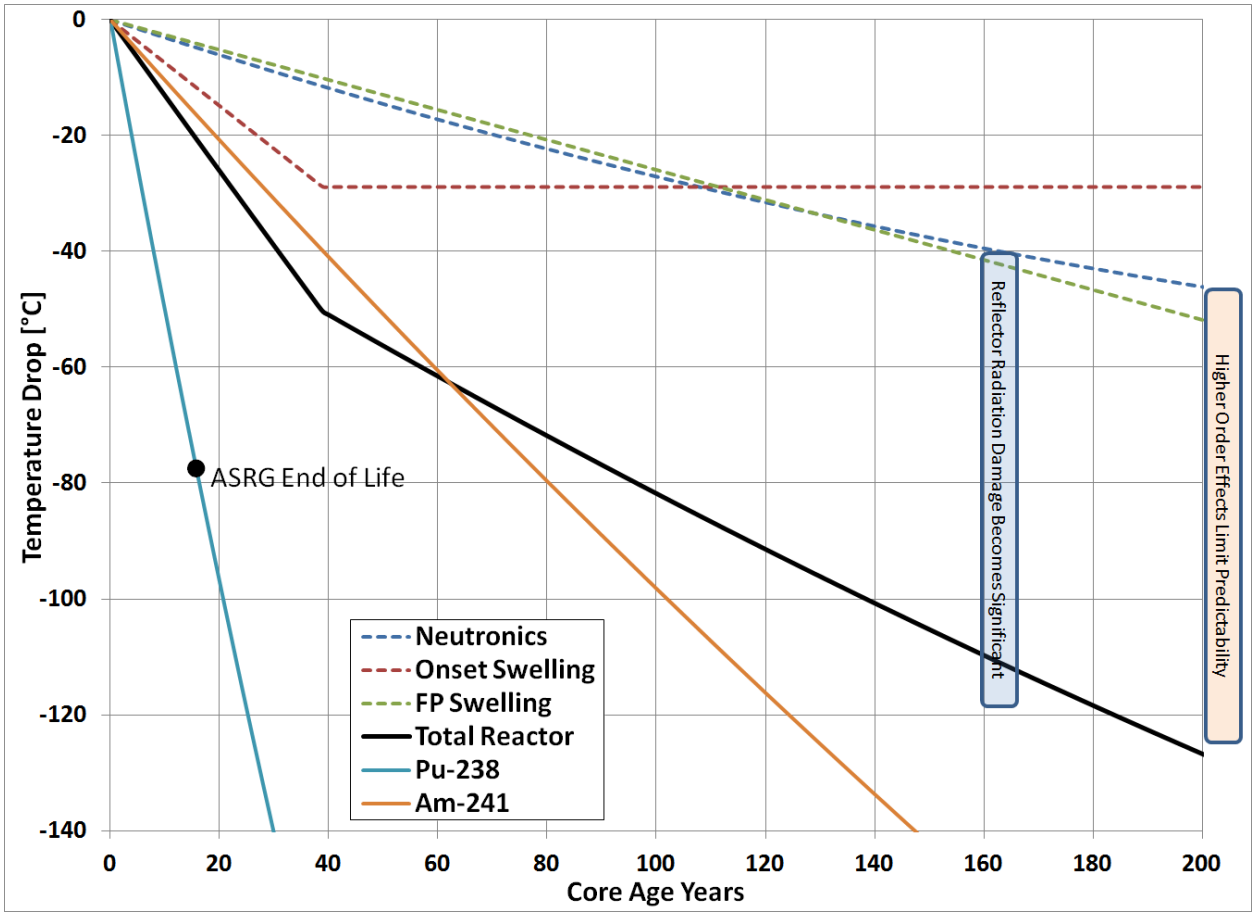

Figure 5.4: Total Temperature drop without poisons. This graph total temperature drop with time with the major components shown. The Pu-238 and Am-241 are based on 650°C source and 80°C with a radiator as a sink and linear relation between Power and Temperature between the sources and sink.

Section 2: Poison Loading

All of the previous effects reduced core temperature because they added negative reactivity. However, the use of pre-loaded poisons will cause the temperature to rise as they are removed by capture. This will add to the mass of the reactor since poisons will have mass and additional fuel must be added to compensate for the negative reactivity to allow the reactor is remain critical [1]. To evaluate this capability we will start using an analytical model based on considering the reactor a thermal system and the use MCNP to evaluate the model.

Additional Poisons: The first step will be to determine which nuclei can be used as a poison. While any material that is not fissile can be a poison, the poison should be selected to have a large cross section for several reasons:

1- Less poison mass will be needed reducing core mass.
2- The poison must be consumed faster than the, fuel which means its absorption cross section should be much larger than U-233 fissions cross section [531b]
3- It is desirable to consume most of the poison by the end of core life [≈2.12% U-233], which means its absorption cross section should be an order of magnitude larger than U-233 fissions cross section [a cutoff of 3000b is used to be >>531b].

Additionally, the poison should be available, not decay [which excludes Xe-135 despite its large cross section] and have a capture product that does not have a significant impact on the core. The list of possible nuclides is shown in Table 5.1.

Of these He-3, cannot be used since the H-3 product will decay back to He-3 and thus the poison will not be consumed [3]. Enriched B-10 is commercially available but enrichment for the other poisons is not currently available. As a result the other elements with low natural enrichments or cross sections are not feasible [Hg and Os]. This leaves 5 elements as possible poisons. One of the possible poisons is Sm-149 which is also a fission product that builds up in the core. As was mentioned earlier, if the core is preloaded with the equilibrium concentration of Sm-149 then there would be no negative effect from Sm-149 build-up [1]. This will be the first poison explored.

Table 5.1: Possible poisons sorted by cross section [2][16][3].

	σ_A [barns]	Elemental Abundance	Element σ_A [barns]	Mass/ σ_A [AMU/10^4 barns]
Gd-157	259,000	15.65%	49,700	31.6
Gd-155	61,100	14.80%	49,700	31.6
Sm-149	42,080	13.82%	5,922	254
Cd-113	20,600	12.22%	2,520	446
Eu-151	9,100	47.81%	4,530	335
He-3	5,333	1.37ppm	0.00747	5.63
B-10	3,835	19.90%	767	26.1
Hg-196	3,080	0.15%	372	5,392
Os-184	3,000	0.02%	16	118,894

Only poisons with thermal cross sections >3000b are shown. Selected Elements in Gold. The Mass/ σ_A Is for Naturally occurring elements except B-10 and He-3 which are 100% enriched.

Samarium Build-up: The Sm-149 build-up was first looked at in chapter 3, however, that early model was based on an thermal system. Since there is large amount of resonance absorption and fast fission in the core, the Samarium is instead modeled in MCNP to determine equilibrium concentration and reactivity effects. This was done by running the MCNP BURN routine, while allowing only Sm-149 to buildup [the fuel was fixed]. This showed that the equilibrium concentration was higher, but the reactivity effect is nearly the same and as a result the build-up time is longer than the Chapter 3 model. The equilibrium concentration is 2.80×10^{-4} atoms per U-233 and causing a reactivity effect of 17.06°C with a life time of 412 years [A factor of ≈2.5x the thermal model].

This was repeated for the other poisons as well [artificially produced as a fission product]. The same effects of resonance absorption and fast fission were seen and this removed B-10 and europium as possible poisons. [B-10 was found to have nearly the same residence time as U-233 meaning it is not removed faster than the fuel].

Equilibrium Samarium: The residence time of preloaded samarium is the same as the build-up time of the fission samarium with an initial temperature drop the same as the final temperature drop of the fission samarium. To counter the initial drop in

temperature the core is loaded with additional U-233. For the equilibrium concentration an added mass of U-233 is 3.42 g and 1.55 g of Sm-149. Since the U-233 is in hydride fuel the mass increase is actually 7.61 g. Additionally the samarium may be added as natural samarium which is only 13.82% Sm-149 and loaded as an oxide as Sm_2O_3. This means the total added Sm_2O_3 mass for one equilibrium loading of samarium is 13.0 g [Only 1.80 g if Sm-149 is enriched]. The effect of pre-loading this samarium on core life is shown in Figure 5.5 and 5.6.

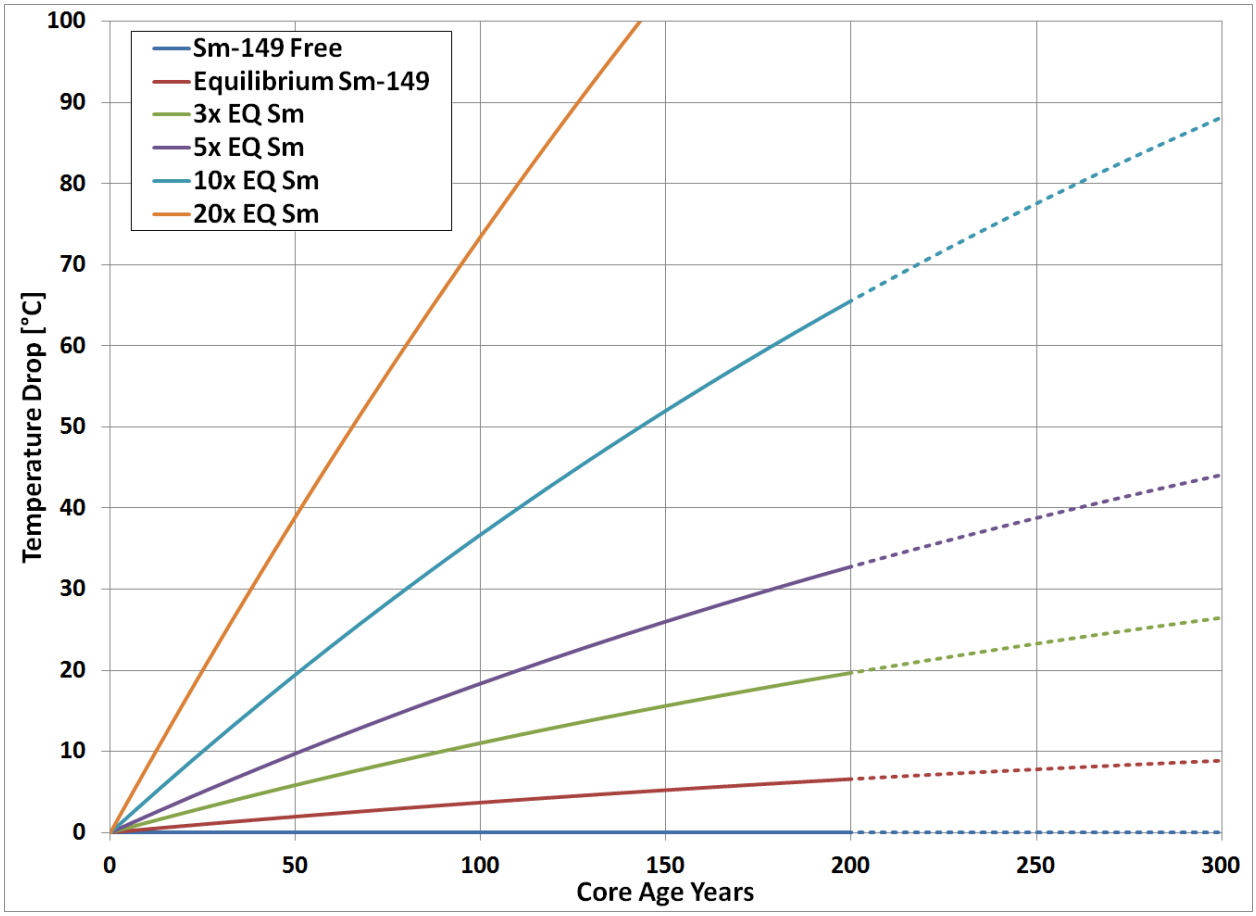

Figure 5.5: Effect of Samarium Loading. This graph shows the temperature rise relative to the poison free model due to the burn-up of poison samarium. 1x EQ Sm is equal to is 13.0 g added Sm_2O_3 plus 7.61 g hydride fuel containing 45 w% U-233.

Since the mass added [20.6 g] is rather insignificant the core can be loaded with greater than one equilibrium concentration samarium. Each additional equilibrium concentration of samarium raises temperature by ≈6.5°C over first 200 years.

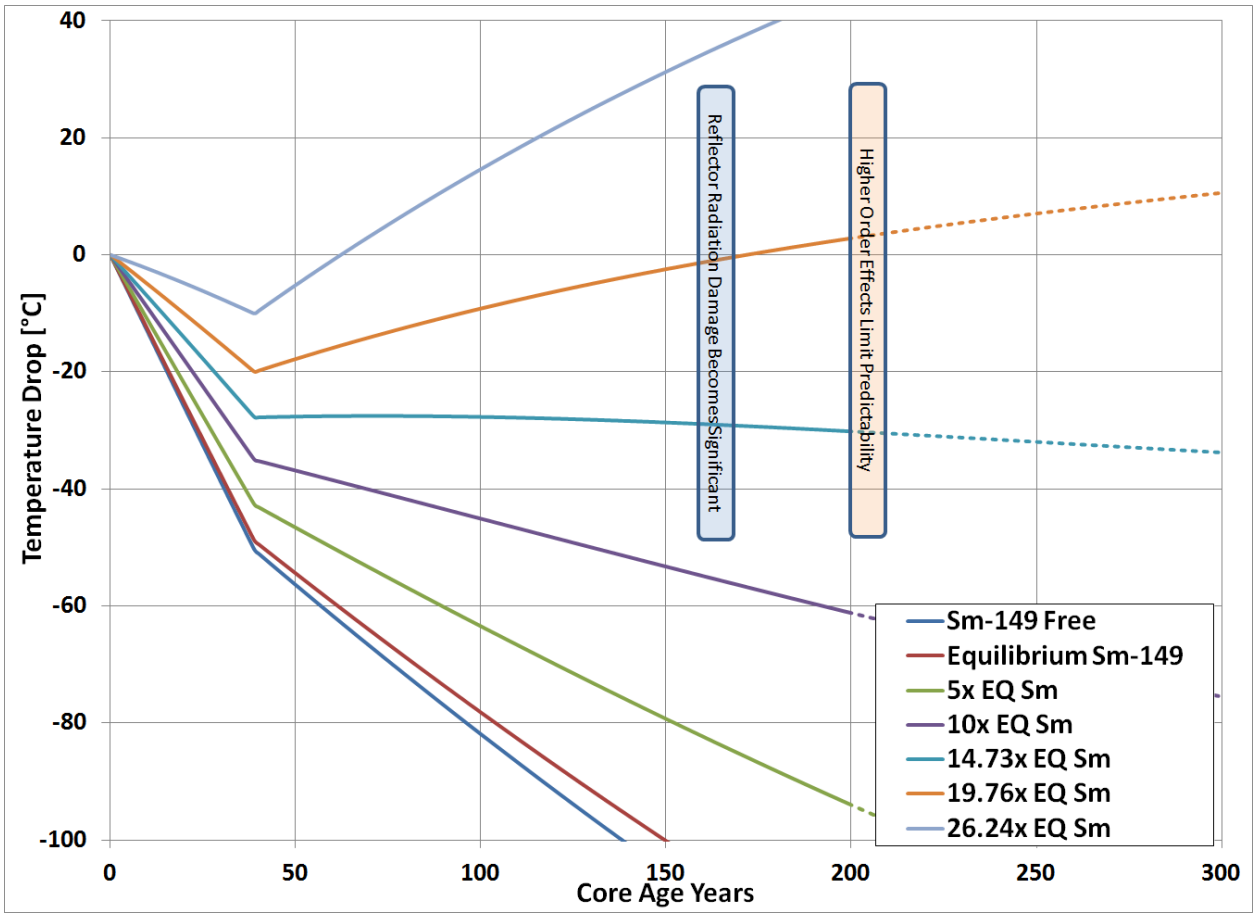

Figure 5.6: Temperature with Samarium loading. This graph shows the total temperature effect due to the burn-up of poison samarium. 1x EQ Sm is equal to is 13.0 g added Sm_2O_3 plus 7.61 g hydride fuel containing 45 w% U-233.

The core could easily be made to stay within the knee definition of core life. The ability of a small added mass [≪Kg] to keep the temperature of the reactor within a much more restrictive band [20°C band in Figure 5.6] for 100's of years is the reason the more restrictive small band definition of core life is able to be used. Using Sm-149 as the Poison the core can be made to stay within a 20°C band by using 407 g of added mass. [This is why Model F of Figure 3.5 weighs slightly more than the other model reactors; it includes poison mass and extra fuel to stay critical].

Gadolinium: These were the only two other possible poisons. Cadmium was found to perform slightly worse than samarium and is not considered further. Gd-155 is

also very similar to Sm-149 in performance. However Gd-157 has a much larger cross section and shorter residence time. Additionally natural gadolinium has both Gd-155 and Gd-157 present which reduces the mass of poisons that need to be added. To add the same 17°C temperature drop only 3.03 g of natural Gd_2O_3 is needed compared to the 13.0 g of Sm_2O_3. The temperature effect of gadolinium is shown in figure 5.7.

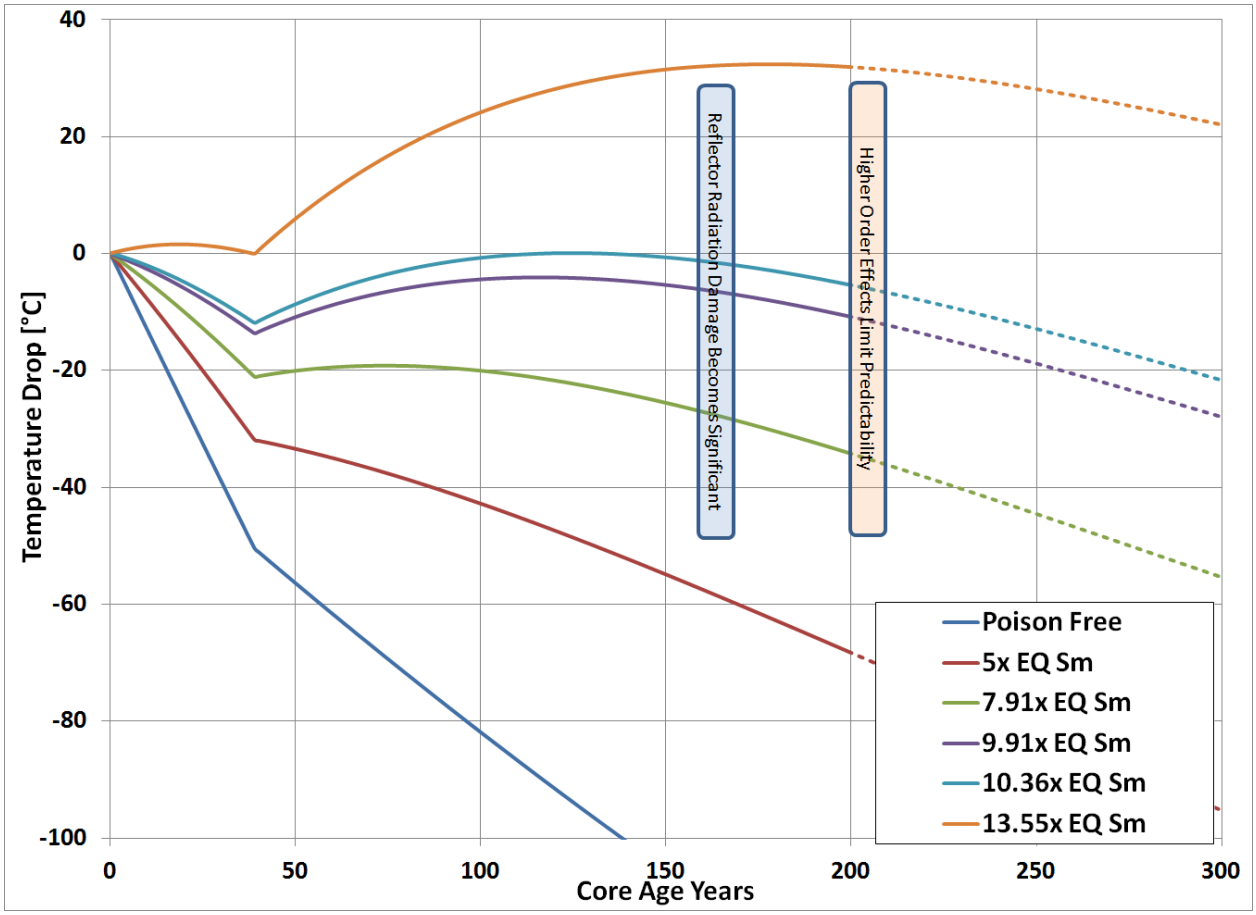

Figure 5.7: Temperature with Gadolinium loading. This graph shows the total temperature effect due to the burn-up of poison gadolinium. 1x EQ Sm is equal to is 3.03 g added Gd_2O_3 plus 7.61 g hydride fuel containing 45 w% U-233.

The smallest temperature band of 11.9°C across occurs with 10.36 time equilibrium Sm-149 loading. Starting the Reactor at 6°C on the high side of the band, the temperature will remain in a ±6°C band. This requires 31.4 g of Gd_2O_3 and 78.8g of added fuel for a total mass increase of 110g [A 0.408% increase in reactor mass].

Detailed Poison Model: The previous model was based a linear response to poison loading with no change to core parameters over the core life. As poisons are loaded, the fraction of neutrons that are thermalized will decrease, which both lowers the temperature coefficient of reactivity and the net worth of future additional poisons. Additionally as the core ages the physical swelling of the core and buildup of fission products will also affect the fraction of thermal neutrons. To address these effects, a more detailed computer model was created. A Matlab routine was created where MCNP would burn the fuel for one year and then the fuel was physically changed to account for offset and linear swelling and the core parameters would be recalculated. This process is then repeated for a total burn-up of 300 years.

While this process should be more accurate than the previous method, it had one drawback: the process is very slow. At each step the core burn-up using BURN is a lengthy process requires nearly a hour of computer time [to determine reactivity to within ±2°C] and then the cores temperature profile and the reactivity coefficients are recomputed [Same methods as Chapter 3 and 4]. As a result, each run of the detailed poison model required nearly two weeks of computer run time.

The results did not significantly change from the previous model. The temperatures dropped more than expected so additional runs were conducted with increased poison loading. The minimum temperature band was found to occur with a Gadolinium loading of 12.1x instead of the previous 10.36x which increased the total mass increase to 128 g from 110 g. The temperature band is also slightly larger at ±≈6.4°C.

While a significant amount of work went into this model, it had little effect on the conclusion that a reactor could be designed to maintain temperature in a very narrow band using burnable poisons over the design core life.

Section 3: Increasing core life

While reactor life could be extended into the 200-1000 year range, there is little use for power durations this long [See chapter 2 for details]. Still it is useful to explore way to extend core life in to this regime.

Reduced Temperature Mode: By using the knee definition of core life and assuming the higher order effects remain small, the core may still produce reliable power for ≈615 years. This mode is akin to the Voyager probes which are still operating with reduced loads [17]. The temperature drop will reduce efficiency and as a result power output. In this region, the core thermal power will remain nearly constant, but electrical power would drop from 500W to ≈300W in the time frame of 200-615 years.

Reduced Power Mode: Alternatively, core life can be extended by using less power and thus there would be less fuel burn-up and core damage. At half power, the core life would be doubled to 400 years. This process however has two limitations: 1-There is a minimum critical heat load and 2-the fuel will alpha decay while in standby power. The minimum heat loads will be radiative losses [140W] and heat leakage through the heat engine [See Chapter 4]. The radiative heat load in standby is ≈10% full power. Reactivity is lost when the U-233 in the core alpha decays to Th-229 with a half-life of 159,200 Years [3]. The temperature of the core would be reduced by 5°C by this process in a period of 749 Year. Combining these two possesses means that the reactor would only operate at half power for 331 Years before temperature dropped 6.4°C.

Use control rods: Adding control rods would allow the core temperature to be actively maintained [18]. This option would not necessarily need initial poison loading but poisons could still be used. Core life using control rods would last until either: 1-the total reactivity worth of the rods is used which could be on the order of 100-200 GWD/MTHM [1,000-2,000 years] or 2-The higher order effect causes a reactivity swing

larger than the rods can control [for example a hydrogen leak]. This method however requires added mass for the rods and control mechanism and reactor instrumentation.

Use chained cores: The probe could be launched with 2 or more reactors. The first core would run until power reached a set level and then the second core would be started up. While this would greatly extend the probe life, it would add considerable mass.

Redesign the reactor: Using control rods or multiple cores would increase the mass of the system. If this additional life is needed, it may be more effective to redesign the reactor instead with more mass to start with. This falls into the category of Mid-Power deep Space reactor of Figure 1.2 and will not be discussed here.

Reduced Temperature and Power Mode: Without adding mass, the core could utilize both the knee region and reduced power to extend core life further than either method alone. Table 5.2 below lists several possible combinations that could be utilized.

Table 5.2: Reduced average power regions.

Thermal Power	Electric Power	Time in ±6.4° Band	≈ Electric Power	≈additional Time in Knee Region
100%	100%	200	61%	415
90%	89%	217	53%	462
80%	78%	238	46%	520
70%	67%	262	39%	595
60%	56%	293	32%	694
50%	45%	331	25%	831
40%	34%	381	18%	1,032
30%	23%	448	10%	1,355
20%	12%	545		

Section 4: Summary

In this chapter, the issue of core life was covered. It should be clear that the reactor could be maintained critical and in a narrow temperature band through the design life of 100 years. Additionally, the core is expected to last to ≈200 years in the narrow temperature range with ≈400 years possible in the knee region. Additionally, it is possible to extend life at reduced power if this is desired.

References [Chapter 5]

[1] J.J. Duderstadt and L.J. Hamilton, “Nuclear Reactor Analysis”, John Wiley & Sons Inc (1975)
[2] National Nuclear Data Center, http://www.nndc.bnl.gov/
[3] Edward Baum, “Nuclides and Isotopes: Chart of the Nuclides”, Lockheed Martin (2009)
[4] Denise Pelowitz, “MCNP User Manual”, Los Alamos (2008)
[5] D. Olander, et al “Uranium-Zirconium Hydride Fuel Properties” Nuclear Engineering and Design, 239, pp. 1406 (2009)
[6] E. Dologlou “Hydrogen and Deuterium Diffusion in Lithium Hydride” Journal of Applied Physics, 107, p. 107 (2010)
[7] S.A. Steward “Review of Hydrogen Isotope Permeability Through Materials” Lawrence Livermore National Laboratory, Livermore, CA (1983)
[8] “Beryllium Properties”, Advanced Energy Technology Group (2012) http://aries.ucsd.edu/LIB/PROPS/PANOS/be.html
[9] R.L. Smith and J.W. Miser “Compilation of the Properties of Lithium Hydride” Lewis Research Center, Cleveland, OH (1962)
[10] “Swelling, Helium release and Creep of Irradiated Beryllium After Annealing” Scientific Report (2005)
[11] M.T. Simnad, et al “Fuel Elements for Pulsed Triga Research Reactors” Nuclear Techonology, 28, pp. 31 (1976)
[12] M.T. Simnad “The U-Zr¬x Alloy: Its Properties and Use in Triga Fuel” (1980)
[13] T.A. Tomberlin “Beryllium-A Unique Material in Nuclear Applications” Idaho National Engineering and Environmental Laboratory (2004)
[14] J.G. Wood, et al “Free-Piston Stirling Power Conversion Unit for Fission Surface Power, Phase I Final Report” NASA (2010)
[15] R.K. Shaltens and W.A. Wong “Advanced Stirling Technology Development at NASA Glenn Research Center” NASA (2007)
[16] Neutron Scattering Lengths and Cross Sections, NIST Data, ATI (2001)
[17] G.L. Bennett “Space Nuclear Power: Opening the Final Frontier” IECEC, San Diego, CA (2006)
[18] D.I. Poston, et al “A Simple, Low-Power Fission Reactor for Space Exploration Power Systems” Proceedings of Nuclear and Emerging Technologies for Space, Albuquerque, NM (2013)

Chapter 6: Shielding

In this chapter the issue shielding the probe from high energy gamma and neutrons produced in the reactor is covered. The objective is to determine the mass of the shielding needed through the design core life. This is a key concern as the mass of shielding can be considerable. The SP100 shielding weighed 970 kg [1], which was more massive than the core itself. Since the design mass limit is 75 kg and the reactor is ≈27 kg this means the shielding should be ≈<48 kg.

Section 1: Sources of radiation

As a starting point the reactor will be considered a point source, but in Section 4, a full 3D model of the reactor source will be used.

Reactor: As mentioned previously, the reactor emits two types of penetrating radiation: gamma rays and neutrons [2]. These account for 2.581% and 6.664% of the fission energy respectively [3]. For the reactor producing 2112 W_{TH} and lasting 200 years this amounts to 1.232×10^{12} J of radiation, which would cause considerable radiation damage.

The reactor, however, is self-shielding. The absorption tenth thickness [absorbs 90% of the incident radiation in this distance] of Uranium for 1 MeV gammas is 2.86 cm [4] and the core is ≈7 cm thick (of 45w/% uranium in zirconium hydride). The fuel will additionally absorb a large fraction of the neutrons. Additionally the moderator and reflector will further attenuate both the neutrons and gammas. To account for self shielding the MCNP model of the reactor was run and the neutron and gamma at 1m from the center of the core was determined.

The self shielding of the reactor attenuates the total neutron and gamma energy release by a factor of 15.5 to only 12.6 W of nuclear radiation energy leaving the core. The total fluence at 1 m from the core is 3.29×10^5 J/cm^2 for neutrons and 3.02×10^5 J/cm^2 for gammas. The resulting gammas and neutron fluence as a function of particle energy is shown are shown in Figure 6.1.

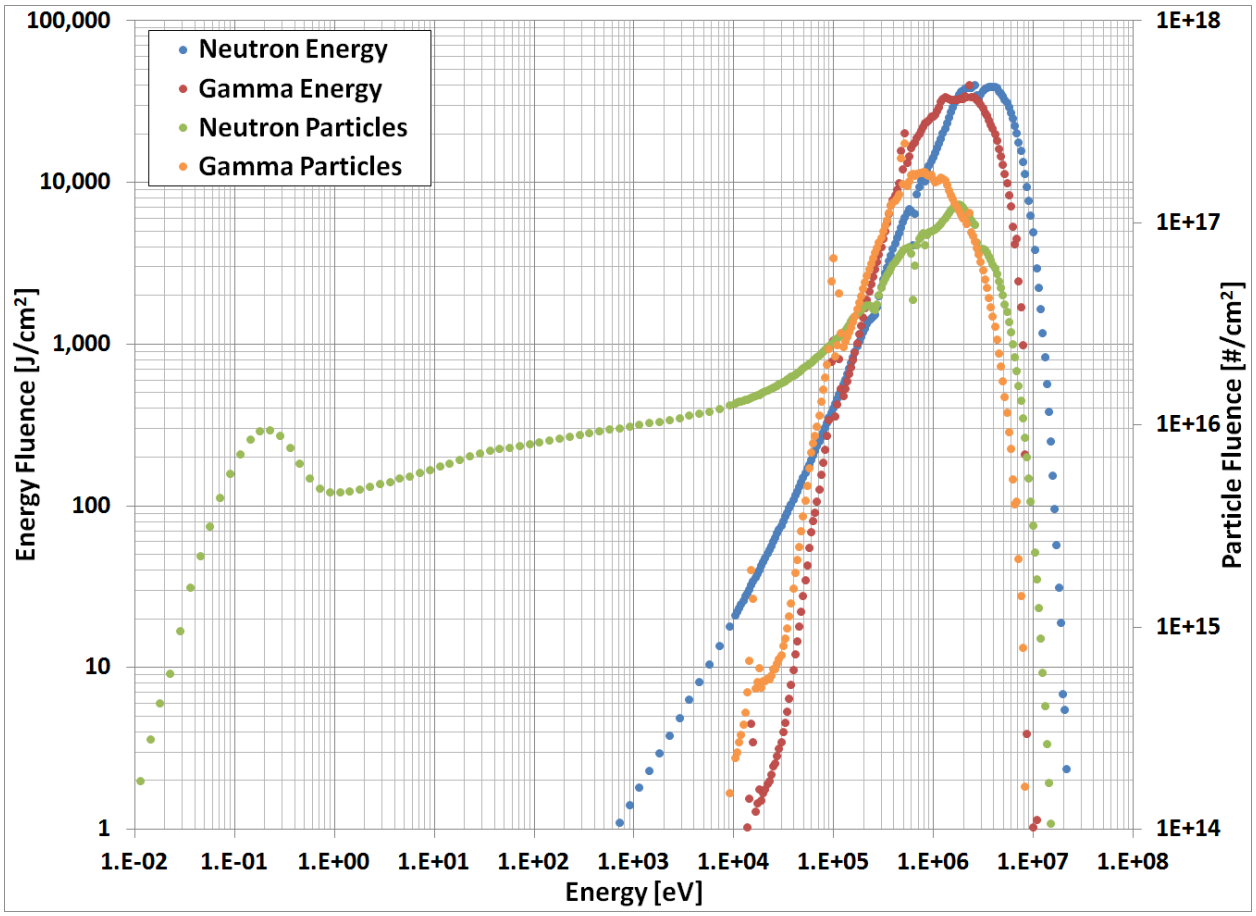

Figure 6.1: Fluence at 1m from the core during 200 years of operation. The fluence is per each logarithmic energy bin with step size of $10^{0.1}$. From 10^{-3} to 10^4 eV the measurement size equals the bin size and from 10^4 to 10^8 eV the measurement size equals ⅛ the bin size. This measurement based on 200 years of operation

From this, the bulk of the energy from gammas [99.8%] and neutrons [98.7%] falls in the range of 0.1-10 MeV and as a result this is the energy range it will be most important to shield. The average energy of the neutrons is 1.15 MeV and the average

energy for the gammas is 1.09 MeV. The thermal tail of neutrons will be insignificant since they are easy to shield and do not significantly affect radiation hardened electronics [5][6].

Just as important as the energy distribution is the radiation angular and spatial direction. MCNP was run to tally the fluence received at the spacecraft payload as a function direction of travel [Actually the cosine of the angle with the radial direction]. This can be interpreted as the radial distance from the origin that the radiation was emitted, which would determine the width of shielding needed [7]. This is shown in figure 6.2.

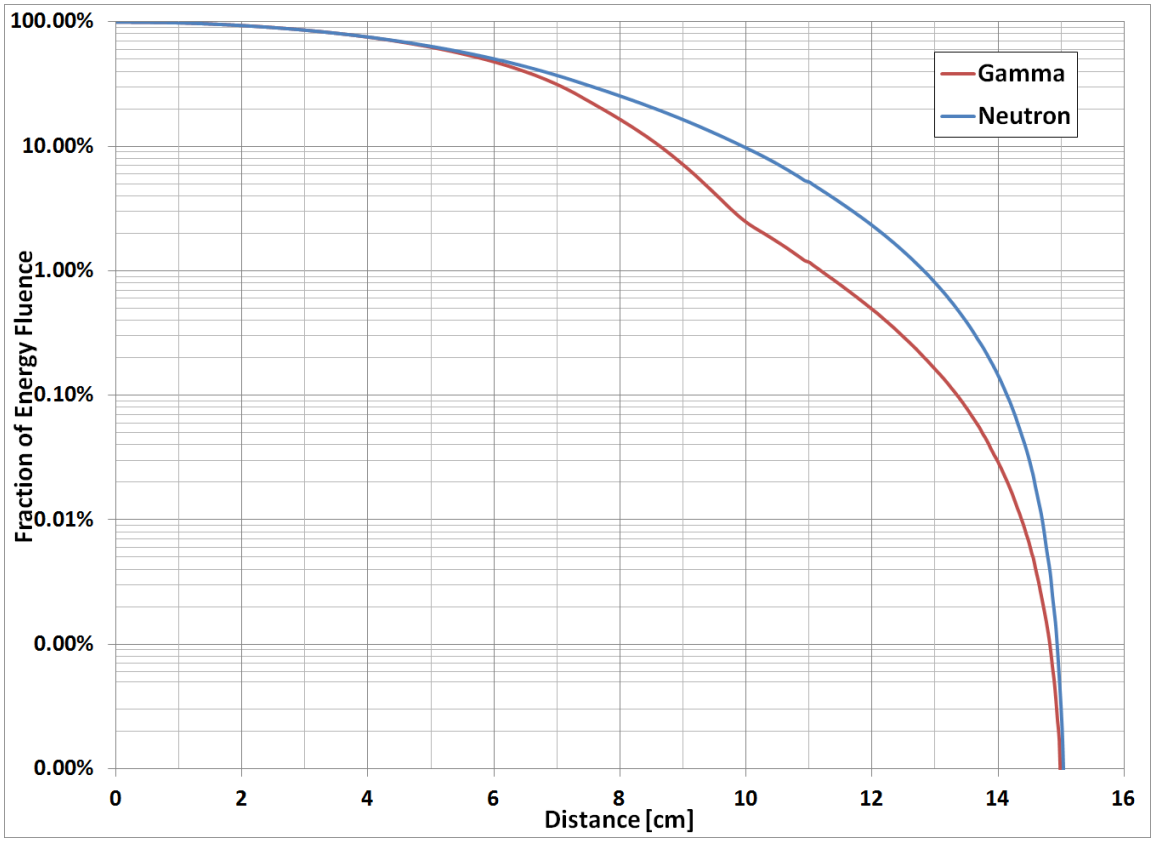

Figure 6.2: Cumulative radiation fraction emitted with distance. This graph is the cumulative fraction of radiation emitted from the reactor as a function of distance. The distance shown is the effective distance based on a straight line trajectory extended to the nearest approach to the center of the core.

Most of the gamma radiation is emitted from the core with the moderator and neutron reflector being less reflective for gamma radiation than neutron radiation [4]. As a result the effective width for gamma shielding should be slightly smaller than neutron shielding. Additionally shielding the edges of the core [the final 10% or 1.5 cm] is much less important [0.1% and 0.5% gamma and neutron] than the centerline between the core and probe. As a result the shield will be expected to have a slightly smaller footprint than the solid angle between the core and probe would suggest [<0.122 sr] [2].

Background Radiation: The background radiation that the probe is subjected to is important as it forms a baseline for radiation shielding. There is no point of shielding the reactor to reduce radiation below this background since it would not effectively reduce the dose to the probe.

In general, the background dose to the probe will be the sum of the dose from galactic cosmic rays, solar radiation, and any local planetary radiation source. Since the probe will be traveling far from the sun the solar radiation will be quite small. Additionally, planetary radiation will have to be tailored to the particular planetary mission and will not be included here. As a result only galactic cosmic rays will be considered. The currently measured galactic cosmic ray flux [8] is ~30 GeV/cm^2-s, which for the 200 year mission is a fluence of ~30 J/cm^2. Unshielded this amounts to a dose of ~4000 Rad(si). Such cosmic rays are within the sun's magnetic envelope. .

As can be seen in Figure 6.1, the neutron and gamma energy fluence exceeds this amount in the energy ranges of ~15Kev to ~10Mev and the total fluence exceeds this by a factor of ≈800 at a distance of 5m from the core. As a result, there would be little utility in shielding the core to reduce the radiation from the core by more than a factor of 800.

Dose Limits: The next step to determine the amount of shielding needed is to determine the notional dose limits for the probe. The probes will be unmanned and thus biological radiation limits would not be applicable. The limiting components for most probes are the microelectronic circuits [5]. The background radiation in deep space means most electronics will have to be radiation hardened. Microelectronic components in general have both total dose and dose rate limits. The dose limits from the SP-100 are used for reference in this work to set the limit for microelectronic components [1]. If specific probe components require higher shielding, they may be separately shielded or the total reactor shielding may be increased. The applicable dose limits are:

1- Total Gamma Dose $5x10^5$ Rad(si) [1]
2- Total Neutron Fluence of 16.0 J/cm^2 [1]
3- Combined Neutron and Gamma Flux of 0.14W/cm^2 [1]

The 3rd limit is a dose rate limit. For this low power of the reactor, this condition is met on the surface of the reactor and does not need to be considered further. The 1st and 2nd limit are however exceeded at 5m from the core as is shown in Figure 6.3. The gamma dose limit is exceeded by a factor of 60.2 and the neutron fluence limit by a factor of 822.

Distance: The distance between the reactor and the probe is important since dose decreases with distance squared [7]. To reduce the radiation below the dose limits by distance alone the reactor would need to be a distance of 144 m from the spacecraft. A boom of this distance may not be practical so shielding will be needed [1]. The probe and the reactor have fixed sizes and as a result the solid angle between them decreases as the distance is increased. A smaller solid angle will allow the shielding material to have a smaller area, which will decrease mass for the same thickness of shielding.

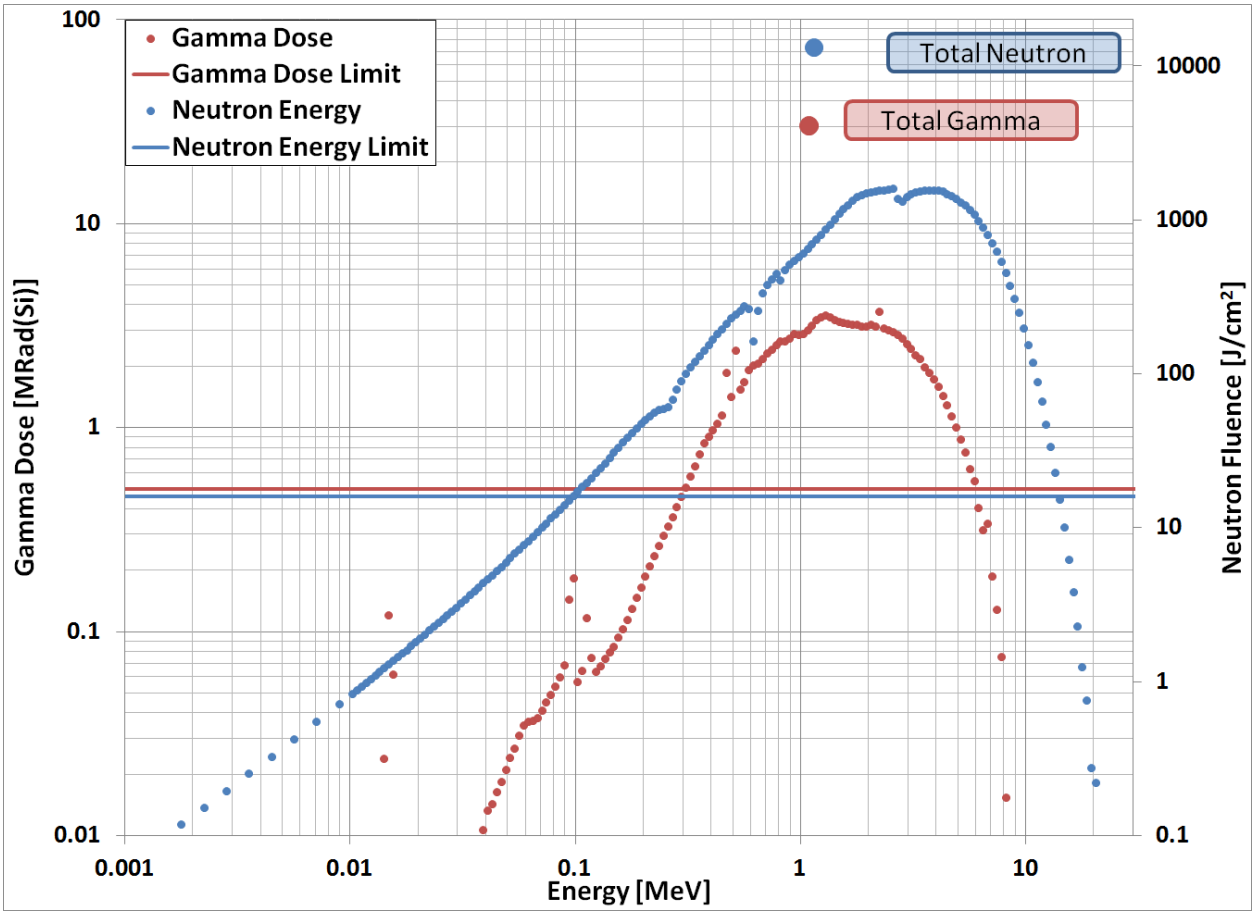

Figure 6.3: Dose at 5m from the Core during 200 years of operation. The Dose and Fluence is per each logarithmic energy bin with step size of $10^{0.1}$. This graph is both the dose as a function of energy and the total dose plotted at the average energy.

For the reference case, the reactor is 5m from the probe, which has a shielded footprint of 1 m radius [These numbers fit well with the size of current probe, but are not definitive]. This is much smaller than past designs such as the SP100 which had a 22.5m boom [1]. If these dimensions are changed based on the actual probe and its mission, then the mass of shielding will have to be recalculated based on the new geometry.

Section 2: Shielding Material

The next step is to select the shielding material which ideally would shield both neutrons and gammas. However, the shielding of neutrons and gammas is significantly different so these will be evaluated separately.

Gamma: The photon mass attenuation coefficients [μ/ρ] for several elements are shown in Figure 6.4 [4]. Also shown is the unshielded gamma dose at 5 m for reference to see what part of the energy spectrum is the most important to shield. Gamma shielding works using 3 effects:

1- Photoelectric effect which dominates at low energy and varies with atomic number Z [$\approx Z^{4-5}$] and as a result this would tend to favor high atomic number material [2].
2- Compton scattering, which dominates at an energy of ≈0.3-6MeV, where most of the dose occurs, and is independent of Z [2]. Compton scattering depends only on the electron density and as a result most materials have nearly the same Compton scattering losses. One exception is H-1, which does not contain neutrons ant thus has only ≈½ the mass per electron [9]. This doubles the μ/ρ of hydrogen relative to other elements [4].
3- Pair production dominates at high energy and varies with atomic number Z [$\approx Z^2$] and as a result this would tend to favor high atomic number material [1].

Because Compton scattering dominates, hydrogen is the best candidate for a gamma shielding material [and is useful in neutron shielding as well]. There are two drawbacks: 1-hydrogen containing materials often have little hydrogen on a mass basis and tend to have low density. The low density is important since the area that needs to be shielded increases with the distance from the reactor. 2- Compton Scattering does not eliminate gammas but scatters gammas to a lower energy and altered direction. If the direction changes enough, the gamma will no longer reach the probe, otherwise a second collision is needed. The second collision will be at a lower energy than the first, which pushes the spectrum into the Photoelectric Effect region [2].

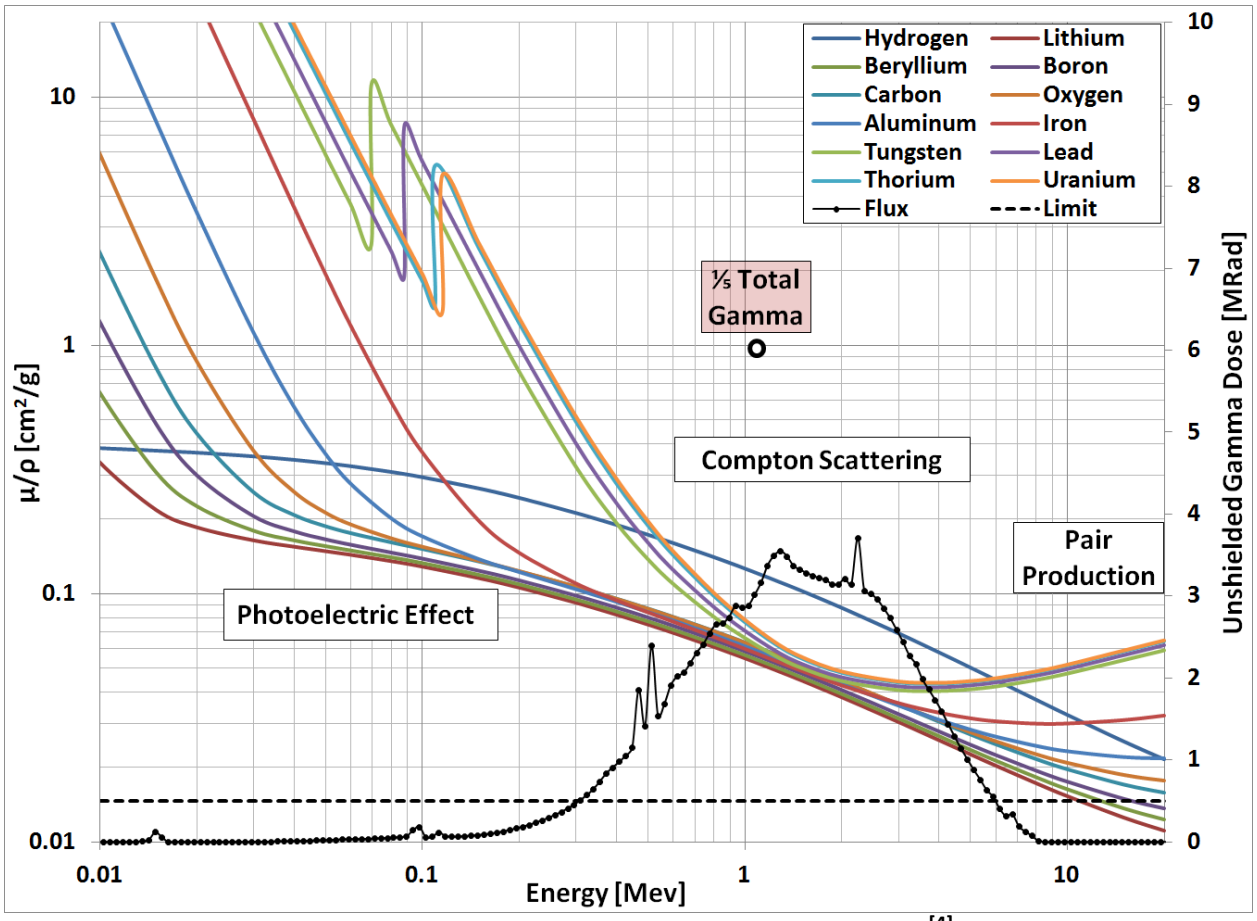

Figure 6.4: Photon Mass Attenuation Coefficients with Gamma Dose [4]. The dose is per each logarithmic energy bin with step size of $10^{0.1}$ at a distance of 5m. This graph is a comparison of gamma shielding effectiveness with the gamma dose to aid in determining shielding materials.

As a result high density, high Z material would be selected as the gamma shielding material. However, materials that may fission should not be used because of the fast neutron flux present which eliminates U-238 and Th-232 as possible gamma shielding materials [3]. The high density, high Z requirement limits the shielding material to Z=72 to 83 [9]. The properties of these elements are listed in Table 6.1. A mixture of these elements may also be useful due to non overlapping K band X-rays and neutron resonances. While rare elements such as gold and platinum are 5%-10% better shielding than tungsten, the high cost of these materials make them much less practical.

Neutrons: The neutrons do not need to be absorbed to be eliminated; deflecting them away from the probe into the vacuum of space is as good as absorption.

Then for neutron shielding a material with either large scattering or absorption cross sections would be needed. Since no material has a high cross section for capturing fast neutrons [3], neutron thermalisation will be needed before absorption. All three of these properties were reviewed earlier.

Table 6.1: Possible Gamma Shielding Materials [4][9].

Element	μ/ρ [mm^2/g]	Density [g/cm^3]	MFP [cm]	Element	μ/ρ [mm^2/g]	Density [g/cm^3]	MFP [cm]
Hf	6.50	13.3	1.16	**Pt**	6.86	21.5	0.68
Ta	6.57	16.7	0.91	**Au**	6.95	19.3	0.75
W	6.62	19.3	0.78	**Hg**	6.99	13.5	1.06
Re	6.69	21.0	0.71	**Tl**	7.03	11.9	1.20
Os	6.71	22.6	0.66	**Pb**	7.10	11.4	1.24
Ir	6.79	22.4	0.66	**Bi**	7.21	9.7	1.42

μ/ρ is at 1MeV. The Mean free path is at the listed density. The shaded materials are the ones commonly used for gamma shielding.

There are however a number of differences:

1- The poison cross section is now less important than the cross section to mass ratio and as a result B-10 and Li-6 will be considered with Gadolinium
2- Poisons that emit little or no capture gammas are preferable and as a result Li-6 or B-10 should be used instead of gadolinium [Gd-157 has 7.94 MeV of capture gammas [3], B-10 has only 0.449 MeV of capture gammas [2] and Li-6 emits no capture gammas [3]]
3- The shield will not be at reactor temperature and should be at ≈room temperature [colder in space] and as a result many hydrogen compounds not considered earlier are possible [liquid H_2, CH_4 and NH_3 are still not possible since they require cryogenics [10]]
4- Reflector and Moderator can also absorb neutrons so Li-6 and B-10 are also considered.

Table 6.2 lists the 12 largest nuclei or elements in terms of Neutron Cross Section per mass at fission spectrum neutron energy which well represents the neutron energy distribution from the reactor.

Table 6.2: Neutron Cross sections [3] [Fission Spectrum Average].

Nuclide	σ_{Total} [barns]	σ_S [barns]	σ_{Total}/Mass [barns/AMU]	Element	σ_{Total} [barns]	σ_S [barns]	σ_{Total}/Mass [barns/AMU]
H-1	3.927	3.926	**3.896**	**C**	2.365	2.352	**0.197**
Li-6	1.900	1.422	**0.316**	**F**	3.610	2.324	**0.190**
Be-9	2.834	2.673	**0.314**	**O**	2.750	2.739	**0.172**
B-10	2.638	2.062	**0.263**	**Mg**	3.429	3.088	**0.141**
Li-7	1.845	1.660	**0.263**	**N**	1.964	1.832	**0.140**
B-11	2.425	2.396	**0.220**	**Na**	3.208	3.024	**0.140**

He and Ne are not included as noble gasses; Also H-2 is not included as since H-1 performs better with the same chemical properties.

From the Table it is clear that hydrogen is an order of magnitude higher in neutron cross section per mass than any of the alternatives. However, high density is also useful therefore hydrogen compounds are considered. Several of these are listed in Table 6.3 which is sorted by the mean free path of fission energy neutrons. Also shown is commercially available high density polyethylene [11] [HDPE or [CH_2]] with boron and lithium additives. As it turns out, the best neutron shielding material is the commercially available polyethylene.

Table 6.3: Possible Neutron Shielding Materials [3][10].

	Phase	Temp [˚C]	σ_{Total}/Mass [barns/AMU]	Density [g/cm^3]	MFP [cm]
AlH_3	Solid	150	0.501	1.486	2.229
BNH_6	Solid	104	0.939	0.780	2.268
[CH_2]	Solid	125	0.730	0.970	2.345
NH_3	Solid	-80	0.809	0.817	2.514
BeH_2	Solid	250	0.972	0.650	2.629
N_2H_4	Liquid	114	0.614	1.021	2.650
$LiBH_4$	Solid	275	1.012	0.613	2.675
Be	Solid	1287	0.315	1.848	2.854
B-10	Solid	2075	0.264	2.177	2.892
LiH	Solid	688	0.832	0.689	2.895

Cryogenic Gasses not included. Shading indicates a thermal poison is present. Only compounds with σ_{Total}/Mass >0.5 barn/Amu [with the exception of solid Beryllium and Boron] and MFP<2.9cm shown in the table above. All materials assume Enriched B-10 and Li-6 and un-enriched for the other elements.

Table 6.4: Commercial Neutron Shielding Materials [3][11].

High Density Polyethylene [CH_2]	σ_{Total}/Mass [barns/AMU]	Density [g/cm^3]	MFP [cm]
5 wt% B-10	0.708	1.076	2.179
5 wt% Boron	0.705	1.080	2.181
30 wt% B-10	0.597	1.164	2.389
30 wt% Boron	0.595	1.190	2.345
7.5 wt% Li-6	0.703	1.049	2.252
7.5 wt% Lithium	0.695	1.060	2.254
No additive	0.730	0.970	2.345

Shield Location: As distance from the reactor increases, the mass of shielding goes up with distance squared due to increased shadow size (slightly less when adjacent to reactor due to solid angle and incidence angle [2]). As a result the shield should be flush to the reactor. This also has a positive effect on reactivity due to in-scatter which reduces mass slightly [12] [This effect is already accounted for in the reference model].

Shield Layout: Since a number of materials are needed to effectively shield neutrons and gammas layering of the materials will be needed. A few key points are the denser material [Gamma shield] should be closer to the core because a smaller area is needed close to the core. The layout of an example shielding is shown in figure 6.5.

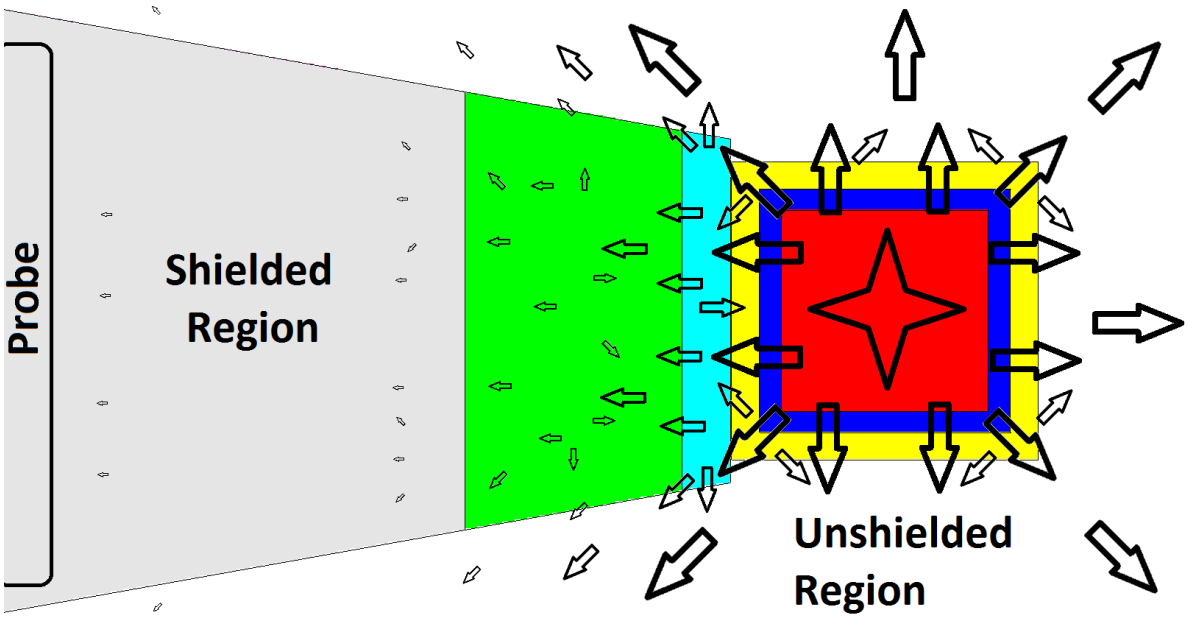

Figure 6.5: Shield Layout illustrating the flow of radiation. The Green and Light Blue regions represent low and high density shielding material respectively. The arrows represent the neutron and gamma fluxes and the Grey area represents the shielded shadow. Arrow size is a qualitative representation of the flux but was not obtained numerically from any calculation.

Section 3: Numerical Results

The next step is to determine the mass of shielding needed. This is done first analytically for illustration and then a computer model was used to solve the shielding mass more exactly.

Analytical: Only two materials will be considered: 1-tungsten as the gamma shielding and 2- 5% B-10 polyethylene as the neutron shield. The gammas will be considered mono-energetic at 1 MeV and only removed by a single collision on the gamma shield. The neutrons will be considered removed following a single collision in the neutron shield. The gamma dose will need to be reduced by a factor of 60.2 and the neutron fluence by a factor of 822. The cross sectional area will be the cross sectional area of the core [451cm^2]. The equation for shielding mass is then Equation 6.1

$$Mass = Area * Density * MFP * \ln\left(\frac{Dose_{Unshielded}}{Dose_{Shielded}}\right) \qquad Equation\ 6.1$$

The gamma shielding will require 4.1 Mean Free Paths [MFP] which is 3.2 cm for a total mass of 27.8 kg. The neutron shielding will require 6.7 MFP which is 14.5 cm for a total mass of 7.04 kg. From this the total shielding mass is 34.9 kg.

The 35 kg of shielding is within the mass limit set and is larger than the mass of the reactor itself. If an additional factor of 10 is used [reduction of gammas by 602 and neutrons by 8220] then the mass of the shielding would be 53 kg, which is not unreasonable given the mass limit of 48 kg. While this result suggests that shielding the reactor is possible, it should be noted that this is an overly simplistic method.

Several issues would raise this mass:

1- The radiation is not mono-energetic and the energies that have the largest MFP will tend to dominate the received dose [13]
2- The cross sectional area is not constant but will increase with distance from the reactor [Cone Shape see figure 6.4]
3- Often 2 or more collisions will be required to remove the radiation

4- Some radiation that is at an angle to leave the cone may be scattered into the shielded region
5- 5-neutron capture will cause secondary gamma radiation [3].

In addition several issues would reduce mass:

1- The neutron shielding is nearly as effective at shielding gammas in the region of interest as the gamma shielding [See Figure 6.3]
2- The gamma shielding will deflect and resonantly absorb neutrons. The high Z material also inelastically scatters neutrons significantly lowering the energy and increasing the collision cross section [3]
3- Many particles travel at an angle through the shield increasing distance traveled
4- Most particles stream from the center of the reactor from the fuel which has ½ the cross sectional area [only 206cm^2].

Since it is difficult to resolve all these issues in an analytical method a more complete model is considered.

Model: MCNP was used to determine the effectiveness of the shield. Matlab was used to create shielding models which were then run in MCNP to determine the neutron and gamma fluence passing through the shield. Similar to Chapter 3, Matlab varied one parameter at a time keeping the shield mass constant until the fluence was minimized in the MCNP runs. Matlab was allowed up to 6 shielding layers [this limited the complexity of the shield] and the shape of each layer was set to be a frustum [7]. Matlab could try any of the 5 gamma shielding materials [shaded in table 6.1] and any of the polyethylene neutron shields. Additionally, the thickness and width of each layer was adjustable. The model varied the ratio between the gamma shielding mass and neutron shielding mass to keep the doses equal relative to the dose limits. The effectiveness of each shield was evaluated by the average dose across a 1 meter radius probe. The results are shown in Figure 6.6.

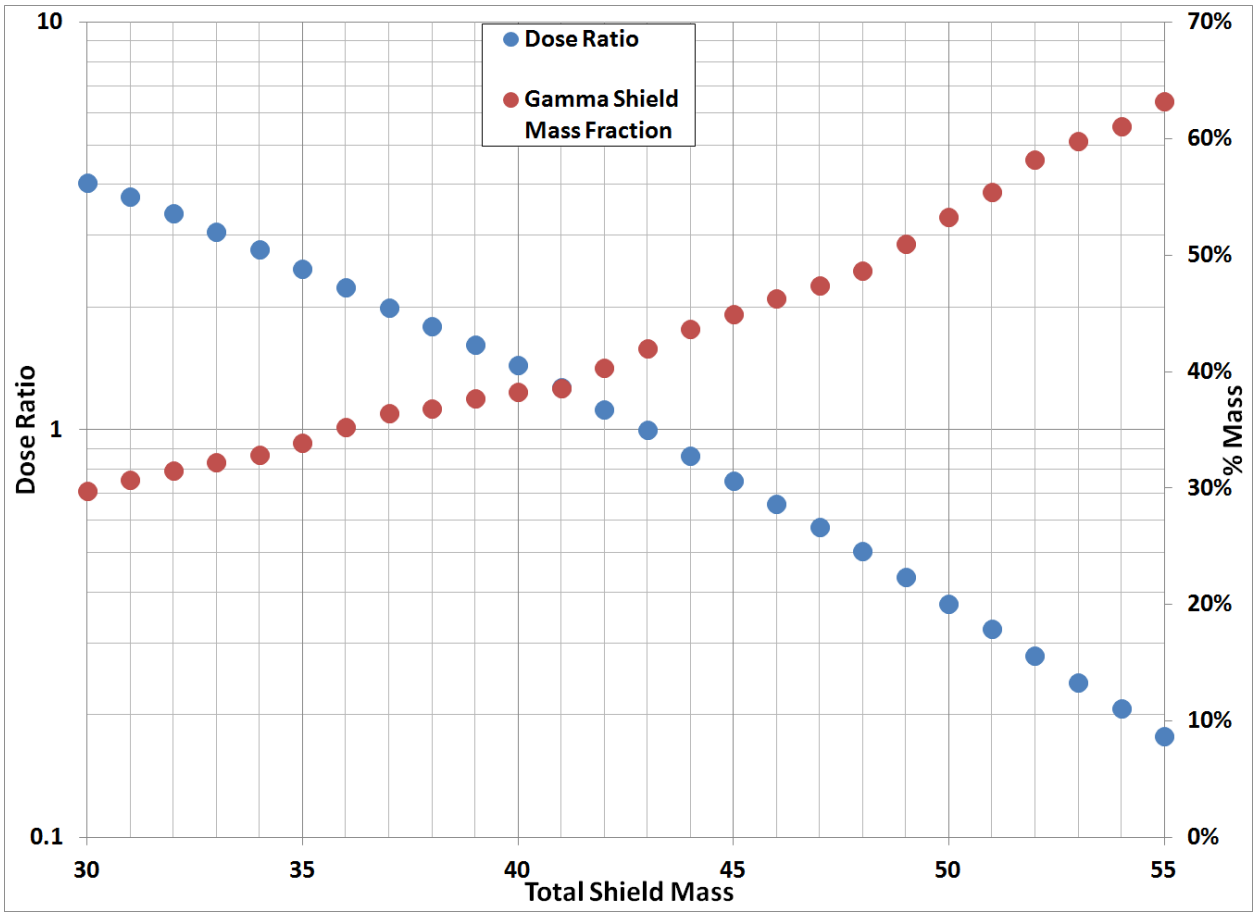

Figure 6.6: Shield Mass Dose and Gamma Fraction. This graph plots the dose ratio and fraction of the total shield devoted to gamma shielding as a function of shield mass allowed. Each mass was individually optimized in Matlab/MCNP.

Variance reduction techniques are needed in MCNP when evaluating shielding due to the nature of Monte Carlo simulation. The specific techniques were used to keep computer run time under 1 minute per evaluation:

1- Geometry splitting [IMP], each shielding layer used an importance function of 4x larger than the previous layer.
2- Exponential Transforms [EXT], the cross sections are artificially transformed to increase mean free path in the direction of the probe.
3- Point detector [F5 Tally], the fluence contribution at the probe is deterministically evaluated at each collision [14].

The shielding that meets the dose limits across the probe has a mass of 43 kg and is shown in Figure 6.7. The computer results of Figure 6.7 are compared to Figure 6.5,

both have the dense gamma shielding adjacent to the reactor. There are two main differences: 1-Figure 6.7 has a layer of polyethylene sandwiched between the denser gamma shielding layers and 2-the width of shielding adjacent to the reactor is less than the width of the reactor to allow the shielding to be thicker for the same mass since most radiation is moving radially [see Figure 6.2].

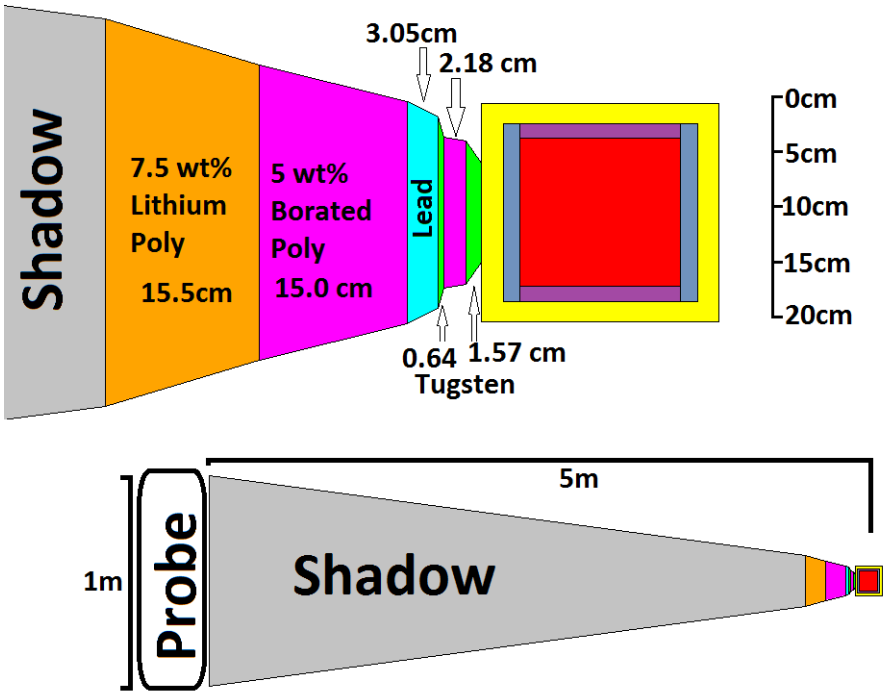

Figure 6.7: Shield layout for the 43Kg Shield. The figure is to scale with the exception of the probe which is taken to be 1m in radius. The shadow region is vacuum and only filled grey for illustrative purposes. There would actually be a gradual transition in radiation levels from the region outside the shadow to within the shadow. The shield layouts for other shield masses differ in geometry and composition as well as the relative position of material layers.

Distance & Time vs. Mass: The mass of the shielding is based on keeping the average dose at the probe 5 m away at exactly the limit based on 200 years of operations. For completeness the model was run several more times at a variety of distances and the results are shown in figure 6.8. Added to the figure is the galactic cosmic ray contribution [8] which will exceed the dose limit in the time frame of 10^4 years [possibly sooner with solar radiation and/or higher galactic cosmic radiation levels

outside the hemisphere]. Additionally, the mass of the shielding can be lowered somewhat by placing the reactor further from the probe [from 43 kg to 20 kg by moving from 5 m to 20 m], but this would be accompanied by increased mass in the boom holding the reactor. At the 5 m distance the change in shielding mass with distance is 3.26 kg/m.

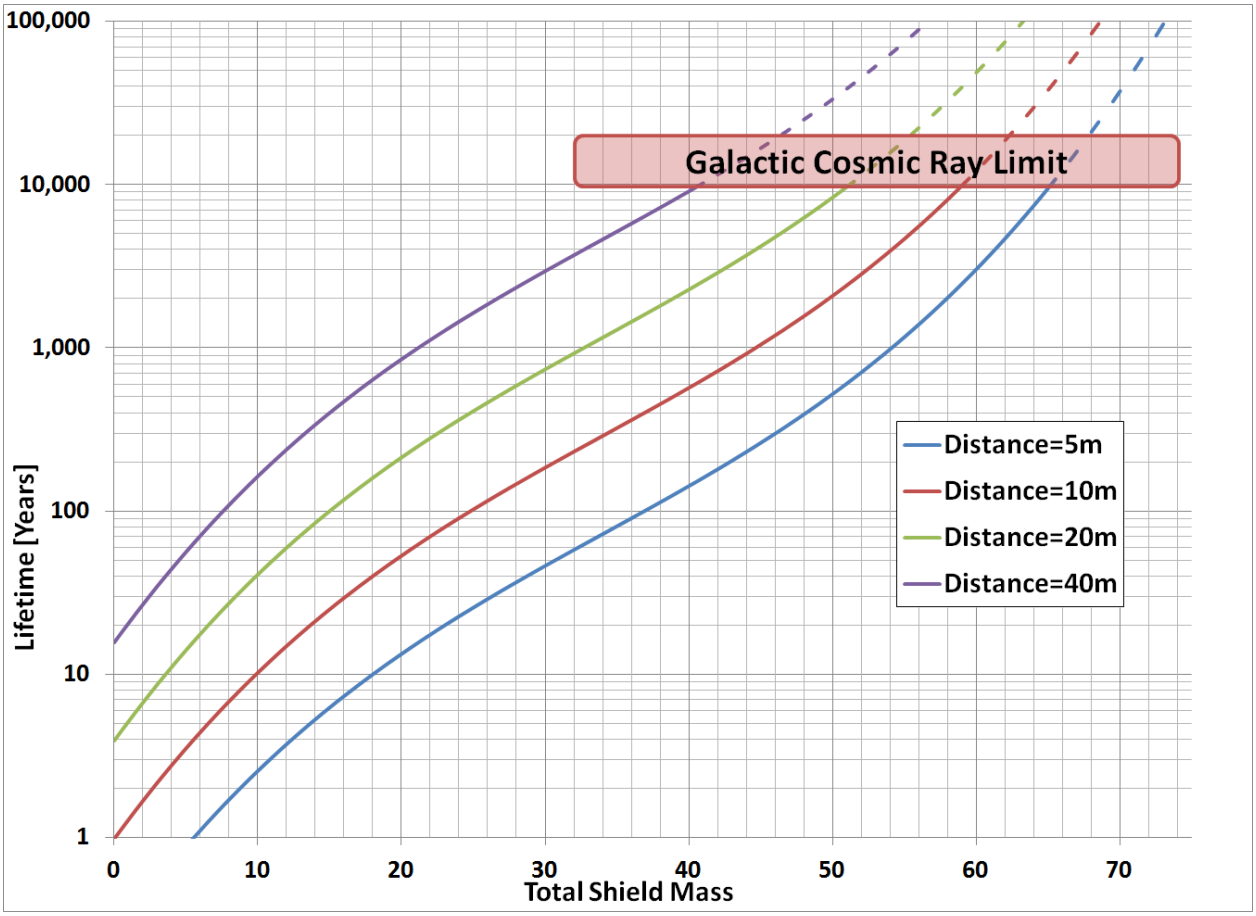

Figure 6.8: Mass vs. time & distance with cosmic rays. This graph plots the lifetime that the probe dose remains within the limits based on shield mass and boom distance. The cosmic ray limit shows that lifetime is limited even without the reactor.

Other shielding not considered: The shielding calculations assume that the only component between the reactor and the probe is the shield. However, this would be a good place to place the heat engine and thermal radiator [See Figure 6.9]. The heat engine and thermal radiator are relatively insensitive to radiation [compared to

microelectronic circuits] and would be within their respective limits even placed adjacent to the shield. The heat engine and thermal radiator would consist of ≈75 kg of metallic mass with iron, copper, titanium and aluminum [15][16] which would provide additional gamma [4] and neutron [3] shielding. However, these would not exist as flat layers and there would be gaps for the radiation to stream between the components. To make proper use of this additional shielding the specific designs of the heat engine and thermal radiator would be needed. Additionally the configuration of the probe would be needed to place the heat engine where it would be most effective [to shadow the most sensitive regions of the probe]. Genetic algorithms should be used in this role to optimize the additional shielding over the current iterative method due to the more complex geometry of the added components. This added shielding will decrease the shielding mass further to <43 kg, but the design mass goal is already met and not considered further at this time.

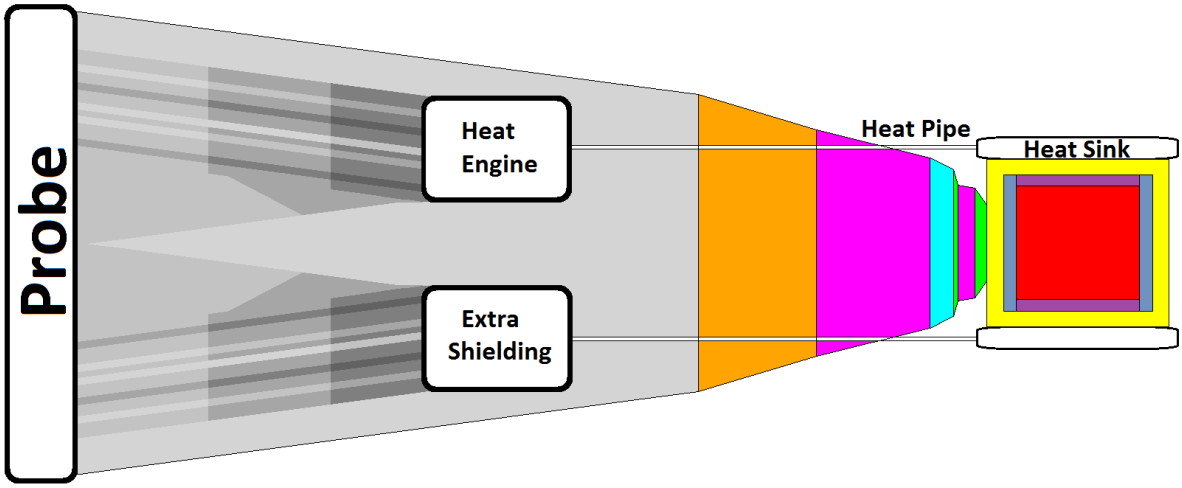

Figure 6.9: The Heat engine acts as additional Shielding. The image above is not to true scale: The length between the probe and reactor was decreased to 200 cm to allow the image to be more readable. The shading in the shadow is for illustration only and is not the result of any calculation.

Section 4: Summary

In this chapter, the issue shielding the probe from high energy gamma and neutrons from the reactor was covered. The mass of the shielding was determined through the design core life to be 43 kg. The mass of shielding is considerable and larger than the mass of the reactor, but is within the design mass limits. The mass of the shielding may be reduced in the future by evaluating the additional shielding, the development of lightweight expanding booms or radiation resistant electronics.

References [Chapter 6]

[1] S.F. Demuth “SP100 Space Reactor Design” Progress in Nuclear Energy, 42, pp.323 (2003)
[2] Glenn Knoll, “Radiation Detection and Measurement”, John Wiley & Sons Inc (2000)
[3] National Nuclear Data Center, http://www.nndc.bnl.gov/
[4] Tables of X-Ray Mass Attenuation Coefficients and Mass Energy-Absorption Coefficients from 1 keV to 20 MeV for Elements Z = 1 to 92 and 48 Additional Substances of Dosimetric Interest, NIST , (2013) http://www.nist.gov/pml/data/xraycoef/index.cfm
[5] George Messenger, “The effect of radiation on Electronic Systems”, VNR (1986)
[6] J.R. Schwank, M.R. Shaneyfelt, and P.E. Dodd “Radiation Hardness Assurance Testing of Microelectronic Devices and Integrated Circuits: Radiation Environments, Physical Mechanisms, and Foundations for Hardness Assurance” Sandia National Laboratories, Albuquerque, NM (2008)
[7] Daniel Zwillinger, “Standard Mathematical Tables and Formulae”, CRC Press (1996)
[8] J.W. Wilson, et al “Galactic and Solar Cosmic Ray Shielding in Deep Space” Langley Research Center, Hampton, VA, NASA Technical Paper 3682 (1997)
[9] Edward Baum, “Nuclides and Isotopes: Chart of the Nuclides”, Lockheed Martin (2009)
[10] David Lide, “CRC Handbook of Chemistry and Physics”, CRC Press (2001)
[11] “Neutron Shielding”, Shieldwerx (2007), http://www.shieldwerx.com/poly-neutron.html
[12] J.J. Duderstadt and L.J. Hamilton, “Nuclear Reactor Analysis”, John Wiley & Sons Inc (1975)
[13] Herman Cember, “Introduction to Heath Physics”, McGraw Hill (2009)
[14] Denise Pelowitz, “MCNP User Manual”, Los Alamos (2008)
[15] J.G. Wood, et al “Free-Piston Stirling Power Conversion Unit for Fission Surface Power, Phase I Final Report” NASA (2010)
[16] R.K. Shaltens and W.A. Wong “Advanced Stirling Technology Development at NASA Glenn Research Center” NASA (2007)

Chapter 7: Safety

In this chapter, the safety of the reactor is explored for both proliferation and criticality risks. The goal is to ensure that there is low radio-toxicity particularly early in the mission where accidents affecting inhabitants on the surface can occur. Since there is no non-zero risk which is considered "safe" by the public, safety can only be considered on a relative scale; thus for reference we will use current RTG materials of Pu-238 and Am-241.

Section 1: Pre-Startup

It is critical to ensure safety prior to the launch and start-up of the reactor. Since the reactor is shutdown prior to and during launch, the activity of the system will be at a minimum. However, while on the ground proliferation and criticality control remain an issue.

Activity: The reactor will have 3 orders of magnitude lower alpha activity than RTG's prior to launch [see Table 7.1]. There are 5 components of the reactor that are radioactive prior to start-up:

1- The fuel U-233 [$T_{½}$= 159,200 Years [1]] which can be considered constant over multiyear storage
2- The U-232 [$T_{½}$= 69.8 Years [1]] which is an impurity in stockpiled U-233 sources which is currently at ≈4.8ppm [2]
3- The fuel decay product Th-229 [$T_{½}$= 7932 Years [1]], which can be considered to build-up linearly from the decay of U-233 over multiyear storage [3]
4- The start-up neutron source Cf-252 [4] [$T_{½}$= 2.645 Years [1]], which would be stored separately and added only shortly before start-up [see Chapter 8]
5- Induced fissions in the sub-critical fuel prior to start-up [K_{EFF} =0.784].

The induced fissions depends on the storage configuration for the reactor but is easily computed in MCNP using a spontaneous fission source of both the U-233 and Cf-252. The number of induced fissions ranges from ≈67 fission per sec in the shutdown core due to U-233 neutrons to ≈63,000 fission per sec when the Cf-252 source in installed [5][6]. Table 7.1 lists the activity of these sources along with the corresponding Pu-238 and Am-241 activity.

Table 7.1: Pre-Startup Activity [1][7][8][5].

	Mass [Kg]	Activity [Ci]	Toxicity [km^3 water]	Gamma [MeV-Ci]	Neutron [s^{-1}]
U-233	8.678	83.74	0.279	0.0153	7.47
U-232	$4.19x10^{-5}$	0.924	0.0154	3.846	0.0544
Th-229	$3.72x10^{-4}$	0.0732	$3.66x10^{-3}$	0.126	-
Cf-252	$4.27x10^{-10}$	$2.29x10^{-4}$	$3.275x10^{-6}$	$9.927x10^{-5}$	10^6
Fissions [No Cf-252]	N/A	$1.83x10^{-9}$	$2.9x10^{-13}$	$2.30x10^{-8}$	168
Fissions [With Cf-252]	N/A	$1.70x10^{-6}$	$2.7x10^{-10}$	$2.16x10^{-5}$	$1.58x10^5$
Total [w/Cf]	**8.678**	**84.74**	**0.298**	**3.99**	**$1.16x10^6$**
Pu-238 [PuO_2]	3.523	60,320	3,020	0.563	$9.12x10^6$ [$5.63x10^7$]
Am-241 [AmO_2]	17.46	59,840	2,990	3.900	$2.06x10^4$ [$4.70x10^7$]

Reactor components are shaded. The thorium activity increases nearly linearly with time from U-233 separation and is shown with 1 decade buildup prior to launch. The Fission Toxicity, Gamma and Neutron are for a 10 year fission product build-up. The Pu-238 and Am-241 are for ideal pure sources at $2KW_{TH}$ with no induced fission. Actual RTG's contain impurities and will have $K_{EFF}>0$ causing self induced fission, both of which increase the total activity.

Prior to start-up the radio-toxicity is 4 orders of magnitude less than an RTG. The gamma activity is comparable in magnitude, but there are two important differences:

1- The gamma from U-232 depends on the build-up of Th-228 with a 1.912 year half-life [1] which allows the Uranium to be worked with for weeks to months [9] with only a fraction of the gamma dose.

2- The gamma dose from U-232 contains a strong 2.614 MeV gamma from Tl-208 [8] which is much harder to shield than the Pu-238 gammas which have energies of 43, 99 and 152 KeV [8][10].

The neutron radiation is smaller than the RTG even with the Cf-252 installed and significantly less prior to inclusion. As a result, the pre-startup activity is well below that of the RTG.

Using a U-235 fueled reactor [eliminating the U-233, U-232 and Th-229] would reduce the pre-launch Radio-Toxicity to 4.2×10^{-4} km^3, which is 7 orders of magnitude below RTG's. However the mass would be significantly increased [see Chapter 3]. Additionally, the toxicity benefit would be significantly reduced after start-up since U-233 and U-235 have similar fission product toxicity.

Criticality: The reactor must remain subcritical [by at least 4$ [11]] until the planned start-up which is evaluated here using MCNP. Prior to launch there are three main effects that drive the reactor to super criticality:

1- The reactor would be highly super critical [25$ worth] at room temperature and it is not feasible to attempt to maintain the reactor hot enough to stay shutdown,
2- There is a small reactivity excess built into the core [4$ worth] [12] and
3- On Earth the reactor will be surrounded by reflective or moderating material such as air and not the vacuum of space. The air would add 0.19$ of reactivity and any additional material would cause a further increase. The worst case scenario is the reactor falling into a pool of cold water, which would add 75.3$ of reactivity [The most likely crash is into the ocean but this is slightly less reactive since chlorine is a moderate poison and doubles the absorption cross section of the water [6][1]].

To ensure the reactor stays shutdown there is a single control rod that is inserted in the reactor. This shuts the reactor down by two methods: 1-some of the fuel is removed from the core and 2-a strong poison is added into the core. The poison to be added should be lightweight so B-10 is used [See Table 5.1].

The design criterion for the reactor has two separate scenarios: 1-The reactor falls into a pool of pure water and the poison rod maintains the reactor subcritical and 2-The rod falls out of the reactor but the reactor remains on a flat surfaces and rolls into a corner where all 3 walls are as reflective as water. Since the fuel rod is stored separately from the reactor prior to start-up, the fuel rod cannot "fall" into the reactor.

Case 2 determined the size of the rod since only the fuel is removed as the rod fell away and case 1 determines the strength of the poison that must be used in the rod. In case 2 the total positive reactivity effects are 52.3$ and as a result the size of the rod is 2.90 cm in radius and removes 2.988 kg of fuel outside the core [1.345 kg U-233]. In case one the total positive reactivity effects are 103$ and as a result the density of B-10 needed is 1.56 g/cm^3 which is 72% of solid density for a total mass of 836 g. Since the density of B-10 is less than the solid density [6], the structure the poison rod was reevaluated as a hollow cylinder and constructed of B_4C [6] [extremely hard, used in commercial reactors and body armor]. The rod would now have a 1.595 cm hollow in the center for a total new mass of 888 g. As a result the core can be maintained subcritical in both cases with a rod that adds ≈1 kg to the system mass [including an allowance for fasteners and the drive mechanism]. During the launch the reactor would be subjects to large vibrations and as a result the control rod mechanism should be vibration tested to ensure the rod is held securely in place.

Proliferation: Prior to launch, theft and proliferation is a concern however there is no comprehensive proliferation standard that exists. As a result the standard for proliferation will be in comparison to RTG fuels [14]. The proliferation issues with RTG fuels were covered in Chapter 2 along with the standard the reactor was expected to meet. These are listed below:

1- <1 Critical Mass [15]	Met: 0.55x Critical Masses
2- Chemically bonded to a moderator [16]	Met: U-233 is in a $ZrH_{1.65}$ Matrix
3- Subcritical on fast neutrons alone [16]	Met: See next paragraph
4- Non-spherical	Met: Cylindrical

The only proliferation concern not covered in the previous chapters was #3. This was verified by using MCNP to evaluate the core. The sub-criticality of the core is measured by two separate methods: 1- Using the CUT command to eliminate neutrons with energy less than 1eV and 2-simulating the reactor at plasma temperatures [at 1 ton TNT equivalent, which is a Uranium temperature of 1.16 KeV], solid density and with all neutrons present. In both cases the reactor is evaluated without the poison rod and with room temperature densities and additional reflector [Solid Be-9] surrounding the reactor. In the two methods the K_{EFF}= 0.92 and 0.90 respectively which meets the requirement that the reactor will be subcritical on fast neutrons alone and as a result cannot be used as is to create an explosion with energy in the kiloton of TNT range.

The only additional proliferation method was to use lower enriched fuel [13]. This was covered in Chapter 3. While this is an option, it would increase mass beyond the design goals and is not used. If in the future proliferation becomes a larger concern then lower enrichment designs should be considered a replacement for RTG's, which are highly enriched [Over 80% enriched Pu-238 with most the remainder U-239, both of which have critical masses less than 10 kg [17][15]]. Conversely if in the future proliferation becomes a lesser concern then standards 3 and 4 may be relaxed to allow the design of a smaller lighter reactor using fast neutrons in metallic fuel [this could cut reactor and shielding mass nearly in half].

Section 2: Activity Build-up

In general, activity builds-up due to radionuclide formation as the reactor operates. This is an issue for 2 reasons: 1-The probe may make a swing-by pass of the Earth after years of operation in space [18] and 2-the reactor may return to earth orbit if the probe speed is less than solar escape velocity [19]. As a result, the long term radio-toxicity of the reactor is explored.

Fission activity build-up: The fission in the reactor causes the build-up of radioactive nuclides by 4 separate processes:

1- Fission product build-up from fission, which is well characterized in the ENDF library [8], at power there are 1,773 Ci of fissions where fission products undergo an average of 5.63 beta decays for 9,986 Ci of beta decay in steady state operation [8].
2- Neutron capture in reactor materials, which is dominated by capture in U-233 [initially 720 μCi/Yr of U-234 which is 2,400 m^3/Yr water [7]]. Be-9 and zirconium have very low capture cross sections [0.38μCi of Be-10, 101μCi of Zr-93 and 453,000 μCi of short lived Zr-95 [8] with respective radio-toxicities of 0.019, 2.52 and 22,660 m^3 water [7] after 200 years]. Li-7 captures to Li-8 which decays with a $T_{½}$ of 0.84 Seconds and H-1 captures to H-2 which is stable and not radioactive [1].
3- High energy neutron reactions in reactor materials, which is again dominated by U-233 and in particular (n,2n) reactions in U-233 to produce U-232 [8] and
4- The alpha decay of U-233 into Th-229 and subsequent decays along the decay chain to Bi-209 [1].

In addition, there will be some activity in non-reactor materials, particularly the shielding. However neither tungsten nor lead will become strongly activated [1] and the B-10 capture produces only stable nuclei [He-4 and Li7]. Only capture in Li-6 will produce significant activity with an equilibrium buildup of 0.41 Ci of Tritium [1] [Tritium has low radio-toxicity or 10^{-3}μCi/ml, which results in a total toxicity of 412 m^3 water [7]].

Overall the activity buildup can be considered the sum of 2 components [The other components contribute $\ll 0.01\%$]: 1-The fission products build-up and subsequent decay and 2-The actinide build-up and subsequent decay.

The Model: There are two separate models for the fission products build-up and subsequent decay and for the actinide build-up and subsequent decay.

The first model for actinides is the same model as Chapter 5, using the BURN routine in MCNP. This works very well to track the actinide build-up since capture in reactor materials is well modeled with the Monte Carlo neutron energy spectrum and the subsequent decay chains are included [20].

However, MCNP only tracks a fraction of the fission products [BURN tracks 210 fission products [20] out of the 1057 fission products in the ENDF library [8]]. The reason for this is many fission products have very short half-lives [Several have $T_{½}$ <1μs [1]] and as a result there are no neutron cross section data for them [8]. Only a few of the fission product radio-nuclides have a cross section large enough to capture an appreciable number of neutrons before decay. As a result only fission products with half-lives comparable to the capture half-life will need to be considered in MCNP with the rest assuming no neutron capture. See Equation 7.1 and 7.2, which is sets criteria for which nuclides in which neutron capture is negligible.

$$\mathbf{T_{½} \ll \tau_A = (\sigma_A \phi)^{-1}} \qquad \text{Equation 7.1}$$

$$\mathbf{\sigma_A \ll (T_{½} \phi)^{-1} \approx \frac{6 \cdot 10^6 barns}{T_{½}[Years]}} \qquad \text{Equation 7.2}$$

Additionally the reactor life sets an upper bound for the time the absorption can happen in [even for stable isotopes]. This in turn sets lower bound for the abortion cross section which is shown in equation 7.3.

$$\mathbf{\sigma_A \ll (200\ Years \cdot \phi)^{-1} \approx 30,000\ barns} \qquad \text{Equation 7.3}$$

Based on this, all fission product nuclides with a cross section of > 1000 barns and 200,000 barns/year of half-live [which is sufficient capture cross section to affecting concentration by >0.76%] are listed in Table 7.2 along with their toxicity and the capture product toxicities.

Table 7.2: Capture in Fission Products [1][8][21][7].

	σ_A [Barns]	$T_{½}$ [years]	Fission Yield	Initial Toxicity [m^3]	Product	$T_{½}$	Final Toxicity [m^3]
Dy-164	2,840	Stable	$2.7x10^{-8}$	-	Dy-165	2.33 Hr	1.E-02
Gd-157	259,000	Stable	0.008%	-	Gd-158	Stable	-
Gd-155	61,100	Stable	0.022%	-	Gd-156	Stable	-
Eu-151	9,100	$\geq 10^{18}$	0.312%	6.E-08	Eu-152	13.54 Yr	96,241
Sm-151	15,140	90	0.312%	21,731	Sm-152	Stable	-
Sm-149	42,080	Stable	0.744%	-	Sm-150	Stable	-
Cd-113	20,600	$8x10^{15}$	0.038%	3.E-08	Cd-114	Stable	-

Initial toxicity assumes no capture and final toxicity assumes capture based on thermal flux of $4.79x10^{9}$n/sec-cm^2. Both assume fission of only U-233. The nuclides that cause a significant change in radio-toxicity are shaded.

As a result of Table 7.2 only Sm-151 and Eu-151 need to be tracked in MCNP [along with the actinides] with all other fission product nuclides insignificantly affected by neutron capture. The nuclide model is then tracked in EXCEL using the fission product concentrations from the ENDF library [8] and the fission nuclide and energy from MCNP [fission in U-233 dominates with 99.98% of fissions with only minor contribution from U-232 at $1.4x10^{-4}$%, U-234 at $3.0x10^{-3}$%, U-235 at $3.6x10^{-4}$% and Th-229 at $1.9x10^{-2}$%].

Results: The radio-toxicity of the reactor combining fission products and actinides is then shown in Figure 7.1 for the buildup of toxicity and in Figure 7.2 for the decay of toxicity following 200 years of operation. Only selected nuclides that contribute >4% of toxicity for a given time and have a half-life of >1 day are shown [for visibility of the graph in Figure 7.1, all 1057 fission products plus actinides are included in sum]. Additionally the toxicity for $2KW_{TH}$ in an ideal Pu-238 and Am-241 RTG is shown for reference [The RTG toxicity includes the daughter products].

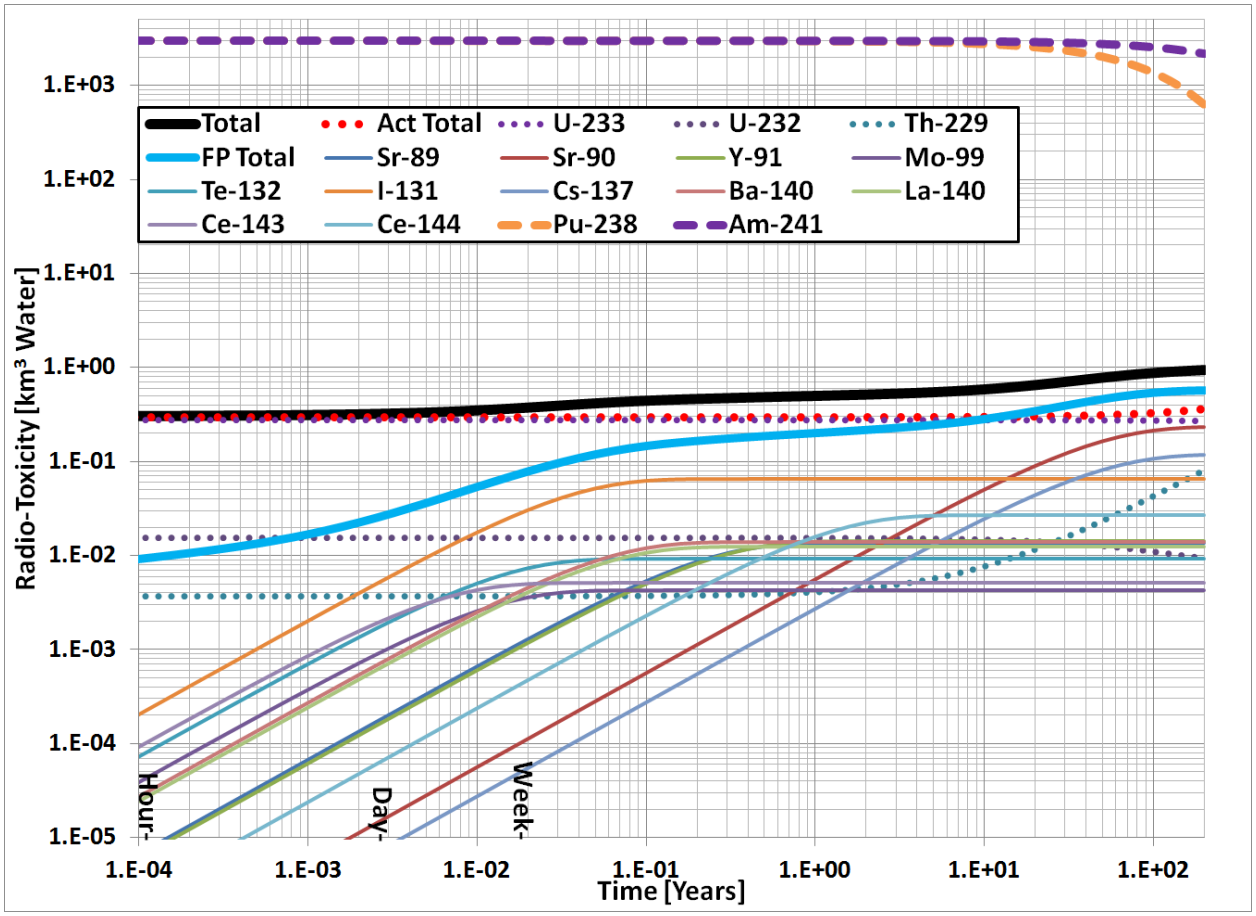

Figure 7.1: Buildup of Radio-Toxicity over 200 Years of Reactor Operation. The graph shows the components of radio-toxicity in the reactor as well as the sum total as a function of time assuming the reactor is operating at full power. The toxicity for Pu-238 and Am-241 are shown for comparison.

In particular, the radio-toxicity of the U-233 is the largest contribution initially starting 94.6% of the total toxicity and remaining at over half the toxicity for the first 6.2 Years. At the end of core life, the radio-toxicity of U-233 is still the largest single contributor at 28.8% of the total with its daughter Th-229 contributing 8.6% more.

The fission products buildup and eventually contribute 61.5% of the total radio-toxicity by end of core life. The short lived beta decay products quickly build-up and within 6 hours are generating over 90% of the total equilibrium decay heat. However, the short lived fission products contribute rather little to radio-toxicity since they decay quickly before they could be absorbed by people [22] [in an accident]. The first major

fission product to build-up is I-131, which accounts for over ⅓ of the fission product radio-toxicity from 4 days to 9 months. Finally, after 1 decade of operation, do the fission products overtake U-233 in terms of radio-toxicity lead by the buildup of Cs-137 and Sr-90 which reach 99% equilibrium concentration by end of core life [200 Years]. At end of core life Sr-90 and Cs-137 account for 24.8% and 12.7% of the toxicity respectively. Since less than 1 in a million fissions produce fission products with half-life between 200 and 200,000 years [8] the fission product toxicity is nearly steady state after 200 years and will not increase even 1% if core life was extended to 1000 years.

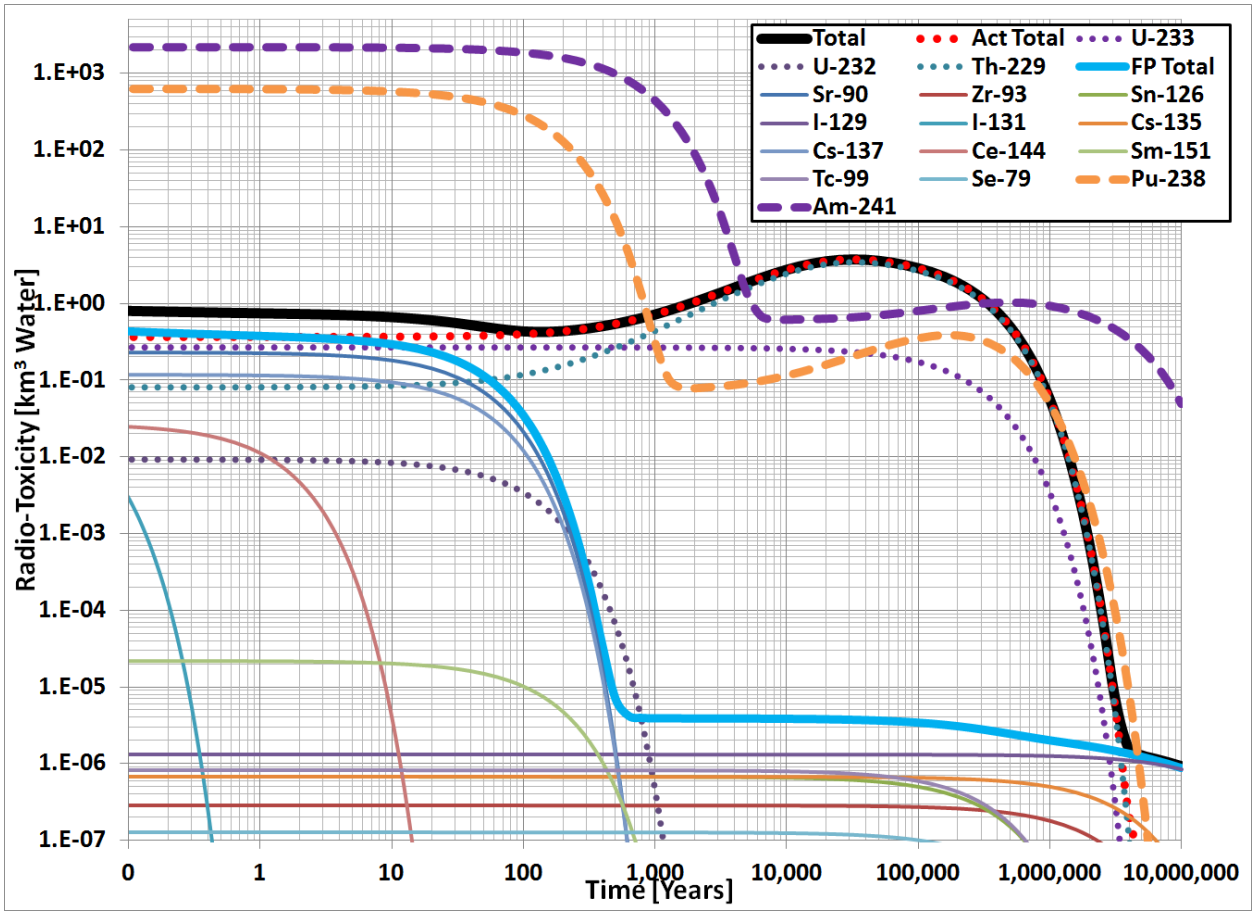

Figure 7.2: Decay of Radio-Toxicity after 200 Years of Reactor Operation. The graph shows the components of radio-toxicity in the reactor as well as the sum total as a function of time assuming the reactor is shutdown after 200 years of operating at full power. The toxicity for Pu-238 and Am-241 are shown for comparison.

After the reactor shuts down, the toxicity drops slowly since the short lived fission products are insignificant contributors to toxicity. It takes 11.3 hours for the toxicity to drop by only 2%. The largest drop in the first month [7.0% with the total drop only 14.9%] is the decay of I-131 with a $T_{½}$=8.02 days. The major components of the residual toxicity are U-233, Th-229, Sr-90 and Cs-137 [75.0% of the total at 200 years of operations]. The Cs-137 and Sr-90 will decay with a $T_{½}$≈30 years and the total toxicity will drop to 45% of the shutdown toxicity in 135 years.

135 years after shut down, the build-up of Th-229 [$T_{½}$=7,932 Years] will exceed the decay of the other components and the total toxicity will increase reaching a peak in 32,300 years at a radio-toxicity of 3.70 km^3 water. Following this, the toxicity then decays as U-233 decays away with a $T_{½}$=159,200 years.

In comparison to Pu-238 and Am-241, the toxicity remains 3-4 orders of magnitude less over the 200 years of reactor operation. However after ≈12$T_{½}$ the toxicity of Pu-238 and Am-241 [1,048 and 4,815 years respectively] will have decayed to approximately the same level of toxicity of the spent core. The RTG will then have comparable radio-toxicity to the reactor since the daughter products of Pu-238 and Am-241 [U-234 to Th-230 and Np-237 to U-233 to Th-229 respectively] have similar half-lives and toxicities as U-233 and Th-229 in the reactor [8][7].

Decay Heat: The fission product decay heat was already covered in Chapter 4. Of possible concern is the higher decay heat as Th-229 builds up since its decay chain is 10.4 times more energetic than the U-233. As it turns out, the Th-229 decay heat after 200 years of operation only reaches 0.50 W_{TH}, which is fairly insignificant. Even at peak Th-229, the heat is only 22.4 W_{TH}, which is well within radiant heat removal of the system [The core is long shutdown at this point].

Waste: Following shutdown the reactor would drift through space and if the probe velocity was insufficient to escape the solar system the probe would return to the inner solar system. It would be extremely unlikely that the probe would impact the Earth on such a return trip. The long term behavior will be based on the decay of U-233 for $\approx 20T_{½}$ [3×10^6 years] after which the decay of I-29 and U-235 will dominate but the total toxicity will be down to <1000 m^3, which is insignificant and need not be considered further.

Section 3: Flight

The reactor will be shutdown prior to launch and not started until the probe reaches Earth escape velocity. There are two possible crash scenarios: 1-the shutdown reactor crashes or breaks up during launch and 2-The operating reactor crashes early in life on a swing-by orbit.

Swing-by Crashes: The swing-by crash would occur at high speeds [>11 Km/sec, Earth escape velocity [19]] and as a result the reactor will burn up during re-entry and dispersed over a wide area. The chief concern is then the total radio-toxicity. The swing-by passes would happen in the range 1-10 years of operation [swing-by times are related to the orbital period of the planet swung past, for example Cassini swing bys includes two Venus passes and one Earth pass in the first 1.84 years of operation]. In this time period the total toxicity will be 4,800-6,000 times lower than both Am-241 and Pu-238 powered probes.

As an option, solar power could be used in this time frame. During swing-by orbits of the Earth the probe would remain near the sun [≈0.5-2 Au] thus solar power is an available option. Using the mass from the Chapter 1 discussion of solar panels and assuming the spacecraft remains within Mars orbit during the maneuvers, the mass of the solar panels would only need to be ≈4 kg to supply system power [500 W_E ÷ 130 W_E/kg, see Chapter 1]. In this option, the reactor would not be started until the probe is leaving the inner solar system after the swing-by maneuvers, which reduces the swing-by toxicity to pre-startup levels and extends the life of the probe by a few years since start-up is delayed.

Launch Crashes: Crashes during launch are more complicated since the probe has not yet reached the high speed of a swing-by crash. There are three cases that are considered:

1- The reactor lands intact in water or land.
2- The reactor is breached by the landing or rocket explosion.
3- The reactor is vaporized or burned up by airspeed or burning rocket fuel.

In all cases the reactor has not yet started–up and only pre launch activity is present, which is 4 orders of magnitude lower toxicity than RTG's.

In case one, the toxicity is well contained in the reactor and the main concern is that the reactor goes critical. The inclusion of the boron rod covered in Section 1 prevents criticality of the reactor submersed in water, which is the most reactive situation the reactor is likely to be in. The rod is fasted securely enough such that crashes severe enough to remove the rod would tear the reactor reflector apart [a case 2 crash] and as a result, in all case 1 crashes the boron rod should remain in place. At this point, recovery of the reactor would be desirable to prevent further damage or proliferation. The probe would have to be traveling slowly to avoid damage in the crash and as a result the crash site would be near the launch site and recovery of the core may be possible. If the reactor is lost in the ocean the total toxicity is insignificant [0.3 km^3 compared to the volume of the ocean $\approx 1.3 \times 10^9$ km^3 [6]] even if the probe corrodes and later releases its contents.

In case two, the breach of the reactor would expose the LiH to air and water. In this case the LiH could chemically combust and/or explode [23] [chemical explosion not a nuclear explosion]. The disassembly of the reactor would now prevent criticality by geometric considerations [the boron fragments will likely be interspersed with the fuel fragments as well]. The chief concern will be toxicity since the reactor parts may be dispersed over a small region concentrating the toxicity. The fuel is relatively inert [24] and as a result most of the toxicity would not be released for several years. This would allow evacuation and/or cleanup [the U-232 gammas would make the larger fragments easier to locate]. However, since the most likely crash site is the ocean, the toxicity would be an insignificant concern as in case 1.

Case three would be similar to swing-by crashes with the exception that the dispersion would be over a much smaller area concentrating the toxicity. In this case, evacuation of affected areas may be necessary [the uranium toxicity would take several days before it could be ingested allowing time for evacuation] [18]. The best solution here would be to have the probe launched in isolated area or over the ocean, which is already the location for most satellite launches in the United States [Cape Kennedy Florida launches towards the Atlantic Ocean].

Finally the mobility of uranium is much less than that of plutonium or americium [the thorium is immobile but as a daughter product of U-233, the thorium will be found wherever the U-233 goes] and as a result less toxicity will move from the crash sites to nearby populated areas [the launch should not be over populated areas]. Due to both the lower toxicity and mobility effects of crashes would be much less severe that crashes of RTG powered probes.

Section 4: Summary

In this chapter, the safety of the reactor was explored for both proliferation and criticality risks and to ensure that there is low radio-toxicity. The proliferation and criticality concerns were all met and the radio-toxicity is well below that of RTG's. The reactor is thus safer than current RTG's and would be a beneficial replacement.

References [Chapter 7]

[1] Edward Baum, “Nuclides and Isotopes: Chart of the Nuclides”, Lockheed Martin (2009)
[2] C.W. Forsberg and L.C. Lewis “Uses for Uranium-233: What Should be kept for Future Needs?” (1999)
[3] Daniel Zwillinger, “Standard Mathematical Tables and Formulae”, CRC Press (1996)
[4] R Martin, “Production, Distribution, and Applications of Californium-252 Neutron Sources”, Oak Ridge (1999)
[5] N. Ensslin “The Origin of Neutron Radiation” Chapter 11, US NuclearRegulatory Commission NUREG/CR-550, (1991), http://www.fas.org/sgp/othergov/doe/lanl/lib-www/la-pubs/00326406.pdf
[6] David Lide, “CRC Handbook of Chemistry and Physics”, CRC Press (2001)
[7] U.S. Nuclear Regulatory Commission Regulations: Title 10, Code of Federal Regulations (2012)
[8] National Nuclear Data Center, http://www.nndc.bnl.gov/
[9] J. Kang and F.N. Hippel “U-232 and the Proliferation-Resistance of U-233 in Spent Fuel” Science & Global Security, 9, p. 1 (2001)
[10] Tables of X-Ray Mass Attenuation Coefficients and Mass Energy-Absorption Coefficients from 1 keV to 20 MeV for Elements Z = 1 to 92 and 48 Additional Substances of Dosimetric Interest, NIST , (2013) http://www.nist.gov/pml/data/xraycoef/index.cfm
[11] J.J. Duderstadt and L.J. Hamilton, “Nuclear Reactor Analysis”, John Wiley & Sons Inc (1975)
[12] D.I. Poston, et al “A Simple, Low-Power Fission Reactor for Space Exploration Power Systems” Proceedings of Nuclear and Emerging Technologies for Space, Albuquerque, NM (2013)
[13] C.W. Forsberg, et al “Definition of Weapons-Usable Uranium-233” (1998)
[14] T.E. Liolios “The Effects of Nuclear Terrorism: Fizzles” EUROPSIS
[15] Van den Berghe “Evaluation of Nuclear Criticality Safety Data and Limits for Actinides in Transport” (2003)
[16] Karl Ott, “Nuclear Reactor Dynamics”, ANS (1985)
[17] M. Ragheb “Ch. 3 Radioisotopes Power Production” (2012), https://dmtpc.mit.edu/twiki/pub/Projects/RadioIsotopeBattery/Radioisotopes_Power_Production.pdf
[18] NASA, “Final Environmental Impact Statement for the Cassini Mission” (1995), http://saturn.jpl.nasa.gov/spacecraft/safety/safetyeis/
[19] Marc Kutner, “Astronomy: a Physical Perspective”, Wiley (1987)
[20] Denise Pelowitz, “MCNP User Manual”, Los Alamos (2008)
[21] Neutron Scattering Lengths and Cross Sections, NIST Data, ATI (2001)
[22] Herman Cember, “Introduction to Heath Physics”, McGraw Hill (2009)
[23] R.L. Smith and J.W. Miser “Compilation of the Properties of Lithium Hydride” Lewis Research Center, Cleveland, OH (1962)
[24] D. Olander, et al “Uranium-Zirconium Hydride Fuel Properties” Nuclear Engineering and Design, 239, pp. 1406 (2009)

Chapter 8: Transients

In this chapter transients in the reactor will be explored to determine the allowable rate of change of reactor parameters and the stability of the reactor during transients such as power changes and startup.

Section 1: The Model

To examine the dynamic behavior of the system a numeric model was developed to relate reactivity, power and temperature and is shown in Figure 8.1. The model was created in Matlab and consists of three components:

1- Neutron kinetics
2- Thermal diffusion [Chapter 4 thermal model without equilibrium]
3- The temperature coefficient of reactivity from Chapter 3.

In addition the model can handle external rod motion and load changes.

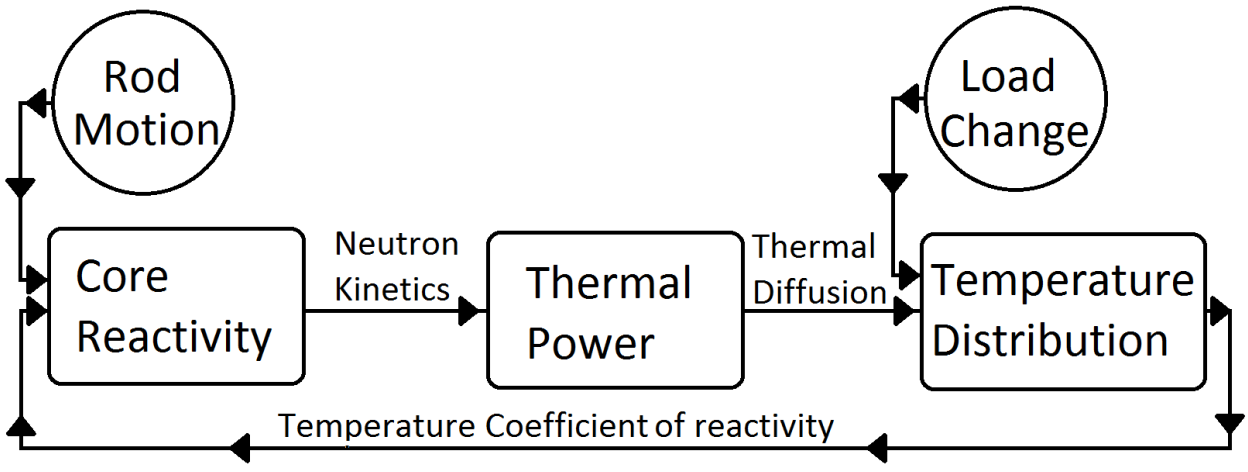

Figure 8.1: Reactor Transient Model. This figure is an illustration of the transient model to determine the power and temperature profile of the reactor.

Neutron Kinetics: The neutron kinetics is well studied [1][2][3] and many simplification methods have been developed based on the particular reactor designs. Since our reactor is small and thus well coupled [small enough that any part of the reactor is only a few MFP from the rest of the reactor], the point kinetics model was used [1] [This was experimentally verified by the DUFF test, and a lesion learned for future space reactors [19]]. For the point kinetics model, the kinetics are based on a set of delayed neutron precursors with group yields [β] shown in Table 8.1. Since the average energy of delayed neutrons is less than fission neutrons [1], MCNP was used to determine the effective utilization of the delayed neutrons to cause fission [$\overline{\beta}$] by imputing the ENDF delayed neutron energy spectrum [4] as a distributed source [based on the power profile] into the reference model [see Chapter 3]. The 6-group set of delayed neutrons was used in this model using Crank–Nicholson implicit method [3] with exponential time stepping. All transients shown in this chapter are based on beginning of core life parameters. The results are similar to end of life transients. The only transient modeled over core life was for heat load changes since start-up and rod motion will only occur at the beginning of life.

Table 8.1: Delayed Neutrons for U-233 [5][1].

		T½ [Sec]	β [x10^{-4}]	$\overline{\beta}$ [x10^{-4}]
6-Group	1	53.7	1.804	2.105
	2	20.8	5.151	6.010
	3	5.96	3.696	4.312
	4	2.36	7.480	8.727
	5	0.873	3.015	3.517
	6	0.292	5.592	6.524
1-Group		9.28	26.74	31.19

Delayed parameters based on thermal fission. Utilization based on the reference reactor model

Heat: The Chapter 4 thermal model for heat flow and heat capacity is used. For reference, the total heat capacity of the reactor components are shown in Table 8.2 to illustrate the time scale to change temperature [Heat-up time=(Heat Capacity)÷(Thermal Power)]. The full power of the reactor is small enough that the reactor will heat-up rather slowly. Thus the time scale that the power responds to temperature is much faster than the temperature changes, aiding stability. Additionally, the heat of fusion of LiH is 2.8 MJ/kg [6], which means that it would take 25 minutes to melt at $2112W_{TH}$.

Table 8.2: Heat Capacities & time [at operating temperature] [7][6][8].

	Mass [Kg]	Heat Capacity [KJ/˚C]	Heat-up Time [Sec/˚C]
Fuel	19.3	8.11	3.84
Moderator	1.13	8.74	4.14
Reflector	6.59	19.44	9.20
Total	27.0	36.28	17.2
LWR UO_2 Fuel [For Reference]			≈0.010

Time scale is based on $2112W_{TH}$ which is full power. Heat-up time is at Full power and operating temperature. The Heat-up time for LWR UO_2 Fuel is for 1 Kg at 37 kW_{TH}/kgU [2].

Limitations: The model assumes that that the LiH does not melt. This sets a thermal limit of 688˚C in the LiH and all transients are designed to limit temperature executions below this temperature. Additionally the model only works when the reactor is prompt sub-critical and as a result any transient causing the reactor to become prompt super-critical is avoided.

Reactor power is not a limitation. The reactor could produce 100's of KW_{TH} and as long as temperature remains within the bounds of Chapter 4, the reactor would be unharmed. Consider a step insertion of 0.321$ of reactivity while at full power [5˚C change]. Reactor power reaches nearly $5.56KW_{TH}$ but only raises fuel temperature by 26˚C [to 773˚C] and LiH temperature by 7˚C [to 685˚C], which are within the transient thermal limits [which are 930˚C and 688˚C respectively]. This is shown in Figure 8.2.

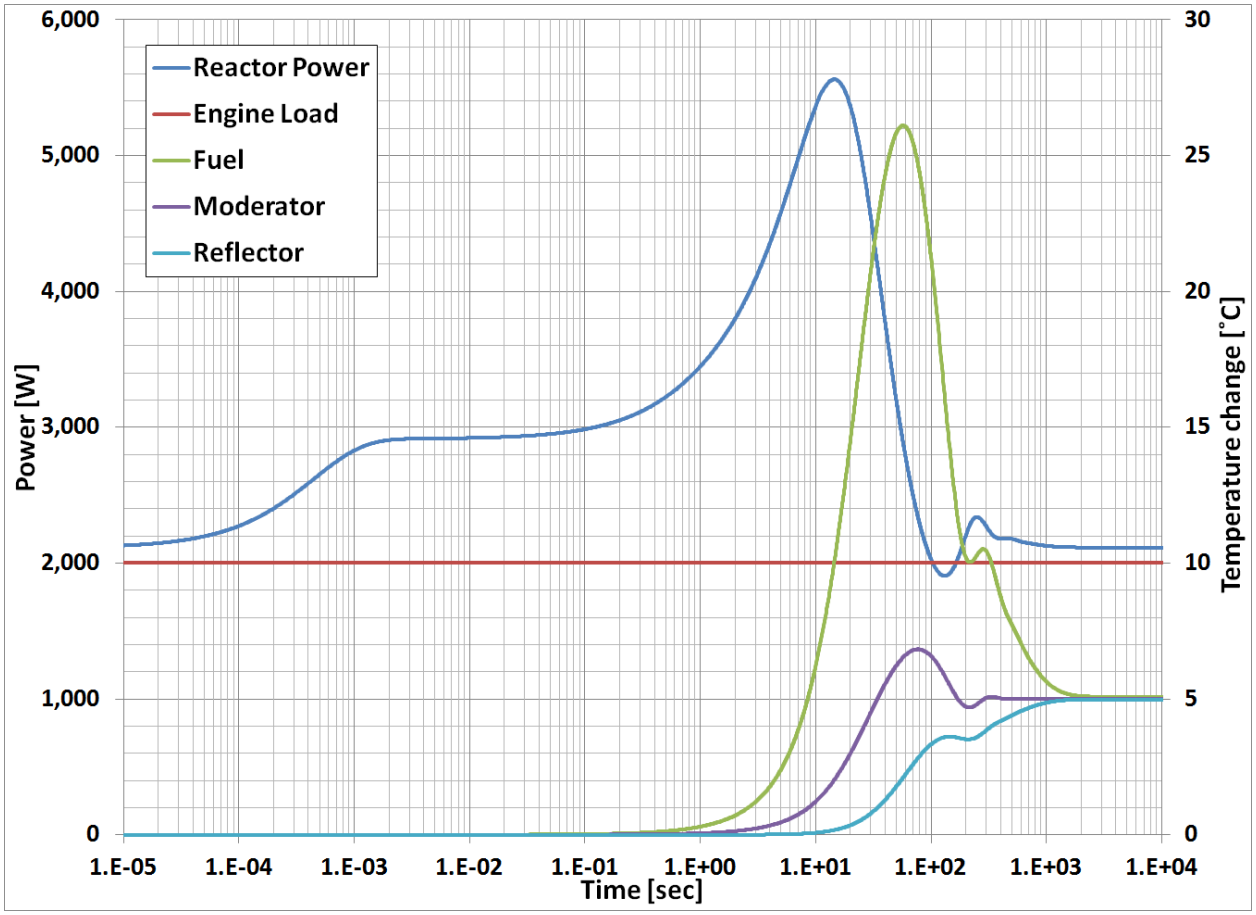

Figure 8.2: Effect of instantaneous 0.321$ reactivity insertion. This is a graph of fission power and reactor temperature as a function of time following a transient. This transient is a 0.321$ step insertion of reactivity. This transient is modeled based on beginning of life parameters.

Section 2: At Power Transients

The stability of the reactor while at power and normal operating temperature is examined for both rod motion and changes in the heat load, which are the two transients the reactor would experience.

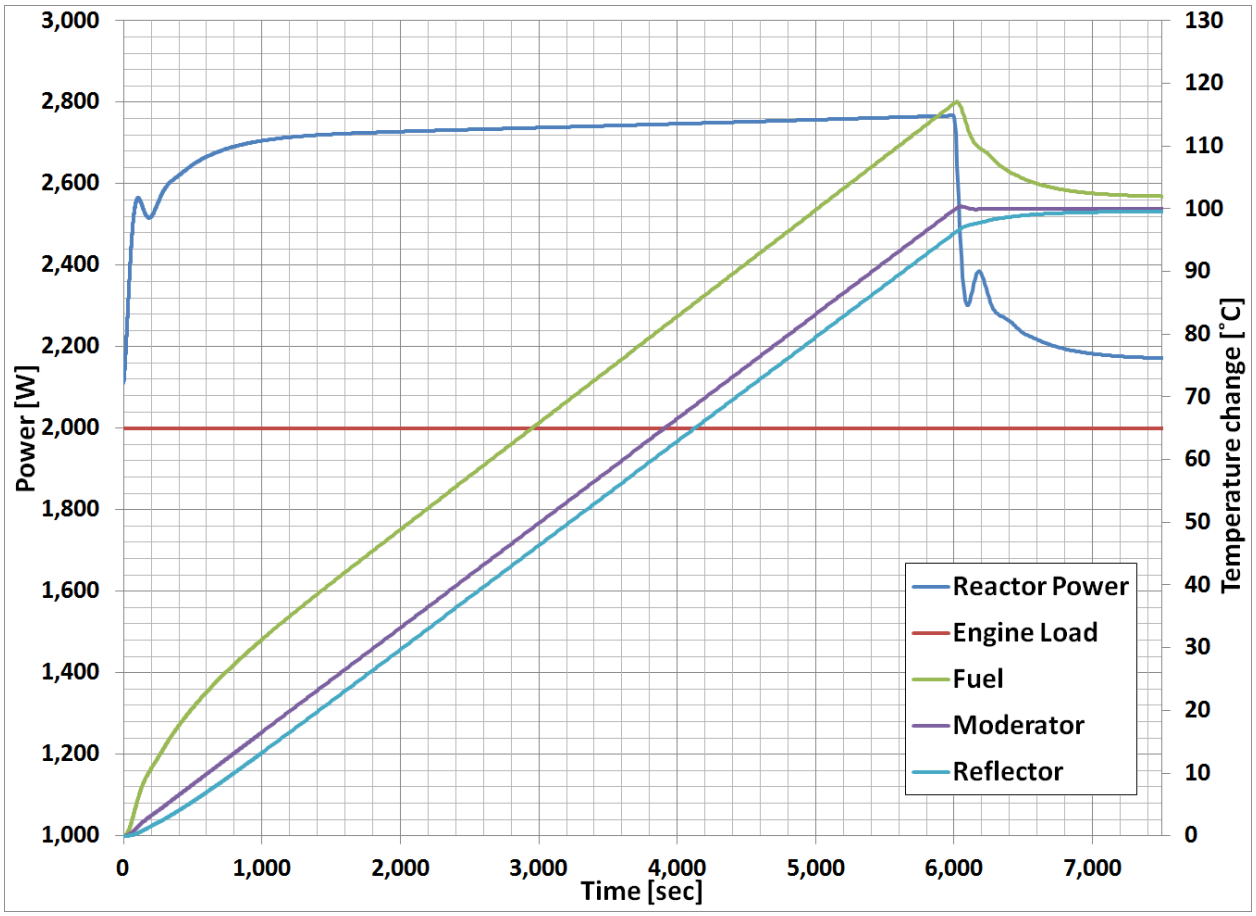

Figure 8.3: Effect of 100˚C heat-up with constant rod speed [≈1˚C/min]. This is a graph of fission power and reactor temperature as a function of time following a transient. This transient is modeled based on beginning of life parameters.

Rod Motion: The rod motion at the beginning of life would be used to set the reactor temperature following start-up. At the conclusion of start-up the reactor would be operating at power, but at a reduced temperature of ≈100˚C below the normal operating temperature [see Section 3]. The control rod is then withdrawn at a constant rate [which adds reactivity and temperature at a nearly constant rate as well]. Figure

8.3 shows the change in core parameters with the rod speed set at 0.326 mm/min [rod speed chosen to produce a final heat–up rate of 1˚C/min].

The temperature of the reactor will overshoot the desired temperature by a few degrees. Varying the rod speed will vary the temperature and power overshoot. This allows a method to select rod speed and associated heat-up rate. The model was run with several rod speeds and the results are plotted in Figure 8.4.

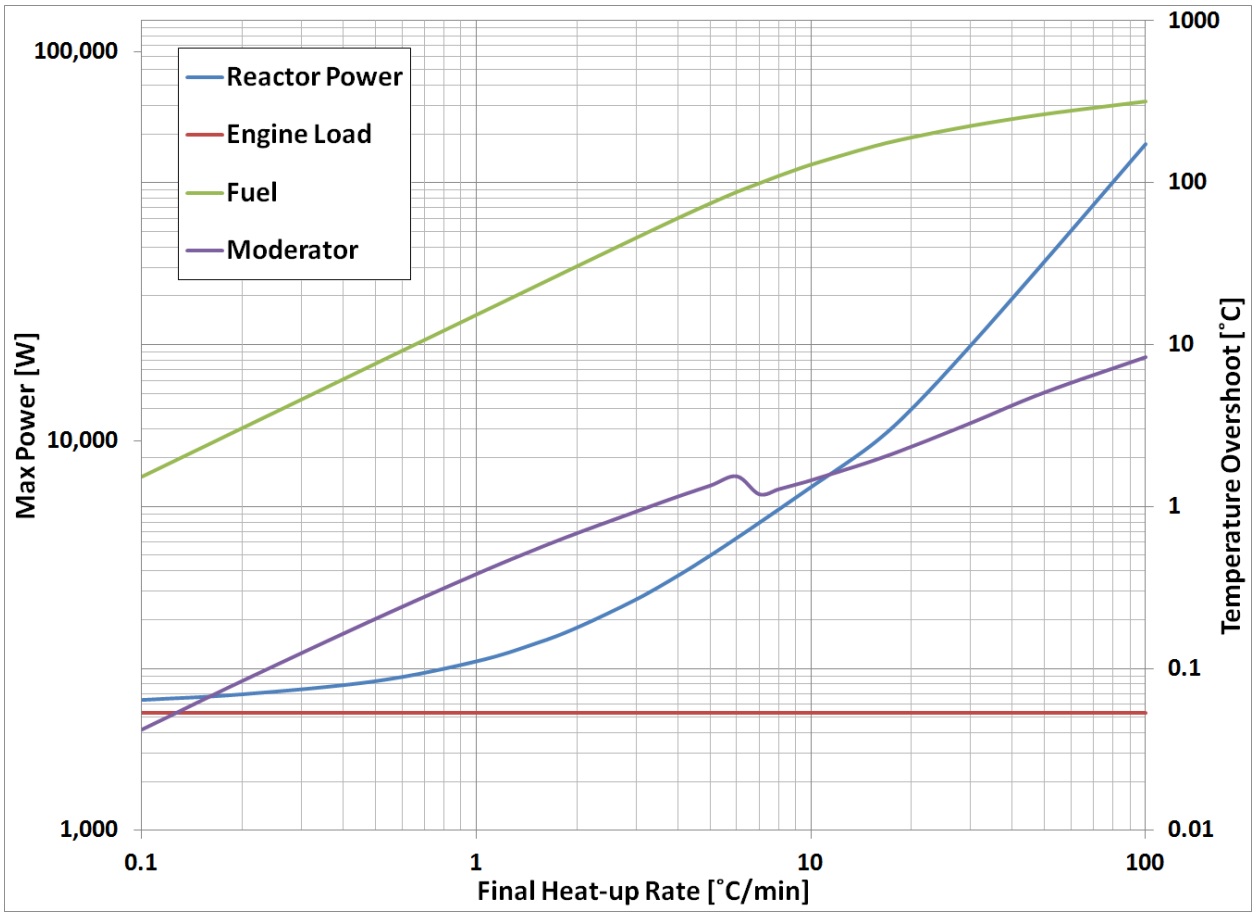

Figure 8.4: Power and Temperature overshoot as a function of Heat-up Rate. This is a graph of maximum fission power and reactor temperature as a function heat-up rate. The transient is caused by rod motion to add reactivity at a constant rod speed. This transient is modeled based on beginning of life parameters. The Kink in the moderator at 7˚C/min is real. Reflector temperature overshoot is insignificant.

The limiting parameter was the fuel temperature, which was limited to 930˚C [see Chapter 4] sets the maximum heat-up rate to 18.4˚C/min [Rod speed of 5.99

mm/min]. In this case, the rod motion would need to stop when the reflector only heated up 31˚C, which requires that the rod control contain anticipatory algorithms and not rely solely on temperature measurements [at 1˚C/min the control is simpler since the reflector heated up 94˚C].

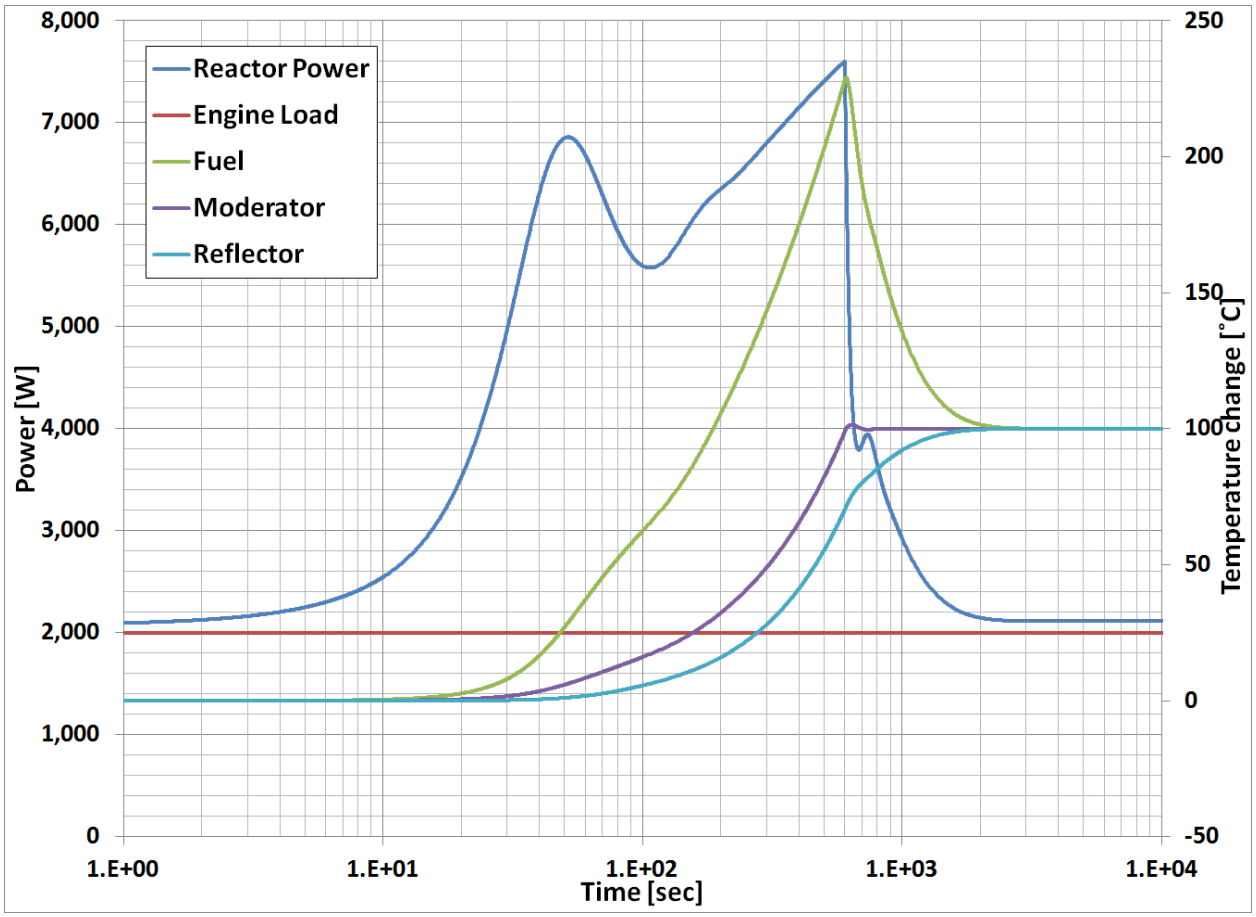

Figure 8.5: Effect of 100˚C heat-up with constant rod speed [10.1˚C/min]. This is a graph of fission power and reactor temperature as a function of time following a transient. The transient is caused by rod motion to add reactivity at a constant rod speed. This transient is modeled based on beginning of life parameters.

The heat-up rate is limited to 10.1˚C/min [3.3 mm/min, see Section 3] and is shown in Figure 8.5. At this heat-up rate, the rod motion will last 10 minutes and reactor power will peak at 7,599 W_{TH} with an average power of ≈6,650 W_{TH}. The LiH will reach 680˚C and the fuel centerline temperature will reach 876˚C [transient thermal limit of 930˚C] and will spend just 18 minutes at greater than 760˚C.

Besides this heat-up the reactor may need to adjust temperature for the first month as the reactor settles into steady state operation [see Chapter 5]. These would occur in small steps of 1˚C with a fuel and LiH overshoot of 3.67˚C and 0.33˚C respectively. For rod insertion to lower temperature, larger steps may be taken since no temperature overshoot occurs [power overshoot does but this is not significant], but limiting the insertions to small steps of 1˚C would not impair reactor operations.

Load Change: Load changes may be used throughout core life to reduce power to conserve core life and later return to full power when it is needed [see Chapter 5]. In this case, both load increases and decreases are considered. Currently Stirling engines designed for RTG's are not designed to change load [9] [since radio-isotopes cannot throttle power [10]], however Stirling designs for Earth based power generation and/or automotive use have been designed for dynamic operation [9] [they are however considered sluggish compared to current internal combustion engines [9]]. While it would be prudent to change power slowly [over the course of hours] for any actual designed operation to limit the transient effects, this section will consider instantaneous changes in load to represent the worst case scenario for a power transients.

The first load change considered is reducing power. The model was run with a matrix of power level changes [an initial power from 5%-100% and a final power from 0-95% in 5% increments]. The largest transient was the 100% to 0% transient which is shown in Figure 8.6. The first effect is the beryllium reflector starts to heat up since less heat is removed. The high heat capacity of the beryllium [9.2 sec/˚C] means that the beryllium will take minutes to heat up. This heat up starts to add a small amount of negative reactivity to the reactor and power drops which reduces heat generation in the fuel causing fuel temperature to drop. Since the neutronics occurs faster than the heat diffusion, the fuel temperature decreases before the LiH heats up appreciably. Since the Beryllium temperature is less important than the fuel to reactivity and the heat capacity

of the fuel is smaller, the dropping fuel temperature nearly adds reactivity as fast as the Beryllium reduces it keeping the core quasi-critical. As a result, the minimum reactivity in the core is only -5.95¢ and the maximum is only +0.29¢ [which is the equivalent of ≈-2¢ and ≈+0.1¢ respectively in LWR's [11]]. With the fuel temperature dropping and the reflector heating up the LiH experiences a comparatively small change of temperature [The peak LiH temperature raises only 1.06˚C].

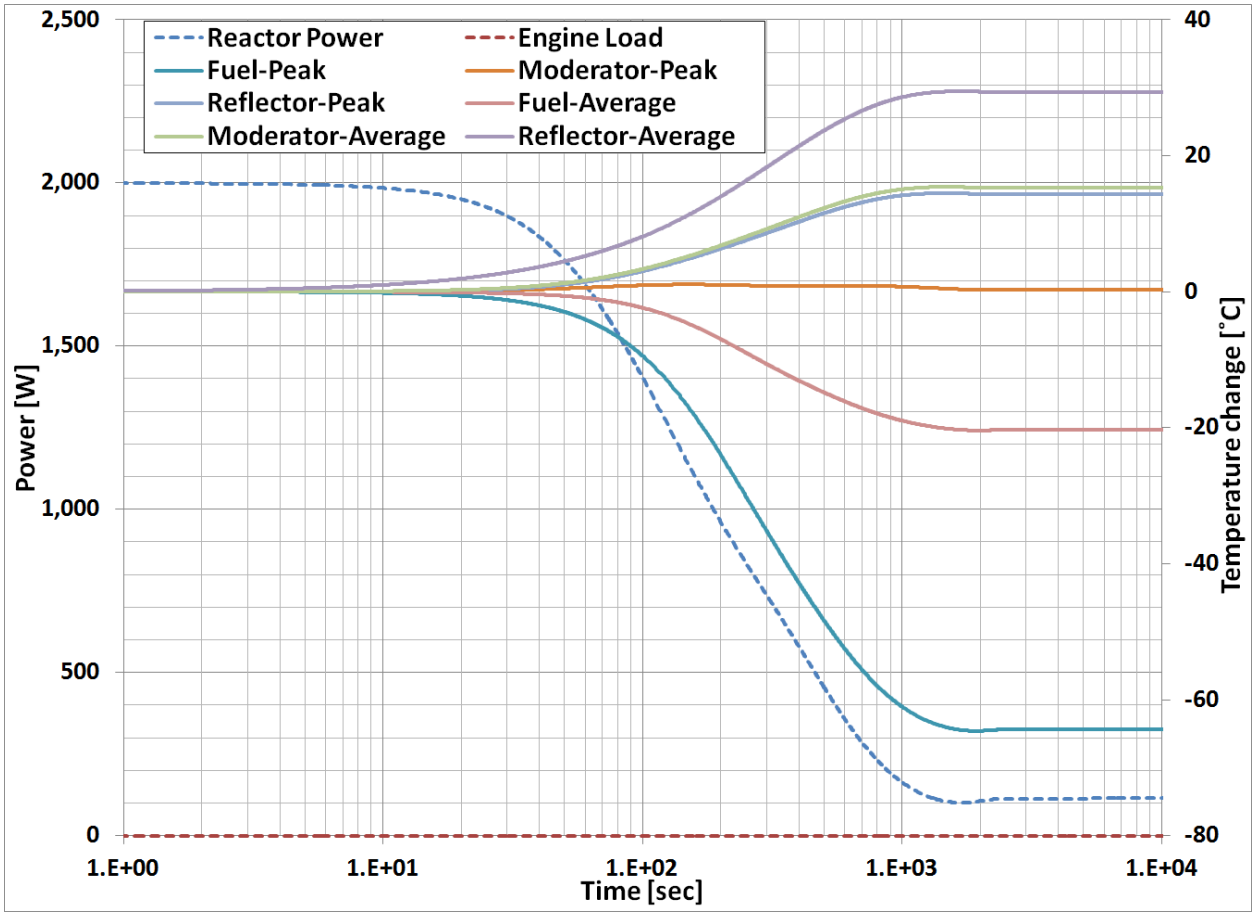

Figure 8.6: Instantaneous load change from 100% to 0%. This is a graph of fission power and reactor temperature as a function of time following a transient. This transient is modeled based on beginning of life parameters. The rise in the Peak LiH temperature is barely visible: The peak at 150 sec is only 1.06˚C.

The final temperature distribution the core contains 541 KJ more heat energy, which is the equivalent of 256 seconds of full power. It takes ≈15 minutes for power to drop below 10%, which allows decay heat to decay significantly [12] [to <40W_{TH}]. As a

result decay heat will be well below radiated power and as a result fission power only drops to 4.8% of full power [instead of ≪1% as in LWR's], which means that the power never reduces below the so called point-of-adding-heat [3][important for reactor stability].

Increased power is considered next. The same matrix of power changes was again considered and the largest transient [0-100% power] is shown in Figure 8.7. The same processes as in the power reduction occur but in the opposite direction. The biggest difference in this case is that the reactivity swing is larger since the power is smaller to begin with, which results in a larger percentage change in power [1600% rise compared to a 95% drop]. In this case, the reactivity will peak at +17.41¢ and have a negative swing of 2.65¢. Again the peak LiH temperature rise is small at only 0.66˚C [the initial drop is larger in magnitude at -2.76˚C but LiH temperature drop is not a concern].

The final temperature distribution the core contains 541 kJ less heat energy, which is the equivalent of 256 seconds of full power. The surprising feature is that the power overshoot that occurs 199 seconds into the transient is smaller than the final power level. Due to the slow nature of the thermal transient the fission power will make several oscillations and overshoots while the thermal load on the core is well below the equilibrium load and as a result the power oscillations are damped out well before the equilibrium power is reached [In most other reactors peak power can be much larger than equilibrium power and as a result large up powers can be damaging to those reactors] [2].

Both load changes shown in Figure 8.6 and 8.7 are with the beginning of life core parameters. Load changes were also simulated throughout the life of the core but did not differ by more than a few degrees [since the heat capacity and temperature coefficient of reactivity are nearly constant throughout core life]. The transients become slightly more severe towards the end of life [the LiH reaches its melting point for 100% to 0% load changes beyond ≈110 years], but this is insignificant for 4 reasons:

1- Realistic load changes will be slower and less severe than instantaneous [9]
2- Load reductions will be less likely to be needed late in core life since power demands for communications and heat would be high due to the distance from the sun and Earth [13]
3- Merely reaching the melting point of the LiH will not cause significant core damage [only lowers temperature slightly]
4- Damage to the core late in life is less significant since most or all of the mission may already be completed.

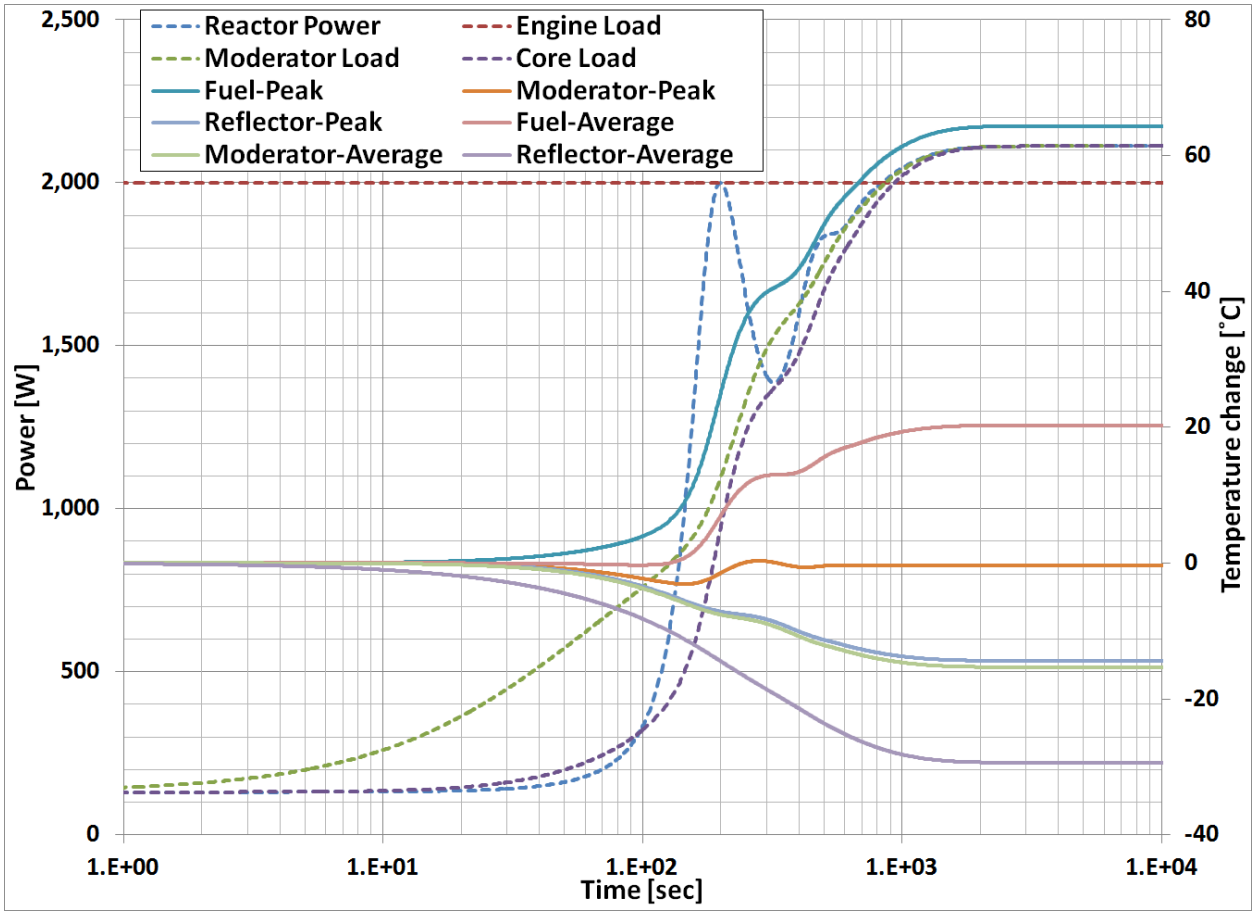

Figure 8.7: Instantaneous load change from 0% to 100%. This is a graph of fission power and reactor temperature as a function of time following a transient. This transient is modeled based on beginning of life parameters.

Section 3: Start-up

The last transient that is considered is the initial start-up. This transient differs from previous transients discussed since the reactor is below the point-of-adding-heat. This is significant since power changes do not necessarily change the temperature of the reactor which means the negative temperature coefficient of reactivity cannot prevent the reactor from going prompt-critical.

Source needed: The first issue that is addressed is the need for an initial source of neutrons. Fission reactors are based on neutron multiplication [1] and if the initial population of neutrons is zero then the final population will zero regardless if the reactor is subcritical or supercritical. To ensure a smooth reactor start-up, the number of neutrons should be sufficient such that the relative statistical fluctuations in the neutron population associated with the source neutrons over the neutron generation lifetime [13.4 Sec when critical] are much less than the reactivity of the core. Since the half-life of neutron source is much greater than the neutron generation lifetime [1], the statistics are will modeled as a Poisson distribution [14]. This leads to Equations 8.1 and 8.2.

$$\frac{\boldsymbol{\sigma_{\text{Source Uncertinty}}}}{\boldsymbol{S_{\text{Source Rate}}\tau}} = \frac{\boldsymbol{\sqrt{S\tau}}}{\boldsymbol{S\tau}} \ll \boldsymbol{\rho} \qquad \text{Equation 8.1}$$

$$\boldsymbol{S \gg \frac{1}{\rho^2 \tau} \approx \frac{10^4}{\rho^2_{[\$]}} \text{Neutrons/sec}} \qquad \text{Equation 8.2}$$

This is why the Cf-252 source mentioned in Chapter 7 was sized to be 10^6 neutrons per second. At this size, the Cf-252 would weigh <1µg [15] and can be incorporated into the rod. The half-life of the Cf-252 source [2.65 Years] [16] would mean that it would not be stored with the reactor and would be attached only during launch

preparation. Cf-252 is commercially available [15]. With the source installed the neutronics during the start-up would behave deterministically and statistical fluctuations will be insignificant.

Criticality: The critical rod position is dependent on small defects, which occur during actual core construction. This makes it necessary to measure the reactor criticality on Earth prior to launch. With proper set-up, the reactor start-up sequence can be done in a laboratory setting with neutron measurement instruments. The Instruments would enable human operators to measure reactor power at very low power levels [~10^{-9} W_{TH}] during the start-up [17]. It would then be possible to measure the zero-power critical rod position for a range of reactor temperatures [the reactor would be externally heated or cooled to change the temperature]. Small adjustments to the measurements would need to be made to account for reflection from air and the laboratory walls, but the error in critical rod position from these effects can be made insignificant.

When the start-up commences in outer space the rod could then be quickly withdrawn to the critical rod position. The reactor start-up is then possible without neutron instrumentation which save the mass of these instruments [≈60 Kg for SP100 [18]] and their electrical load.

To reach the expected critical rod position the rod will need to be moved a total distance of ≈37 cm [Boron Rod 20.4 cm + Spacer 5 cm + Fuel Rod ≈ 12.1 cm into the core]. There would be no speed limitation on this rod movement since the reactor would be subcritical and at zero-power. For safety the rod would actually be moved to a position that is just slightly subcritical [≈-4$] to account for small variations of disturbance in the system due to the vibrations that occur during launch.

Point of Adding Heat: The next step in the reactor start-up will be to proceed from criticality at source neutron levels [~10^{-9} W_{TH}] to the point of adding heat [≈10's W_{TH}] without going prompt critical. Then the power and temperature would be raised from the shutdown condition to power at a reduced temperature [reaching 540˚C, see Section 2]. For this computation, the initial temperature is taken to be 0˚C but the initial temperature is not significant.

With neutron instrumentation, it is possible to precisely control the reactor start-up by measuring in core power levels. However, to save mass it is assumed that no neutron instrumentation will be used in space. This means the rod will be pulled at a constant rate to start-up the reactor. Once the rod motion stops, the reactor power will follow the thermal load. If the reactor has not heated up, the thermal load will be zero and core power will return back into the source region, negating the start-up [2]. As a result of this, the start-up and heat-up will need to occur in a single step. The core will need to heat-up sufficiently such that thermal radiated power becomes significant but below normal operating temperature to leave a large thermal margin for the transient. The reactor is designed to heat-up 540˚C [the 100˚C margin from 640˚C, see Section 2] and the radiated thermal loads will reach ≈70 W_{TH}.

At this point, the model was then run with a variety of rod speeds and the resulting power and temperatures are shown in Figures 8.8 and 8.9. The 3.3 mm/min corresponds to a peak fuel temperature of 930˚C and will spend just 8.5 minutes at greater than 760˚C.

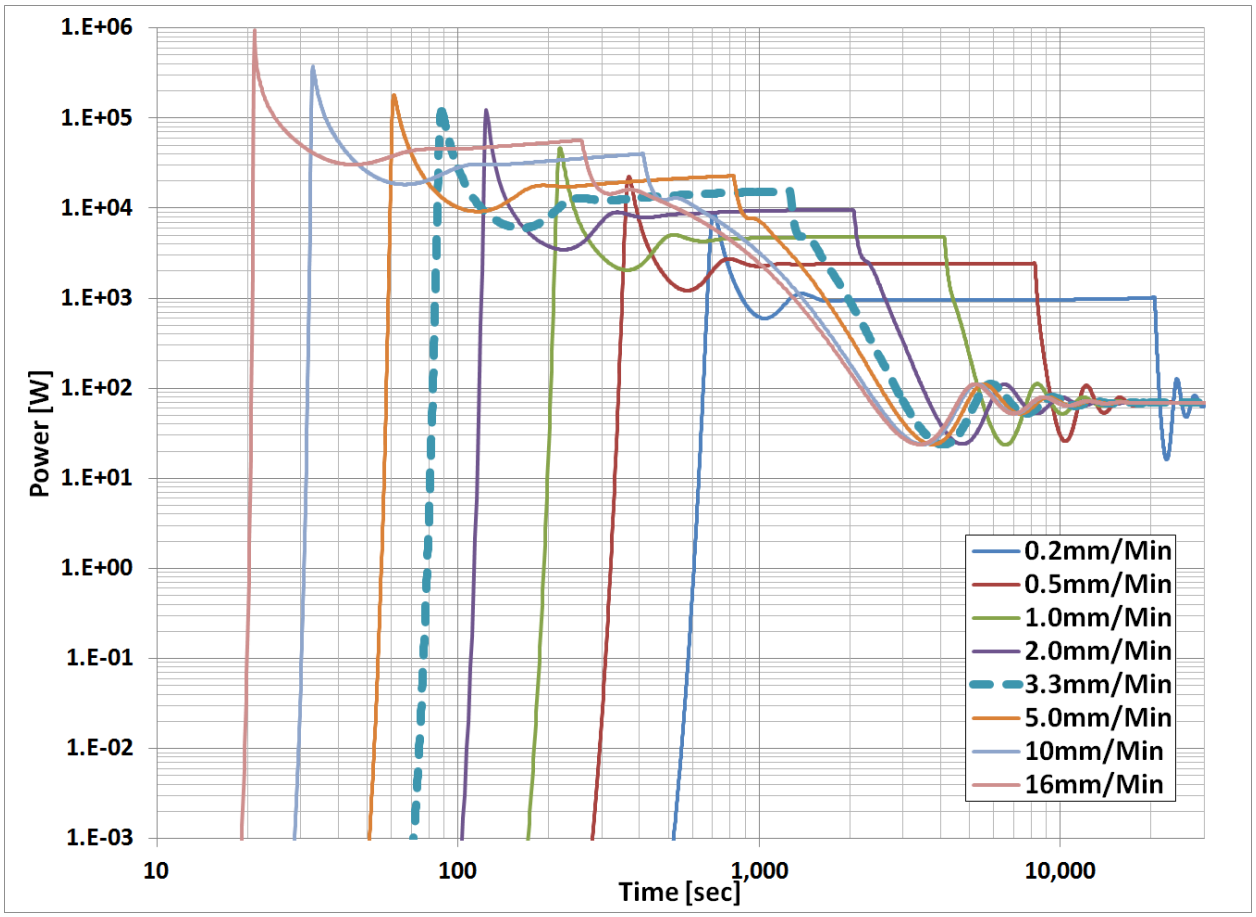

Figure 8.8: Power profile for various rod speeds. This is a graph of fission power as a function of time following a transient. This transient is modeled based on beginning of life parameters. The transient is caused by rod motion to add reactivity at a constant rod speed. Rod motion starts at T=0.

At all rod speeds, the transient runs a similar course. The reactor is super-critical [37¢ at 0.2 mm/min to 95¢ at 16 mm/min] as the power reaches the point of adding heat and power spikes. The power spike for the 3.3 mm/min reaches 120 kW_{TH} or only 13.8 kW_{TH}/kgU, which is a lower power density than TRIGA/SNAP reactors at 90/150 kW_{TH}/kgU [7] [LWR are ≈35 kW_{TH}/kgU [2]]. At this point, the reactor heats up rapidly adding negative reactivity, reducing reactor power. The reactor power then stabilizes at the given heat-up rate associated with the rod speed. At this point, the transient proceeds similar to the heat-up in Section 2. The only difference is that the thermal

load is only ≈70 W_{TH} at the end of the transient. This causes the reactor to experience a large power down at the end of the heat-up. A more detailed graph of the 3.3 mm/min is shown in Figure 8.10. Following the heat-up, the heat engine would be started, which would proceed similar to the load increase shown in Figure 8.7.

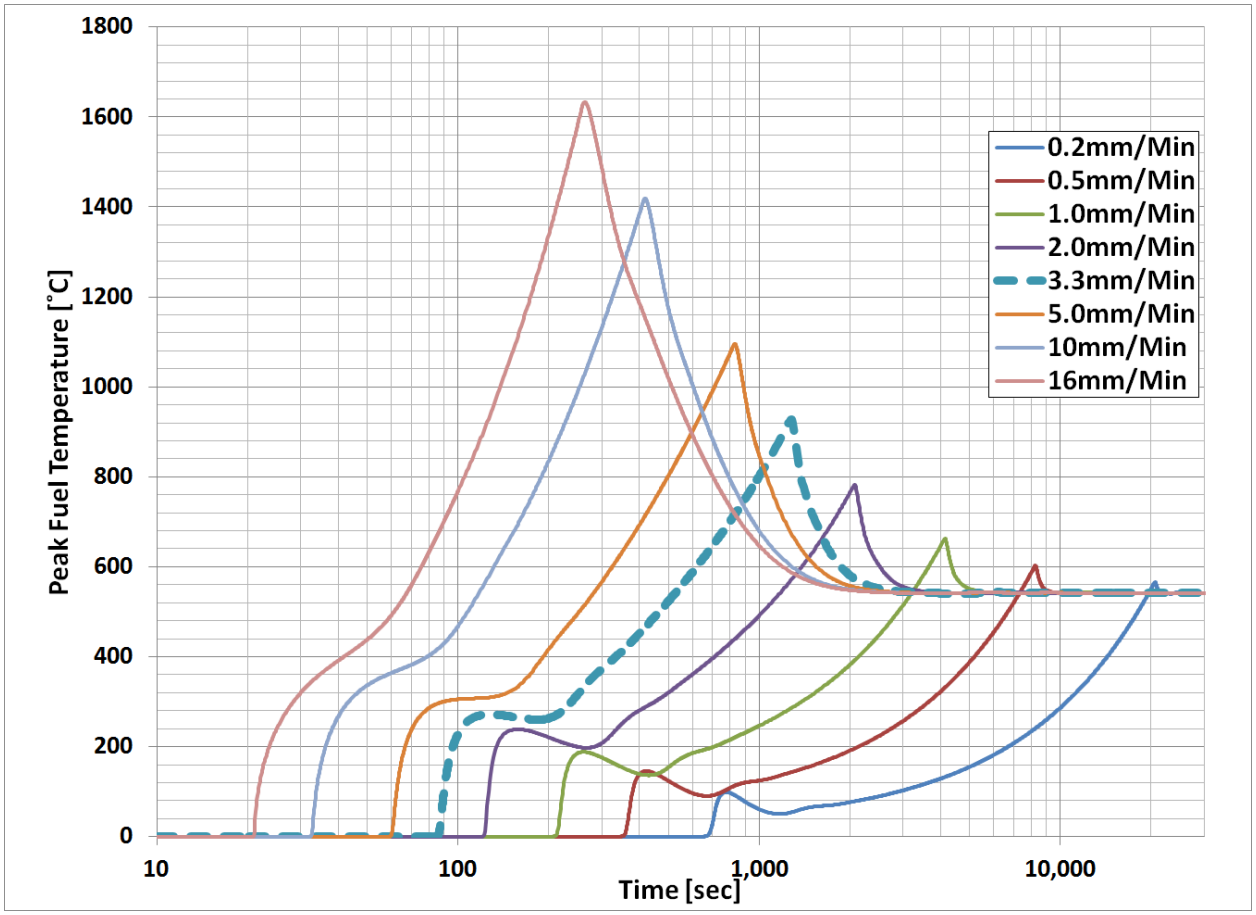

Figure 8.9: Temperature profile for various rod speeds. This is a graph of reactor temperature as a function of time following a transient. This transient is modeled based on beginning of life parameters. The transient is caused by rod motion to add reactivity at a constant rod speed. Rod motion starts at T=0.

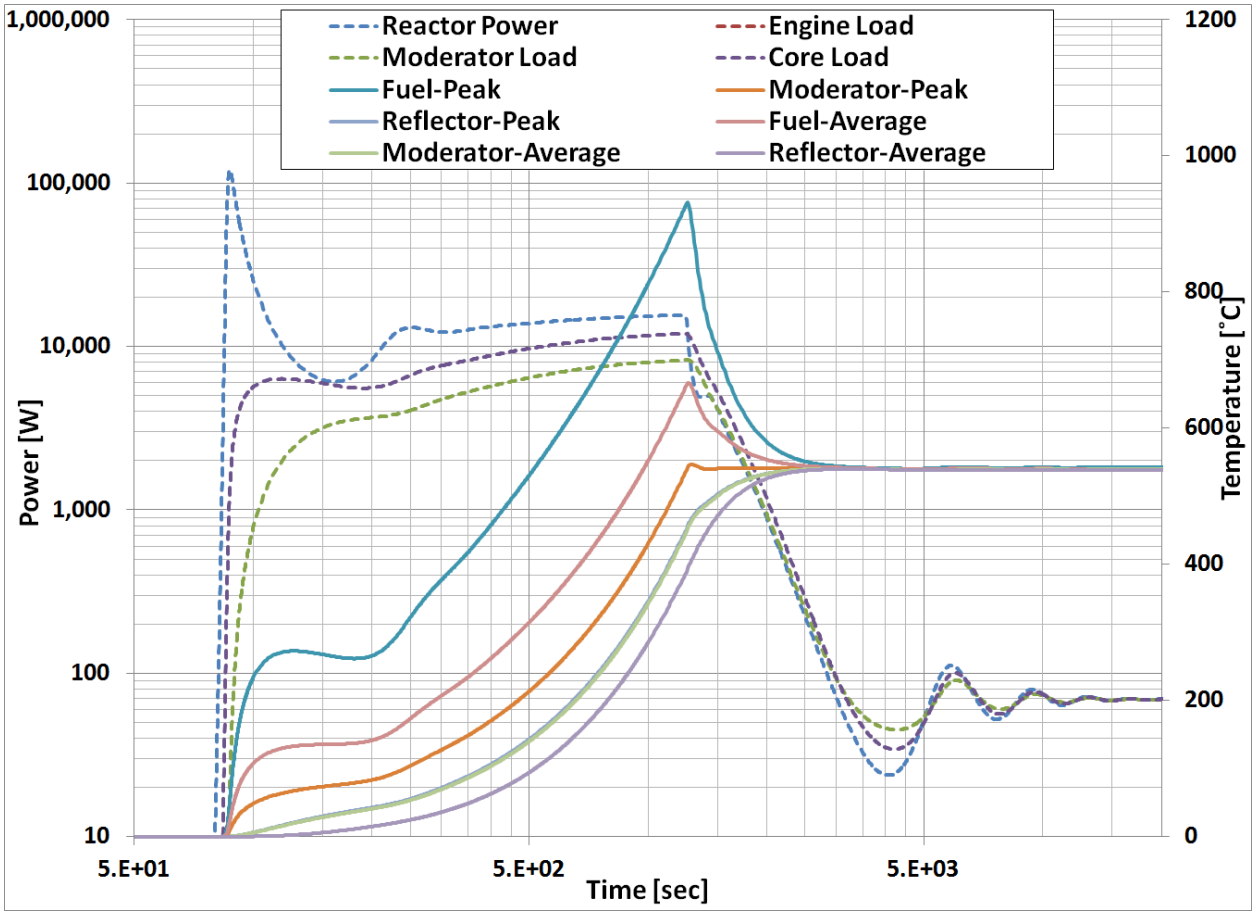

Figure 8.10: Start-up Power and Temperature profile at 3.3mm/Min rod speeds. This is a graph of fission power and reactor temperature as a function of time following a transient. This transient is modeled based on beginning of life parameters. The transient is caused by rod motion to add reactivity at a constant rod speed. Rod motion starts at T=0.

Start-up duration: The start-up duration depends on the design of the control rod drive mechanism. To minimize transients the rod speed was set at ≤3.3 mm/min. In this case, the start-up would take ≥131 minutes to bring the heat engine online to produce power. This consists of 112 minutes for the rod to be moved to the critical position [≈37cm] and 21 minutes to raise the power the reactor to and heat-up to 540˚C at which time the heat engine could be brought online.

If instead, the rod speed was variable, then the initial rod movement to the critical position could proceed at a much faster rate [reducing the 112 minutes to a few], thereby reduce the time to start-up the reactor significantly. Additionally, the start-up

and heat-up transients can be reduced by reducing the rod speed. This creates a margin and can reduce the thermal stress of the heat-up. The 3.3mm/min was the maximum rod speed that kept the reactor within the thermal limits. Slower rod speeds are acceptable as well.

In any case the probe will need to have a supply of power for at least several hours after launch [battery]. The probe would have to leave Earth orbit and then take hours to start-up before generating electricity. If initial solar panels are used [Chapter 7 Section 3] while near the sun the start-up can be delayed [months to years] and start-up speed is not an issue [the reactor could be started slowly over weeks]. Otherwise the probe design should ensure there is sufficient battery power to start-up the reactor.

Rod Shutdown: The reactor can also be shut-down by the insertion of the control rod. This transient is not covered because of the difficulty in restarting the reactor. Since the core life is sufficient at full power and other life extension options exist [see Chapter 5] there is no need for the reactor to shut down and restart later in deep space. At the very end of life, the reactor may be shut down with the rod if it is still operable [they will likely be stuck but in this case the reactor will shut itself down as in Chapter 5, plus the alpha decay of the fuel will add additional negative reactivity].

Section 4: Summary

In this chapter, the reactor transients were explored and the allowed rate of rod motion and load changes was determined. It was determined that the reactor is very stable due to the negative temperature coefficient as well as a large heat capacity in relation to the core power levels. This stability of load changes allows the reactor to change power levels with demand to conserve fuel and increase core life if needed. The reactor start-up was analyzed and is possible without neutron instrumentation.

References [Chapter 8]

[1] Karl Ott, “Nuclear Reactor Dynamics”, ANS (1985)
[2] J.J. Duderstadt and L.J. Hamilton, “Nuclear Reactor Analysis”, John Wiley & Sons Inc (1975)
[3] Edward Larsen, “Nuclear Engineering Problems and Solution Techniques”, NERS 490 Lecture notes, University of Michigan (2008)
[4] National Nuclear Data Center, http://www.nndc.bnl.gov/
[5] N. Kocherove, M. Lammer, and O. Schwerer “Handbook of Nuclear Data for Safeguards” Nuclear Data Section, IAEA (1997)
[6] R.L. Smith and J.W. Miser “Compilation of the Properties of Lithium Hydride” Lewis Research Center, Cleveland, OH (1962)
[7] D. Olander, et al “Uranium-Zirconium Hydride Fuel Properties” Nuclear Engineering and Design, 239, pp. 1406 (2009)
[8] “Beryllium Properties”, Advanced Energy Technology Group (2012) http://aries.ucsd.edu/LIB/PROPS/PANOS/be.html
[9] D. Thimsen, “Stirling Engine Assessment”, EPRI (2002), http://www.engr.colostate.edu/~marchese/mech337-10/epri.pdf
[10] M. Ragheb “Ch. 3 Radioisotopes Power Production” (2012), https://dmtpc.mit.edu/twiki/pub/Projects/RadioIsotopeBattery/Radioisotopes_Power_Production.pdf
[11] “The Westinghouse PWR Nuclear Power Plant”, Westinghouse (2006)
[12] A.L. Nichols “Nuclear Data Requirements for Decay Heat Calculations” Internal Atomic Energy Agency, Nuclear Data Section (2002)
[13] IAEA “The Role of Nuclear Power and Nuclear Propulsion in the Peaceful Exploration of Space” (2005)
[14] Daniel Zwillinger, “Standard Mathematical Tables and Formulae”, CRC Press (1996)
[15] R Martin, “Production, Distribution, and Applications of Californium-252 Neutron Sources”, Oak Ridge (1999)
[16] Edward Baum, “Nuclides and Isotopes: Chart of the Nuclides”, Lockheed Martin (2009)
[17] Glenn Knoll, “Radiation Detection and Measurement”, John Wiley & Sons Inc (2000)
[18] S.F. Demuth “SP100 Space Reactor Design” Progress in Nuclear Energy, 42, pp.323 (2003)
[19] D.I. Poston, et al “The DUFF Experiment-What Was Learned?” Proceedings of Nuclear and Emerging Technologies for Space, Albuquerque, NM (2013)

Chapter 9: Conclusion

The need for decades long electrical power for deep space probes is currently filled by RTG's using Pu-238 [1]. The safety and proliferation risks of radionuclides warrant a renewed investigation of fission nuclear power as a RTG replacement [2]. Since most past fission reactor designs were not designed for this role [3], a fresh investigation into this option was conducted here. In this work several unique contributions to space reactor designs were developed as well as a continued evolution towards lighter and lower power designs [1].

Section 1: Chapter Summaries

A summary of each individual chapter results is included in this section.

Chapter 1: The possible sources of energy for space power were examined and this analysis concluded that nuclear power was only viable when solar power is not an option. The major use for this energy would be for electrical power generation. The high initial power of short-lived radionuclide's such as Sr-90 [4] and the distance to reach the outer solar system pushed core life-time to at least 2 decades. The effect of radiator mass was considered, which limited the possible specific powers that the reactor could realistically achieve [5]. A region of core age and specific energy of the fuel was developed.

Chapter 2: The mission requirements for deep space probes were examined along with past reactors and RTG's. The reactor would be in direct competition with alpha decay RTG's that produce initial specific power of 3-6 W_E/kg [6] [average specific

power of 2-4 W_E/kg] and the reactor would not be able to significantly improve upon these [the specific power is limited by the heat engine mass, which is similar for both heat sources; fission and alpha decay]. However, there was large room for improvement in safety and proliferation [7]. Based on this review, the specifications of the reactor required a mass of <≈150 kg producing ≈500 W_E for a time of ≈100 years with significantly less toxicity and proliferation risk less than current RTG's.

Chapter 3: The materials from which the core is to be constructed were selected. The high temperature of the core [650˚C] significantly limited the materials that contained hydrogen at low pressure [8]. The neutronics of reactor was then examined for a large number of core configurations. The minimum critical masses of the various core designs were very close in final masses, which were ≈25 kg [well within the design mass]. The core was designed as a thermal reactor and as a result showed strong negative temperature coefficients of reactivity, which will keep the reactor stable at steady power [9]. In addition, the very low power of the core meant that Xe-135 transients would be insignificant [10].

Chapter 4: A thermal analysis of the core was performed. The temperature limits of the core materials were examined and limited by hydrogen retention and melting. Since heat transfer in the core is limited to conduction, to eliminate pumps, the temperature gradient across the core set a limit for thermal efficiency. This eliminated the use of thermocouples and required dynamic heat engines such as Stirling and Brayton [11] [Stirling is selected for this paper]. A more detailed analysis of the heat conduction in the core was then undertaken allowing thermal power of 2112 W_{TH} from the core [243 W_{TH}/kg_{FUEL}] at a temperature of 640˚C. Additionally, the reactor could be operated at reduced power if desired. Finally, higher power could be generated with greatly reduced lifetime, but this was not utilized in the base design.

Chapter 5: The lifetime of the reactor was analyzed. The core lifetime is based on maintaining a steady reactor temperature. As the cores fuel is burned, poisons build-up and radiation damage accumulates [12]. These add negative reactivity, which results in lowering core temperature [10]. To counteract the temperature drop, burnable poisons are investigated as a means to keep temperature steady in a much smaller temperature band of ±6.4°C. This allows for reactor lifetimes of up to 200 years with constant power, which is significantly longer and steadier than RTG sources [6].

Chapter 6: The issue of shielding the reactor is covered in detail. This is a key concern as the mass of shielding can be considerable. The SP100 shielding weighed 970 kg [13], which was considerably more massive than the core itself. The sources of radiation as well as the applicable dose limits are covered. The materials used for shielding are then selected. Numerical modeling of the shielding was then done to minimize the mass of the shield. The shield would be 43 kg, which is larger than the core itself but not prohibitive.

Chapter 7: The core safety is compared to current RTG's. The pre-launch safety design consists of criticality control using a shutdown rod. The toxicity of the core is 4 orders of magnitude lower than RTG's [14]. Further toxicity reduction can be achieved using U-235, but increases the mass of the system considerably. The proliferation risks are also lower than Pu-238 and Am-241 [15]. Further reduction in proliferation by using low enriched fuel would significantly increase the mass of the reactor [55]. The reactor would not start-up until Earth escape velocity is reached to minimize risk to the Earth [7]. Following start-up, the build-up of fission products and actinides is tracked and the total toxicity is computed. Throughout the entire life of the core [and thousands of years after] the toxicity is much lower than for comparable RTG's. This lower toxicity means that the risk during crashes will be significantly lower.

Chapter 8: The reactor transients are covered. Due to the small size of the reactor, point kinetics are used to model the transients [17]. The reactor is very stable due to the negative temperature coefficient as well as a large heat capacity in relation to the core power levels [9]. The allowed rod speed during heat-up [10.1˚C/min] and start-up of the reactor was found. Due to the heat capacity of the Beryllium, the effect of load changes was quite small. Even instantaneous load changes of 0-100% and 100-0% are easily handled by the reactor. The reactor start-up was analyzed and is possible without neutron instrumentation. The duration of the start-up would be on the order of hours and external power [solar or battery] would therefore be necessary to start the reactor.

Section 2: Overall Conclusions

Specific Power: In total, the mass of the reactor, start-up rod and shielding as designed here was 71.0 kg. The reactor would generate 2 kW_{TH} at 640˚C at the heat engines. Using the ASRG, the heat engine would be ≈84 kg and generate ≈560 W_E [18] [3.6W_E/kg], which meets the design goal. This is the same average power that the GPHS-RTG generates over half the half-life of Pu-238 [19] [see Chapter 2 Section 2]. With the heat engine adapted to the size of the reactor, the electrical output would be 500-800 W_E with an Engine/Radiator mass of 50-80 kg [5] [4.1-5.3 W_E/kg]. This would be the equivalent to beginning of life RTG specific power of 6.0-7.7 W_E/kg.

Unique Design: There have been several designs for space nuclear in the past [1][20] and it is important to highlight the design aspects of this reactor that are unique to this design. These are listed below [21][22][20][1]:

1- Use of a thermal reactor design in space.
2- Use burnable poisons instead of control rod movement.
3- No moving fluids for heat removal [no pumps or moving parts]
4- The shield footprint is smaller than the reactor to reduce mass.
5- All transients are stable without operator response.
6- Reactor is subcritical on fast neutrons alone.

Additionally, it is important to point out aspects of the design that differ in magnitude from previous designs [1][20]. These represent evolutionary improvements as space reactor designs shift to smaller and lighter. These are listed below:

1- Small size of only 28 kg for the reactor and rod and 43 kg for the shield.
2- Low power of 2,112 W_{TH}.
3- Long lifetime of 200+ years.
4- Moderate core temperature of 640°C to 750°C.
5- High heat capacity to thermal power ratio [3.5°C/min heat-up at 100% power].

The primary contribution of this dissertation, by designing a RTG replacement reactor, was thus to push the reactor design envelope to smaller size and lower power, into the region where reactors were previously considered not feasible.

Path Forward: To move forward from this initial design work to utilize reactors in space requires several steps. These are listed below.

1- Maintain the U-233 currently stored in the US. Disposal of this potential fuel would leave only U-235 reactors as a possibility. It would be a shame to waster such excellent potential fuel [23][24].
2- Develop a scalable set of heat engines [likely Stirling] and associated radiators so that the electrical output can be varied based on mission requirements. This would also be useful for future RTG's as well [11].
3- Determine one or more specific missions for the reactor to power in the near term. The specific payloads and budgets would allow the reactor to be well matched with the mission. These reactors would not be mass produced so each one could be customized to a degree [within the window of Figure 1.2].
4- Develop a complete shielding model with genetic algorithms to determine the shielding requirements for each individual mission. The shield is the heaviest component of the reactor and reducing this mass would be significant.
5- Complete the analysis of the reactor system to include launch vibration tests, crash simulations and fitting the pieces together to telescope after launch to fit compactly in the launch vehicle.
6- Build and test a reactor on Earth. The construction should be simple and quickly completed. The difficulty in this step would lay in obtaining regulatory approval and building the reactor with all the Earth required safety components. It may be practical to simulate the reactor instead and perform this step computationally [17].
7- Construct the reactors to be used in space and perform zero-power measurements on it [critical position]. Have proper storage facilities available until needed for launch.

The first 2 steps, in particular, should be started within the next few years. The U-233 is a valuable resource regardless of the final design of a reactor and the cost to store the U-233 is tiny compared to creating fresh U-233 [23][24].

While this dissertation was being written a separate low power design was initiated; the DUFF and KRUSTY reactors [3][22][26][17]. An alternative path forward would be to merge the results found here into the DUFF designs. For example, a merged reactor design might utilize the U-233 thermal reactor with burnable poison temperature control and the improved shield design of this study [for low mass and longevity of core life] and the heavy block beryllium reflector and higher power of 1 kW_E

of the DUFF design [for simplicity and cost]. The merging of these two designs would require additional study that is not included here.

Conclusion: Using a fission reactor would significantly decrease the radio-toxicity and proliferation risks of current RTG's. The reactor design is well suited to the long duration deep space mission with a power supply lifetime significantly longer than any possible RTG. The shielding required is significant, but not prohibitive with a mass comparable to that required for the heat engine. Due to the steady nature of the generated power and the long life, the specific power generation would exceed current RTG's and match planned advances.

Small low power reactors should be used to replace RTG's!

References [Chapter 9]

[1] IAEA "The Role of Nuclear Power and Nuclear Propulsion in the Peaceful Exploration of Space" (2005)
[2] M.S. El-Genk, Space Safety Regulations and Standards, "Chapter 26 Safety Guidelines for Space Nuclear Reactor Power and Propulsion Systems" pp. 319 (2010)
[3] L. Mason, et al "A Small Fission Power System for NASA Planetary Science Missions," NETS–2011, Paper 3318 (2011)
[4] National Nuclear Data Center, http://www.nndc.bnl.gov/
[5] L.S. Mason "Realistic Specific Power Expectations for Advanced Radioisotope Power System" Journal of Propulsion and Power, 23, pp. 1075 (2007)
[6] M. Ragheb "Ch. 3 Radioisotopes Power Production" (2012), https://dmtpc.mit.edu/twiki/pub/Projects/RadioIsotopeBattery/Radioisotopes_Power_Production.pdf
[7] Friedensen, " Protest Space: A Study of Technology Choice, Perception of Risk, and Space Exploration" Chapter 3 How NASA Calculates Risk (1999), http://scholar.lib.vt.edu/theses/available/etd-120899-134345/unrestricted/06chapter_3.PDF
[8] David Lide, "CRC Handbook of Chemistry and Physics", CRC Press (2001)
[9] Karl Ott, "Nuclear Reactor Dynamics", ANS (1985)
[10] J.J. Duderstadt and L.J. Hamilton, "Nuclear Reactor Analysis", John Wiley & Sons Inc (1975)
[11] D.J. Anderson, et al "An Overview and Status of NASA's Radioisotope Power Conversion Technology NRA" NASA Glenn Research Center, American Institute of Aeronautics and Astronautics (2005 year)
[12] D. Olander, et al "Uranium-Zirconium Hydride Fuel Properties" Nuclear Engineering and Design, 239, pp. 1406 (2009)
[13] S.F. Demuth "SP100 Space Reactor Design" Progress in Nuclear Energy, 42, pp.323 (2003)
[14] U.S. Nuclear Regulatory Commission Regulations: Title 10, Code of Federal Regulations (2012)
[15] J.C. Mark and E. Lyman "Explosive Properties of Reactor-Grade Plutonium" Science and Global Security, 17, pp.170-185 (2009)
[16] C.W. Forsberg, et al "Definition of Weapons-Usable Uranium-233" (1998)
[17] D.I. Poston, et al "The DUFF Experiment-What Was Learned?" Proceedings of Nuclear and Emerging Technologies for Space, Albuquerque, NM (2013)
[18] R.K. Shaltens and W.A. Wong "Advanced Stirling Technology Development at NASA Glenn Research Center" NASA (2007)
[19] G.L. Bennett, et al "Mission of Daring: The General-Purpose Heat Source Radioisotope Thermoelectric Generator" IECEC, San Diego, CA (2006)
[20] G.L. Bennett, et al "Status Report on the U.S. Space Nuclear Program" Acta Astronautica, 38, pp. 551 (1996)
[21] George Scmidt, "Nuclear Systems for Space Propulsion and Power", NASA Glenn Presentation (2010)
[22] D. Poston "The Demonstration Using Flattop Fissions (DUFF) Experiment" Los Alamos National Laboratory (2012)

[23] C.W. Forsberg and L.C. Lewis “Uses for Uranium-233: What Should be kept for Future Needs?” (1999)
[24] J.W. Krueger “U-233 Disposition Project Update” (2011), http://www.oakridge.doe.gov/em/ssab/Minutes/FY2011/Presentations/U-233ProjectUpdate.pdf
[25] D.I. Poston, et al “A Simple, Low-Power Fission Reactor for Space Exploration Power Systems” Proceedings of Nuclear and Emerging Technologies for Space, Albuquerque, NM (2013)